School of Medicine
Oregon Health & Science University

CERTIFICATE OF APPROVAL

This is to certify that the Ph.D. dissertation of

Carley A.E. Shaut

has been approved

[redacted]
Mentor/Advisor – H. Scott Stadler

[redacted]
Committee Chair – Jan Christian

[redacted]
Member – Jonathan Zonana

[redacted]
Member – Cheryl Maslen

[redacted]
Member – David Ransom

[redacted]
Member – Philip Copenhaver

Hoxa13 is essential for placental vascular patterning and endothelial cell integrity

By Carley Ann Egelston Shaut

A DISSERTATION

Presented to the Department of Molecular and Medical Genetics

and the Oregon Health & Science University

School of Medicine

in partial fulfillment of

the requirements for the degree of

Doctor of Philosophy

Approved by the Oral Examination Committee

December 13th, 2006

Table of Contents

Chapter Five: The HOXA13 transcription factor directly regulates expression of Tie2 and Foxf1

Chapter Six: Materials and methods

Chapter Seven: Conclusions and Discussion

Appendix

List of Figures and Tables

Figures

Chapter One

Chapter Three

Chapter Four

Chapter Five

Tables

List of abbreviations

A13-DBD	HOXA13 DNA Binding Domain
Adrb1	Adrenergic receptor beta-1
ANOVA	Two-Factor Analysis of Variance
CAM	Chorioallantoic membrane
ChIP	Chromatin Immunoprecipitation
bp	Base-pairs
D13-DBD	HOXD13 DNA Binding Domain
E	Mouse embryonic day
EC	Endothelial cell
ECM	Extracellular matrix
EMSA	Electrophoretic mobility shift assay
FDR	False discovery rate
GFP	Green fluorescent protein
IA	Intussusceptive angiogenesis
ISH	*In situ* hybridization
IHC	Immunohistochemistry
IMG	Intussusceptive microvascular growth
K_d	Dissociation constant
Lyve1	Lymphatic vascular endothelial marker 1
MAGE	Melanoma Antigen-encoding Gene
Nrp1	Neuropilin-1

PBS	Phosphate-buffered saline
PDGF	Platelet derived growth factor
PECAM-1	Platelet endothelial cell adhesion molecule-1
PFA	Paraformaldehyde
qRT-PCR	Quantitative real-time polymerase chain reaction
TEM	Transmission electron microscopy
UA	Umbilical arteries
VEGF	Vascular endothelial growth factor

Acknowledgements

So many people have influenced and helped me throughout my graduate career, so many that it is hard to begin thanking them all!

A big thank you to Scott Stadler for his dedication to my learning and development as a scientist and researcher. Yes, I learned a lot in this lab! Thank you for encouraging me to stick with it and to see my potential.

Thank you to my Thesis advisory and exam committees, Jon Zonana, Jan Christian, Cheryl Maslen, David Ransom, and Phil Copenhaver. Thank you so much for your dedication to helping me with my thesis writing and editing, and thank you for your words of advice and encouragement through the years of graduate school. I wouldn't have made it this far without your encouragement and support!

Through graduate school, I've been very blessed by amazing friendships, both inside and outside of science and OHSU. I'm grateful for my "girls", Jodi, Wendy, Patrice, Martha, Lara and others, the amazingly talented ladies whom I've walked along side during graduate school. We are a team for life, I feel, and you're the best teammates a gal could ask for. I'm also grateful for the great friendships built in the lab, with Wendy, Gin, Susan, Emily, Chie, Diane, Crystal, and Siming. Who else could you talk to about mouse "pee-pees" and such! Boy do we have some crazy stories!

My never-ending love to my husband and parents. To my parents, thank you for always believing in me and supporting me though it all. You are my touchstone to peace and understanding. Dave, I am a complete person, an extremely happy person, and a *sane* person, because of our relationship. Thank you for caring about me and loving me every day. I am excited to see what our next adventure will be together.

Thank you to everyone who has guided me through these important, sometimes tumultuous, years of graduate school. Graduate school has been both extremely challenging and very rewarding, and it's all worth it in the end. I am happily on my way to new and exciting adventures!

Abstract

Eutherian embryonic survival is dependent on the formation of a functional and properly vascularized placenta that allows efficient blood flow between the embryo and the placenta. While the molecular signals are only now being elucidated, it is clear that the steps of placental formation and vascularization are highly regulated. *Hoxa13*, a gene encoding a member of the highly conserved HOX family of transcription factors, is strongly expressed in the developing umbilical arteries and placenta endothelial cells. Mice lacking *Hoxa13* exhibit umbilical artery stenosis, a thinned placental labyrinth, and lethality at embryonic stages E12.5 to E14.5 due to cardiac defects. From its newly recognized expression pattern, we hypothesize that HOXA13 plays an essential role in patterning the umbilical arteries and chorioallantoic placenta. To test this hypothesis, we utilized detailed histological analysis, *in situ* hybridization, and microarray analysis. Using placental and vascular markers, we have shown that the vascular labyrinth layer of the mutant placenta is greatly reduced in size with a smaller and less branched vascular tree. While unaffected placentas contain a highly ordered vascular network that becomes more compact and branched with maturation, the mutant placentas are deficient due to less structure and vascularization. Then, we utilized Affymetrix microarray technology to examine the effect of loss of *Hoxa13* function on placental gene expression. Several interesting candidate genes were identified, including genes involved in vasculogenesis and cell adhesion. Furthermore, we performed *in situ* hybridization, immunohistochemistry, and quantitative RT-PCR to confirm the

results of the microarray analysis. To identify direct transcriptional targets of HOXA13, the candidate gene promoters were evaluated by chromatin immunoprecipitation, luciferase assays, mobility shift assays, and fluorescence anisotropy. From this analysis, we concluded that HOXA13 directly activates *Tie2* and *Foxf1*, important molecules for proper vascularization and embryonic development. Overall, our study reveals an important role for *Hoxa13* in patterning the placental vasculature. Consequently, the study of *Hoxa13* will provide insight into the molecular and genetic regulation of placental size and vascularization which are key factors in creating a functional placenta that supports embryonic health and survival.

Chapter One

Introduction

Introduction

The Placenta

1A. The placenta in folklore and medicine

Extensive mythology and lore has surrounded the birth, life, and death of humans, including many traditional beliefs regarding the placenta, the "flat cake" and highly-vascularized fetal organ that unites the developing fetal and maternal blood at the maternal uterine wall. Peoples following tribal or ancient traditions have attempted to explain the placentas physical and spiritual function using folklore and traditions. Some groups believed it held the spirit of the child or acted as a sibling, and so great care was taken to preserve or bury the placenta. Others considered it evil and wretched, casting ill-will to the child, and so the placenta would be burned or stabbed. (Long, 1963). Overall, the connection of the baby and placenta was understood and respected at a basic level, and so the placenta was praised or feared. Even today, while not the norm, some mothers choose to consume the placenta of their new baby, hoping this will alleviate such post-partum difficulties as depression, bleeding, and hormonal imbalances, or to simply offer nutrients and energy to the mother (Field, 1984). Others save the placenta for ritual ceremonies such as tree plantings, while most don't give it a second look and simply consider it biological waste after delivery. Past and present, medical and spiritual, the placenta has been recognized as a powerful and essential component to the health and well-being of human life.

The mammalian placenta is one of the first organs to arise during early fetal life, and this multi-functional organ is clearly imperative for proper fetal

development, health, and survival (Simmons and Cross, 2005). The placenta functionally substitutes for the lungs, kidneys, and the intestines because the maternal-fetal connection at the placenta interface allows for the exchange of respiratory gases, waste, and nutrients. In humans and mice, this point of exchange occurs between a minimal number of cell layers to allow for the closest interaction of maternal and fetal blood supplies, revealing how intimate a connection is made between the mother and her offspring (Faber and Thornburg, 1983).

Mammalian embryonic survival is dependent on the formation of a functional and properly vascularized placenta that allows efficient blood flow between the embryo and the placenta. This is highlighted by the fact that embryos with malformed placentas will die, even with no other physical defects (Rinkenberger and Werb, 2000). In human pregnancies, placenta defects are among the most common pregnancy complications during the second half of pregnancy (Craven and Ward, 1999). Furthermore, many serious placenta-related defects which commonly afflict human pregnancies and fetal health (preeclampsia, intrauterine growth restriction, chorioamnionitis) have no effective treatments to alleviate the physical problem (Krebs et al., 1996; Wang et al., 2003; Redline, 2006). Importantly, these pregnancy complications significantly increase the risk of fetal mortality, as well as having an affect on adult cardiovascular health (Cetin et al., 2004; Louey and Thornburg, 2005; Morley, 2006). Therefore, more research is needed to shed light on common pregnancy complications.

Fortunately, the placentas of mice and primates share a similar structure, genetic patterning, and vascular branching (Rossant and Cross, 2001). For example, the highly branched and vascular human chorionic villi are analogous to the vascular-dense labyrinth layer of the mouse placenta. Therefore, the mouse placenta is a suitable model for studying the genetics and development of the human placenta.

1B. Formation of a working placenta

In mouse and human, the steps of placenta formation and morphology are well characterized. Placenta initiation occurs early during development at E8.5 in the mouse, when the extra-embryonic chorion comes in contact with and fuses to with the allantois, the mesodermal outgrowth of the hindgut (Figure 1.1). The nascent umbilical vessels are formed by vasculogenesis within the allantois, and these vessels grow toward the chorion and form a branched network of vessels within the labyrinth (E10.5-E11) (Downs et al., 1998; Downs, 2002). During this process, trophoblast cells, which are derived from the trophectoderm surrounding the blastocyst inner cell mass, differentiate into diverse trophoblast cell types which have unique gene expression profiles and positions within the placenta (Adamson et al., 2002; Simmons and Cross, 2005).

By E11.5, the placenta has three defined layers: the proximal labyrinth layer consisting of the embryonic vascular network and surrounding syncytiotrophoblast cells, an outer trophoblast layer of giant cells into which the maternal spiral arteries intercalate to provide nutrient-rich blood to the labyrinth, and a middle barrier layer of spongiotrophoblast cells that defines the labyrinth

border (Rossant and Cross, 2001) (Figure 1.1). All layers are derived from fetal tissue, although only the mesenchyme and vasculature of the labyrinth contain fetal tissue derived from the inner cell mass and embryo proper (Hemberger and Cross, 2001).

Within the labyrinth, endothelial-lined fetal vessels branch to fill in the labyrinth. The endothelial cells (ECs) are adjacent to a syncytium of trophoblast cells comprised of three layers in the mouse (hemotrichorial) and one layer in the human placenta (hemomonochorial) (Figure 1.2). The fetal ECs, connective tissue, and trophoblasts encompass the hemochorial placenta interface or barrier, the location where fetal and maternal blood comes in close contact for the exchange of nutrients and waste (Faber and Thornburg 1983).

After its initiation, the labyrinth becomes denser with fetal and maternal blood spaces and the vasculature becomes more integrated by the angiogenic remodeling of the fetal vascular tree (Figure 1.3). This process leads to maximum surface area at the placental interface for maternal-fetal exchange, occuring between E11.5 and E14.5 of mouse placental maturation (Hemberger and Cross, 2001; Adamson et al., 2002). In mouse and human placentas, this is characterized by increased fetal blood vessels, compaction of the villous/ labyrinth, and overall growth of the placenta.

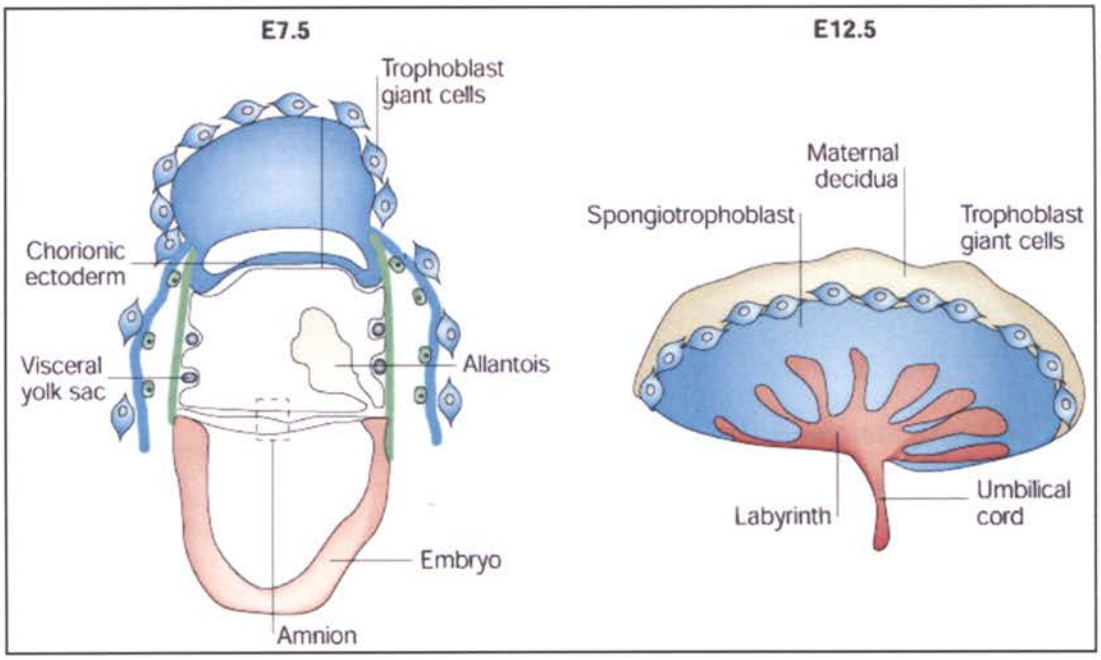

Figure 1.1: Mouse placental development

Post-implantation at E7.5, the allantoic bud grows into the extra-embryonic space towards the chorionic ectoderm and these tissues fuse at E8.5 to form the nascent chorio-allantoic placenta (left). By E10.5 in the mouse, the three define placenta layers are observed: the labyrinth, the spongiotrophoblast, and the decidua (right). Used with permission from McMillan (Rossant and Cross, 2001).

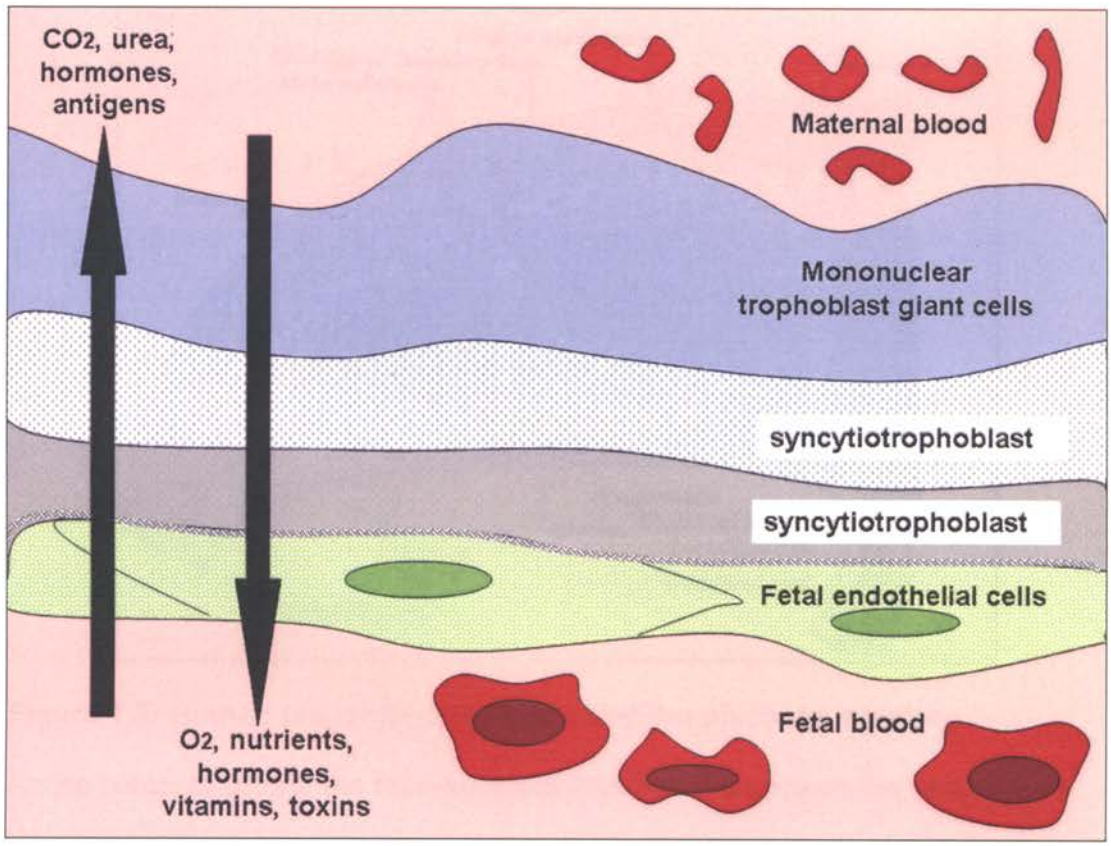

Figure 1.2: The maternal-fetal interface

The maternal and fetal blood supplies are separated by three trophoblast layers and the fetal endothelial cell layer. It is between these few cell layers that the exchange of nutrients, waste, and gases occurs.

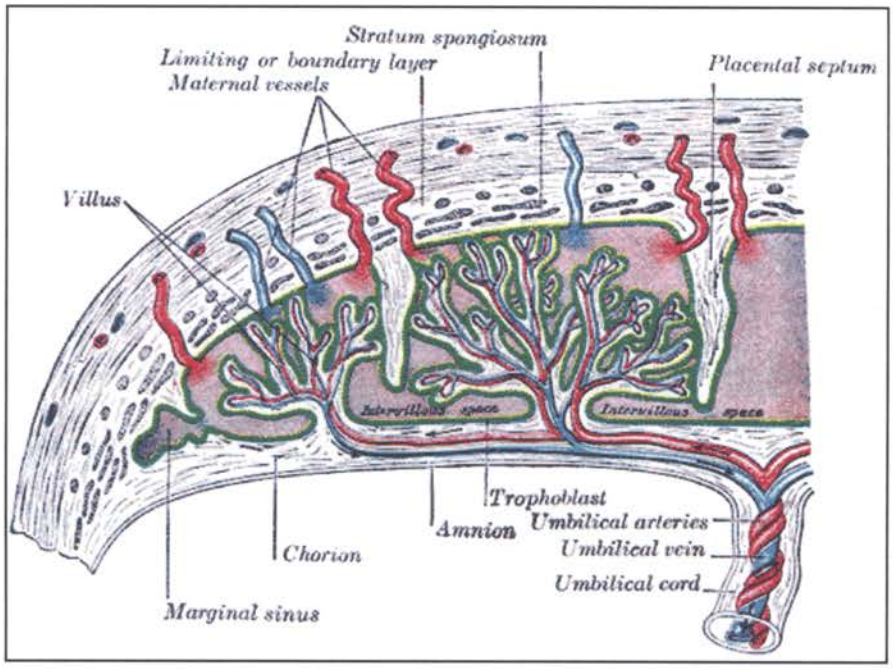

Figure 1.3: Human placental circulation and the placenta interface

As the placenta grows, the fetal-maternal interface expands as the vasculature branches and become more dense (left to right above). Similar to humans, the mouse labyrinth grows and become more vascularized from E11.5 to E14.5. Drawing by Henry Gray (1825–1861). Anatomy of the Human Body, 1918.

1C. Placental defects and essential placental genes

Since the mouse is a good model for understanding the human placenta, many studies and reviews have described essential genes for placental initation, chorioallantoic fusion, trophoblast differentiation, and labyrinth vascularization (reviewed by Rossant and Cross, 2001; Hemberger and Cross, 2001). Many genes have been linked to trophoblast differentiation, and deletion of these genes prevents proper labyrinth formation or vascularization. These include several genes encoding for transcription factors (*dlx3, esx1, arnt, tcfeb, gcm1, cdx2/4*), growth factors and their receptors (*pdgfb, hgf, met*), and cell cycle regulators (MAP kinases, *erk2*, *vhl*) (Rossant and Cross, 2001; van Nes et al., 2006). For example, null mutations of *vhl* (Gnarra et al., 1997), *gcm1* (Anson-Cartwright et al., 2000), *arnt* (Adelman et al., 2000), and *erk2* (Hatano et al., 2003) result in a small, avascular labyrinth. Interestingly, most of these genes are classified as trophoblast-expressed genes, and lethality and placental defects of many mutants can be rescued by tetraploid aggregation assays which confirm a functional requirement for these genes in trophoblast cells (Rossant and Cross, 2001). Within the mouse, a few genes are associated with the labyrinth vasculature during labyrinth initiation (*notch1, dll4, hey 1/2*), although neither expression patterns nor roles in labyrinth morphogenesis have been clearly revealed (reviewed by Cross et al., 2006).

While many genes play critical roles in chorio-allantoic formation and morphogenesis, the molecular regulation of placental size and vascularization is not fully understood. For example, while many studies have described the

importance of trophoblast differentiation in proper placental morphogenesis and structure, the critical role of the vasculature has not been fully addressed (Rinkenberger and Werb, 2000; Adamson et al., 2002). While the integration of fetal blood vessels is required for a working placenta and proper trophoblast interactions, mouse studies have not identified genes specifically required for definitive labyrinth vascularization. Furthermore, important questions remain concerning the molecular interactions between fetal ECs and trophoblasts (Cross et al., 2006). In this study, we identify an EC-specific gene required for complete vascular patterning and maintenance within the labyrinth.

The Vasculature

1D. Vascular endothelial cells

The blood vessels that feed all organs of the body consist of a tight arrangement of endothelial cells and a strong support structure of smooth muscle, pericytes, and extracellular matrix. Vascular ECs are specialized epithelial cells lining all blood vessels of the body. They are positioned between the blood and the vascular wall which correlates with their multiple functions such as regulating molecular signaling, transendothelial permeability, clotting, and response to physical factors such as pressure and shear stress, which are often accompanied by changes in EC gene expression (Malek and Izumo, 1995; Dye et al., 2004). Beyond their characteristic morphology, endothelial cells are molecularly distinct (Figure 1.4). For example, platelet endothelial cell adhesion molecule-1 (PECAM-1) and von Willebrand factor are typical EC-specific markers used for vascular identification (Baldwin et al., 1994). Furthermore, ECs display molecular heterogeneity depending on their location within the vascular tree. ECs have unique molecular signatures (i.e. matrix, surface molecules, and pathways) for artery/vein and capillary/vessel specification (Kumar et al., 1987). For example, arterial-specific (*neuropilin-1, ephrin-B2, gridlock, foxc1/c2,* notch receptors) and venous-specific (*epbB4, coup-tfII*) markers establish the molecularly distinct arterio-venous system (reviewed by Lamont and Childs, 2006).

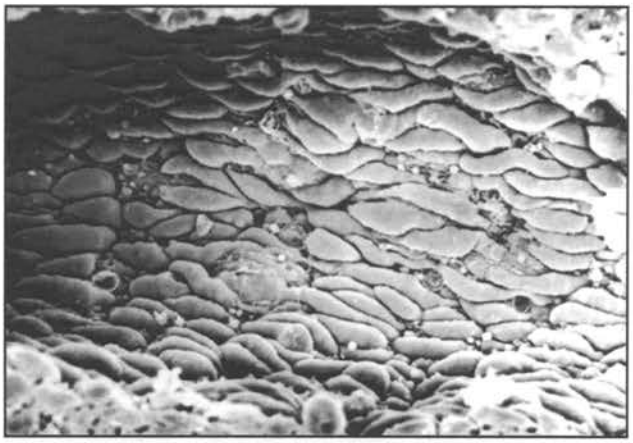

Figure 1.4: Vascular endothelial cell are specialized epithelia lining blood vessels - As shown by electron microscopy of a dissected mouse umbilical vessel, endothelial cells are tightly aligned and oriented in the direction of blood flow (horizontal flow in image).

1E. Mechanisms of vascular patterning

To support the health of a tissue, a highly integrated vascular system must supply cells with oxygen-rich blood and nutrients. The vascular system must be properly arranged into arteries and veins of varying sizes and must anastomose at the smallest of vascular structures, the vascular capillary bed. During embryonic development, vascularization arises by two distinct mechanisms, vasculogenesis and angiogenesis, which are molecularly regulated by multiple cues such as hypoxia and vascular-specific growth factors (Beck and D'Amore, 1997). The mechanisms of vasculogenesis and angiogenesis work together to create and refine the vascular tree.

Vasculogenesis

During early embryonic development, vascular initiation, differentiation, and primary vascular plexus formation occur by a mechanism called vasculogenesis. While the exact mechanism is controversial, the initiation of vasculogenesis seems to occur by the differentiation of common blood and EC progenitors called hemangioblasts from mesoderm and their alignment to form primary vascular blood islands. In this process, the inner hemangioblasts differentiate into blood cells progenitors, while the outer angioblast progenitors differentiate into endothelial cells that encircle the emerging blood cells (reviewed by Poole et al., 2001; Ingram et al., 2005). As this process proceeds, blood islands fuse to create tubes and finally a primary vascular plexus, a web of primary vessels (Figure 1.5). Vasculogenesis occurs due to initiation growth signals such as VEGF from the surrounding tissue, which activates the associated receptors Flk1 and Flt1 on the angioblasts (Poole et al., 2001). Development of cardiac endocardium and the major blood vessels (including the umbilical vessels) occur by vasculogenesis (Downs et al., 1998).

While this mechanism effectively initiates blood vessel formation, the primary plexus must be remodeled and pruned by angiogenesis to create the hierarchical vascular tree. Soon after vasculogenesis commences, and before it is even completed, remodeling of the vasculature takes place.

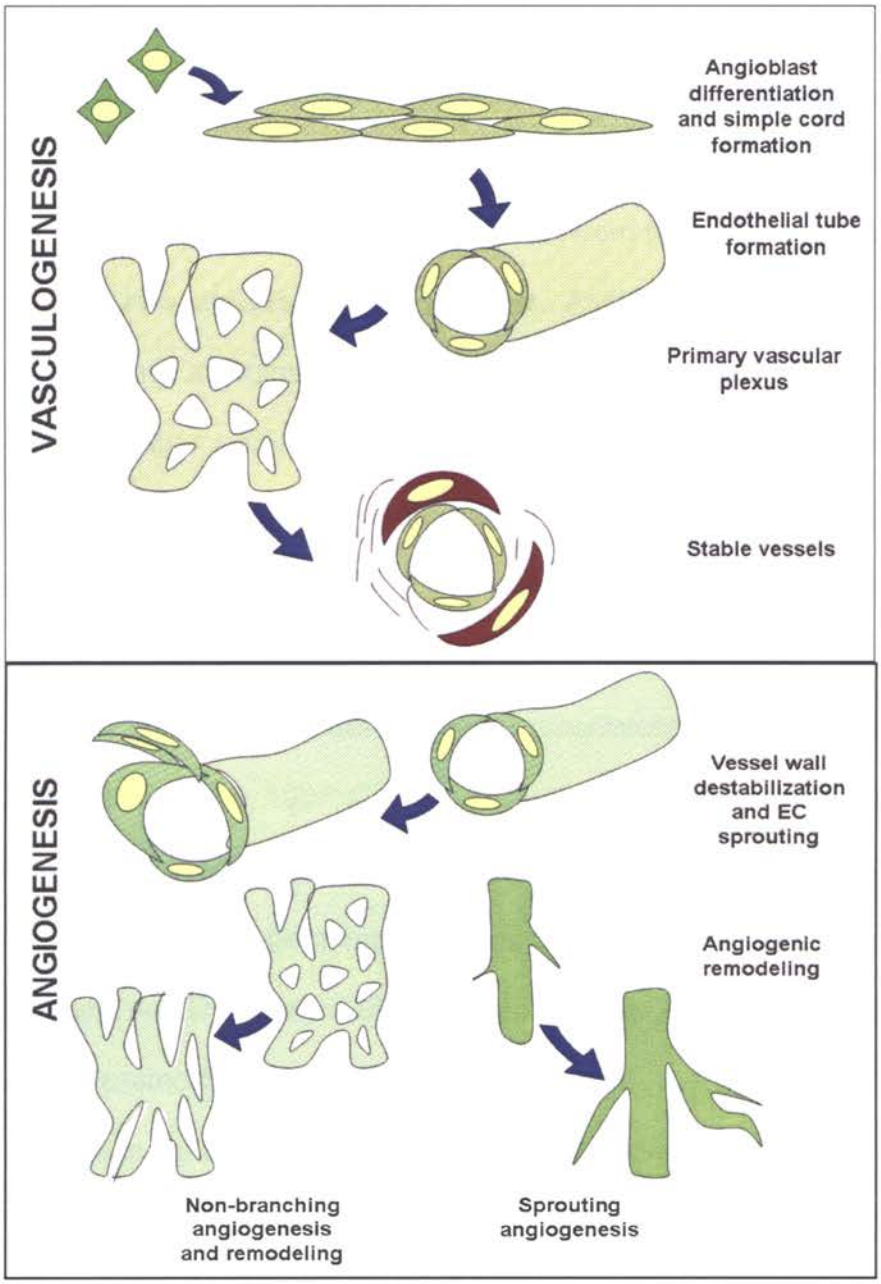

Figure 1.5: Blood vessel are shaped by vasculogenesis and angiogenesis

Angioblast differentiation follows several steps: simple cord and tube formation and establishment of the primary vascular plexus. Next, the primitive vasculature is remodeled by angiogenesis. ECs lining the vessels are activated: they alter their ECM and become motile to sprout or rearrange the vascular structure.

Angiogenesis

Angiogenesis is the remodeling of the primary vasculature into a more complex, functional, and integrated vascular network. Importantly, the efficient hierarchical structure of the vascular tree, from tiny capillary beds to large elastic vessels, is established by angiogenesis. Angiogenesis ensures that every part of the body has an intimate connection to the vasculature. For example, the vascularization of the brain, kidney, placenta and the coronary tree occur by angiogenesis. (Reviewed by Beck and D'Amore, 1997; Folkman, 2006).

Angiogenesis occurs by several physical mechanisms including sprouting of new vessels to make new branch points, remodeling and pruning of existing vascular branches, and non-sprouting intussusception of vessels (Figure 1.5, Figure 1.6) (Risau, 1997; Charnock-Jones et al., 2004). To initiate angiogenesis, ECs become "activated" which includes degradation of the underlying matrix, increased vascular permeability, increased proliferation, and migration of the ECs (Darland and D'Amore, 1999; Yancopoulos et al., 2000). Angiogenic activation of ECs promotes cell proliferation to expand the vasculature (such as in sprouting angiogenesis) and rearrangement and movement of existing ECs to increase vascular complexity and structure.

Intussusceptive angiogenesis (IA)

One angiogenic mechanism that is often overlooked is intussusceptive angiogenesis (IA). IA creates new vessels by the splitting of an established vessel lengthwise into two distinct vessels, thereby increasing vessel numbers and density without an increase in ECs (Figure 1.6). Its importance has been

recognized in the vascularization of the placenta, lung, kidney, ovary, coronary vessels, and in cancerous tumors (Ratajska et al., 2003; Charnock-Jones et al., 2004; Ribatti et al., 2005; Makanya et al., 2005; Macchiarelli et al., 2006). IA occurs in several steps that can be visualized by electron microscopy, vascular casts, and live imaging of chick chorioallantoic membrane (Djonov et al. 2000). First, ECs from opposite sides of the vessel wall begin to protrude and extend into the vessel lumen. Next, the ECs make contact and a thin cytoplasmic bridge creates a "trans-capillary pillar" dividing the vessels (Figure 1.6) (Burri et al., 2004). IA has several different outcomes depending on the location of the pillars and the type of vessels being remodeled. For example, IA might split existing capillaries to expand the capillary bed density, IA can occur repeatedly to create and add to the distal capillary tree, or it might occur at small vessel bifurcations leading to vessel pruning (Djonov et al., 2002; Burri et al., 2004).

Due to the relatively recent recognition of IA as a mechanism of angiogenesis, we are just beginning to understand the molecular and physiological signals regulating IA. Vascular signaling molecules such as Tie2/Ang and PDGFB/PDGFβR are implicated in regulating IA in the placenta and other organs (Patan, 1998; Bjarnegard et al., 2004). Both signaling pathways are important for pericyte recruitment and matrix remodeling during EC activation, and knocking out these pathways causes intussusceptive angiogenic defects (see section below). Overall, much more work is required to parse out the molecular signals governing IA.

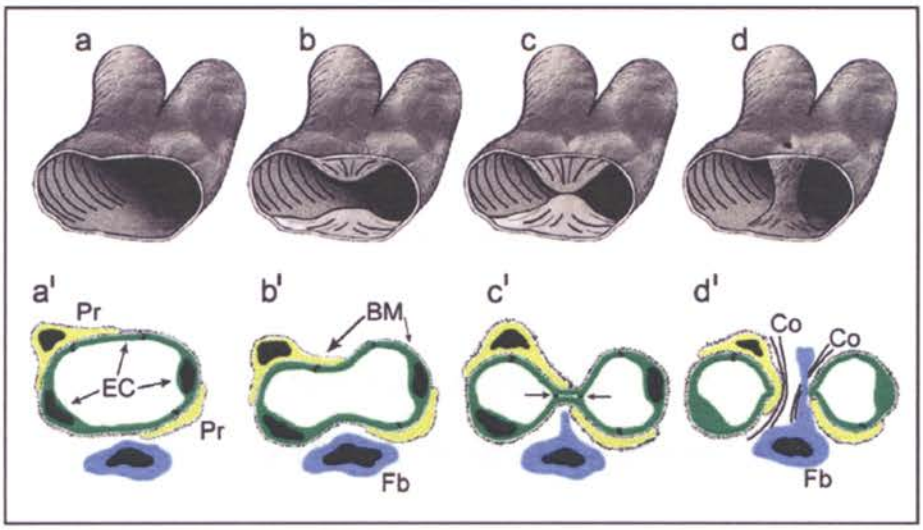

Figure 1.6: Intussusceptive angiogenesis (IA) is a mechanism for vessel remodeling - Intussusceptive angiogenesis occurs when endothelial cells from opposites sides of a vessel grown inward and meet (b-c), creating a trans-capillary pillar (b) into which support cells (pericytes, Pr; fibroblasts, Fb) and extracellular matrix molecules can invade (d). In this way, new smaller vessels are created from large ones, thus effectively increasing the complexity of the vascular bed. Used with permission from Wiley Publishing (Burri et al., 2004).

1F. Molecular mechanisms of vascularization in the body and placenta

Key molecular signals and growth factors regulate vasculogenesis and angiogenesis, and the molecular characterization of these vascular factors is supported by functional studies, expression analysis, and mouse models (Beck and D'Amore, 1997; Yancopoulos et al., 2000). Focusing on the placenta, vasculogenesis and angiogenesis are tightly regulated by the expression of locally acting factors such as vascular endothelial growth factors (VEGFs) and

their cellular receptors Flt1, Flk1, and Neuropilin-1, and angiopoietin growth factors 1 and 2 and their associated EC-specific receptor TIE2. Other vascular markers are noteworthy (platelet-derived growth factor, fibroblast growth factor, transforming growth factor-β, HGF, platelet-derived growth factor), but the following discussion will focus on VEGF and TIE2 systems and their known role in the embryo and the placenta (reviewed by Ahmed et al., 2000; Kaufmann et al., 2004; Demir et al., 2005; Folkman, 2006) (Figure 1.7).

VEGF

VEGF was first identified as a vascular-specific mitogen that promoted angiogenesis (Connolly et al., 1989; Gospodarowicz et al., 1989; Ferrara and Henzel, 1989). Mouse knockout studies have shown that deleting a single *vegf* allele causes severe vasculogenic defects in the heart, brain, yolk sac, and placenta, leading to early embryonic lethality (Carmeliet et al., 1996; Ferrara et al., 1996). There is a critical dose-dependent requirement for *vegf*, since homozygous null mice have severe vasculogenic defects and die during early development, while mice with a hypomorphic *vegf* allele survive and display fewer vascular defects (Carmeliet et al., 1996). Embryos deficient in the VEGF receptors *flt-1* and *flk-1* also show dramatic vasculogenic defects in the body and yolk sac and lethality by E8.5-E9.5 (Fong et al., 1995; Shalaby et al., 1995). These studies reveal the significant influence of VEGF and its receptors on regulating early embryonic vascularization that is critical for embryonic survival.

Consistent with its essential role in the vasculature of the embryo, VEGF is a key angiogenic factor in placental vascularization. Early trophoblast

differentiation is directly promoted by VEGF-expressing macrophages (Hofbauer cells), and VEGF-A is expressed later by trophoblasts and vascular smooth muscle while its receptors VEGFR-1, VEGFR-2, and Neuropilin-1 are localized to the angiogenic stem cells and labyrinth ECs (Clark et al., 1996; Zhou et al., 2002; Tsoi et al., 2002; Demir et al., 2004) (Figure 1.7). Furthermore, levels of VEGF decrease as the placenta becomes functional and oxygenated through increased vascular density, while high levels of placental VEGF and placenta growth factor (PlGF) are associated with aberrant angiogenesis and preeclampsia (reviewed by Ahmed et al., 2000). Clearly, the placenta is sensitive to changes in powerful vasculogenic signals such as VEGF.

Tie2 and angiopoietins

Similar to the VEGF effect, the vascular-specific growth factors angiopoietins (ANG1 and ANG2) and their EC-specific receptor TIE2 (i.e. TEK), play essential roles in angiogenic remodeling and EC integrity. Their expression patterns and mouse knockout models confirm their importance in angiogenesis in the body and within the placenta. *Tie2* is highly expressed on ECs involved in active angiogenesis (Sato et al., 1993; Dumont et al., 1995). TIE2 phosphorylation and activation by ANG1 leads to vessel stabilization and maintenance. Conversely, ANG2 functions as a TIE2 antagonist by binding TIE2 and inhibiting ANG1 binding and activating TIE2, leading to vessel destabilization and angiogenic remodeling (Maisonpierre et al., 1997; Gale and Yancopoulous, 1999). Functional studies show that ANG1 promotes network stabilization, cell survival and vascular sprouting in conjunction with VEGF (Koblizek et al., 1998;

Papapetropoulos et al., 1999; Ward and Dumont, 2002). Consequently, *Ang2* is expressed in tissues involved in active angiogenic remodeling such as the ovary, uterus, and placenta, while *Ang1* is expressed in more stable vasculature like the intestines, skeletal muscle, and myocardium (Maisonpierre et al., 1997). However, questions still remain concerning the exact mechanism of TIE2-ANG2 signaling. While ANG2 typically acts as a TIE2 antagonist, higher concentrations or longer exposures of ANG2 lead to TIE2 activation and vascular sprouting (Kim et al., 2000; Teichert-Kuliszewska et al., 2001). Overall, the TIE2-ANG signaling pathway in ECs is physiologically complex and crucial for angiogenic remodeling.

Compared to mouse knockouts of VEGF and its receptors, *Tie2* and *Ang1* knockout mice die later on during development from angiogenic defects. Mice lacking *Tie2* or *Ang1* die at mid- to late-gestation (E13.5-E14.5, Puri et al., 1995; E18.5-birth, Sato et al., 1995; E12.5 for *Ang1*, Suri et al., 1996) from defects in angiogenic remodeling and EC integrity such as edema, microvascular hemorrhaging, and loss of vascular maintenance. The blood vessels of these mutants display defective intussusceptive angiogenesis: large sinusoidal vessels with incomplete lumen divisions, blind end vascular sprouts, round EC that do not spread out, and loss of EC-matrix interactions (Patan, 1998). Similarly, overexpression of *Ang2* produces the vascular remodeling and cardiac defects seen in the *Ang1* and *Tie2* knockout mice, confirming ANG2 as a TIE2 antagonist (Maisonpierre et al., 1997).

In humans and mice, the *Tie2-Ang* angiogenic pathway plays a significant role in placental vascularization. *TIE2* is expressed in the ECs of human

placental villi, and the levels of activated TIE2 remain constant during early pregnancy (Vuorela et al., 1997; Zhang et al., 2001; Kayisli et al., 2005). *Ang2, Ang1*, and *VEGF* are expressed at similar time points as *Tie2* within the syncytiotrophoblasts and around fetal blood vessels (Zhang et al., 2001; Geva et al., 2002). Interestingly, in first trimester placentas, *ANG2* expression levels are 400 times higher than *ANG1* and 100 times higher than *VEGF-A*, and this trend holds throughout gestation (Geva et al., 2002). While *ANG1* is negligibly affected by changes in growth conditions, *ANG2* expression is sensitive to changes in oxygen levels since it is elevated in hypoxic conditions (villous culture) and reduced in human placentas affected by preeclampsia (Zhang et al., 2001). Overexpression of *Ang2* within the placenta leads to dilated vessels, edema, ECM remodeling, and a larger placenta, confirming *Ang2* function in angiogenic remodeling of the placenta (Geva et al., 2005). Likewise, loss of *Tie2* causes defects in IA, the primary angiogenic remodeling mechanism for placental vascular complexity and density (Patan, 1998). Overall, in the placenta ANG2 is the primary regulator for TIE2 signaling in labyrinth vascularization.

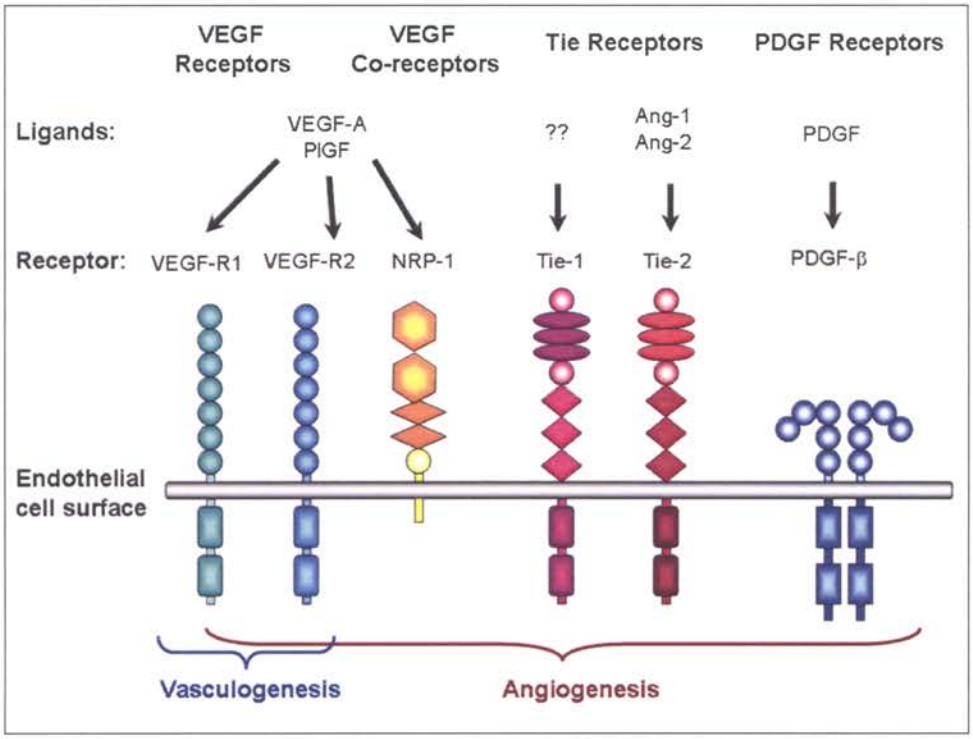

Figure 1.7: Vascular receptors and signals that regulate vasculogenesis and angiogenesis – Receptors on the vascular cell surface can be activated by their ligands to promote and regulate initial vasculogenesis and secondary remodeling by angiogenesis. VEGF binds to VEGF-R1/R2 and NRP1, Angiopoietins bind to Tie2, and PDGF binds to its receptor PDGF-β. All of these vascular markers are expressed in the placenta vasculature.

Hox Genes

1G. An introduction to *Hox* genes

Hox genes were first discovered in the fruit fly, *Drosophila melanogaster,* as essential genes for body patterning and morphogenesis (Lewis, 1978; McGinnis et al., 1984b; Manley and Levine, 1985). A characteristic of *Hox* genes is their ability to control homeotic transformations, the change of one body part into another. Classical experiments in *Drosophila* depict the homeotic transformation capabilities of *Hox* genes. For example, by the deletion or misexpression of *Hox* genes in *Drosophila*, whole body parts can be transformed into other distinct body parts, such as haltere to wings or mouth pieces to legs (reviewed by Graba et al., 1997; Hombria and Lovegrove, 2003). Mouse studies performed in our lab reveal that loss of HOXA13 function alters the cellular morphology of the urethral plate epithelium in the external genitalia and the epithelia of the bladder (Morgan et al., 2003; unpublished data, Stadler lab).

Hox genes are structurally and functionally conserved among many diverse species (Krumlauf, 1994; McGinnis et al., 1984a). The human and mouse genomes contain 39 *Hox* genes which are arranged in clusters on four different chromosomes (Figure 1.8). *Hox* genes contain a homeobox motif that encodes the 60 amino acid homeodomain, the DNA-binding domain of the transcription factor. The protein homeodomain confers DNA binding specificity through its direct interaction with a core DNA binding site and by its interactions with other proteins (Mann and Affolter, 1998). These interactions allow HOX transcription factors to effectively activate or repress target gene transcription.

Hox genes follow rules of colinearity which define their spatial and temporal expression based on their linear order within the Hox cluster (Lewis 1978). Genes positioned more 3′ within the Hox cluster are expressed in the anterior body and genes positioned at the 5′ end of the cluster are expressed more posteriorly (Figure 1.8). In general, 3′ genes are expressed at earlier developmental stages than 5′ genes. For example, *hoxa13* is positioned most 5′ on the mouse chromosome 6, and therefore its expression is restricted to the posterior urogenital tissue and the distal tips of the limbs during mid- to late-

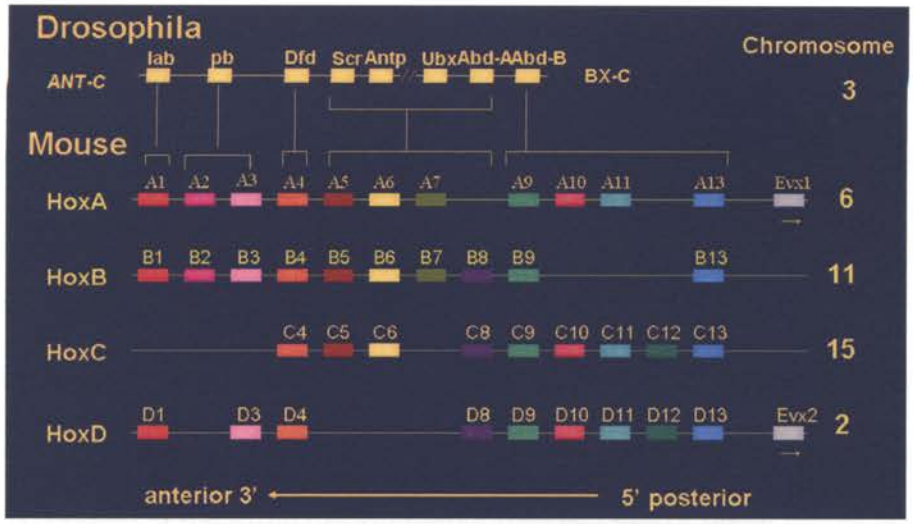

Figure 1.8: The Hox gene clusters

The mouse genome contains homologous genes that reside on four different chromosomes, an evolutionary product of gene duplication. Paralogous genes are denoted by the same color bars on different chromosomes. Hox genes follow the rule of colinearity: genes that lie more 3′ on the chromosome are expressed in the anterior tissues while 5′ genes are expressed in the posterior of the body. Figure reprinted with permission from the author (Scott et al., 2001).

gestation (Stadler et al., 2001). Alternatively, *hoxa1* and *hoxb1* are expressed in the developing brain and rhombomeres during early development (Rossel and Capecchi, 1999). In this way, Hox genes control the anterior-posterior axis of the developing body and the proximal-distal axis of the limb.

1H. *Hox* genes in the vasculature and placenta

Several *Hox* genes function in ECs and during angiogenesis while retaining functions in other tissues. *Hoxd3* and *hoxb3* promote angiogenesis by directly regulating expression of integrins and vascular factors (Boudreau et al., 1997; Myers et al., 2000), while *hoxa5* and *hoxd10* inhibit angiogenesis by down-regulating pro-angiogenic genes and promoting quiescence (Myers et al., 2002; Rhoads et al., 2005). Furthermore, these genes have separate and defined roles in other tissues such as the adult kidney and spinal cord, and in embryonic development of the hindbrain, spinal cord, limb, and gastrointestinal tract, revealing their pleiotropic nature.

Likewise, expression of several *hox* genes has been noted in the placental trophoblasts and pregnant uterus. *Hoxa9, hoxa10, hoxa11, hoxb6,* and *hoxc6* are all expressed in maternal decidual/endometrial cells or distal placental trophoblasts, and *hoxa10* mutant mice have progesterone resistance and premature labor (Gao et al., 2002; Amesse et al., 2003; Sarno et al., 2006). Furthermore, *hoxa11, hoxb6,* and *hoxc6* are also expressed in abnormal molar trophoblast growths and in the BeWo choriocarcinoma cells (Zhang et al., 2002; Amesse et al., 2003). Finally, screens to find homeobox genes within the placenta identified *gax, msx2*, and *dlx4* (Quinn et al., 1997). While no other *hox*

gene has been described in the placental vasculature besides *Hoxa13*, it is clear that many *hox* genes have multiple roles in diverse tissues throughout development.

1I. *Hoxa13* in the mouse and human

HOXA13, a member of the highly conserved HOX family of transcription factors, is a transcriptional regulator that is essential during embryonic development. *Hoxa13* expression was first characterized in the murine limb (Dolle and Duboule, 1989; Haack and Gruss, 1993), and functional studies of HOXA13 have primarily focused on the limb mesenchyme where it plays an important role in patterning the digits of the forelimb and hindlimb (Fromental-Ramain et al., 1996, Post et al., 2000). Specifically, precise expression of *Hoxa13* is required for its proper function in promoting cartilage condensation and differentiation, cell-cell adhesion, and interdigital apoptosis (Fromental-Ramain et al., 1996; Stadler et al., 2001). Consequently, *Hoxa13* mutations or deletion leads to hypodactyly and fusion of digits (Stadler et al., 2001; Goodman and Scambler, 2001).

Hoxa13 is also important for embryonic patterning of the male and female genitourinary tract and external genitalia, and loss of *Hoxa13* causes multiple patterning defects of the urogenital sinus, bladder, and ureters, and the adjacent rectum and umbilical arteries (Warot et al., 1997; Morgan et al., 2004). Supporting the mouse phenotypes, mutations in human *Hoxa13* lead to Hand-Foot-Genital syndrome (HFG) which presents with digit and genital

malformations such as hypospadias in males and uterus and ureter-bladder integration defects in females (Mortlock and Innis, 1997; Warot et al., 1997).

Hoxa13 knockout mouse models have been effective tools to study developmental patterning (Fromental-Ramain et al., 1996). Our characterizations of *Hoxa13* in the limb, UG, placenta, and umbilical cord have utilized a $Hoxa13^{GFP}$ knockout mouse model (Stadler et al., 2001; Morgan et al., 2003; Knosp et al., 2004) (Figure 1.9). In this unique mouse model, the portion of *Hoxa13* exon 2 encoding for the homeodomain's third alpha-helix is replaced with a cassette coding for green fluorescent protein, GFP (construct published in Stadler et al., 2001). This creates a mutant allele that effectively deletes functional HOXA13 and marks the *Hoxa13*-expressing cells with GFP, a visible fluorescent tag that is retained in the nucleus (Stadler et al., 2001). Importantly, the $Hoxa13^{GFP}$ mutant mouse phenocopies many of the urogenital and limb defects seen in humans affected by *HOXA13* mutations that lead to HFG syndrome.

Functional studies of the HOXA13 transcription factor reveal that it binds to unique DNA binding sites *in vivo* and *in vitro*. *In vitro* screens for HOXA13 binding sites show that it binds to TA-rich sequences, most preferentially the site AAATAAAAA (Knosp et al., 2006). By scanning candidate gene promoters *in silico*, the HOXA13 preferred binding site can be found and is often conserved among species. By focusing on these sites for further promoter analyses (chromatin immunoprecipitation, luciferase assays, etc.), we can determine whether HOXA13 binds to these sites *in vivo* (Knosp et al., 2006). For example,

HOXA13 binds to the *Enpp2* promoter *in vitro*, and cells overexpressing HOXA13 show activation of *Enpp2* (Innis et al., 2005; McCabe and Innis, 2006). In limb tissue, HOXA13 represses *Sostdc1* and activates *BMP2* and *BMP7* (shown by ChIP and luciferase assays) leading to misexpression of BMP target genes (Knosp et al., 2004; Knosp et al., 2006). Therefore, this is an effective strategy for the discovery of HOXA13 targets.

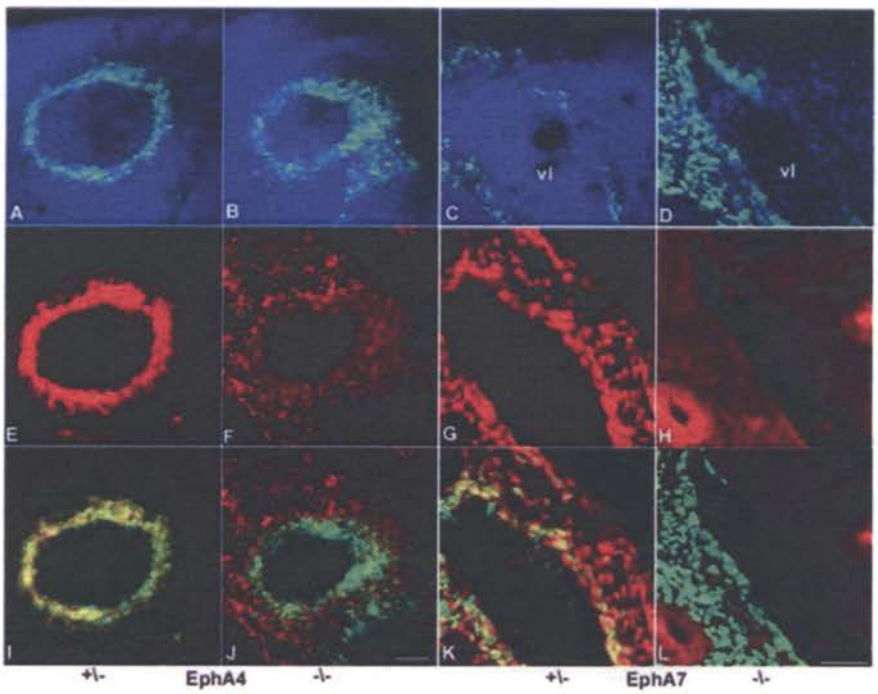

Figure 1.9: HOXA13 is required for proper EphA4 and EphA7 expression in the umbilical arteries

Both EphA4 and Epha7 co-localize with *Hoxa13*^{GFP} in the umbilical arteries of *Hoxa13* heterozygous (A, E, I, C, G, K) and *Hoxa13* mutant mice (B, F, J, D, H, L). Figure reprinted with permission from the author (Stadler et al., 2001).

1J. *Hoxa13* and placenta vascularization

The *Hoxa13* knockout mouse is the only *Hox* gene knockout that leads to embryonic lethality, occuring around E12.5 to E14.5, signifying that *Hoxa13* is essential for early development and survival. However, the cause of lethality is unknown since the umbilical artery stenosis phenotype is insufficient to cause mid-gestation lethality. While previous studies have reported *Hoxa13* expression in the chorioallantoic placenta and umbilical arteries (Figure 1.9), neither placental expression analysis nor extra-embryonic defects have been well established (Warot et al., 1997; Stadler et al., 2001). Furthermore, no functional studies of HOXA13 in the UA or placenta have been reported. However, since the placenta and its distinctive vascular network are required for mammalian embryonic survival (including proper heart development), we hoped to reveal a role of *Hoxa13* in the placenta. Therefore, my research began from this starting point in hopes that more could be revealed about HOXA13 in these tissues.

During human pregnancies, placental defects are among the most common pregnancy complications in the second and third trimesters (Craven and Ward, 1999). Therefore, the study of placental development has strong clinical significance since placental defects (including preeclampsia and intrauterine growth restriction) are a common complication to an otherwise healthy pregnancy. Furthermore, a healthy and well-functioning placenta is critical for the proper development of the heart, survival and growth of fetus, and future adult cardiovascular health. (Hemberger and Cross, 2001; Cetin et al., 2004; Louey and Thornburg, 2005; Morley, 2006; Redline, 2006).

Chapter Two

Hypothesis and Specific Aims

Hypothesis and Specific Aims

Consistent with the newly recognized *Hoxa13* expression pattern, we propose that the transcription factor HOXA13 plays an essential role in placental vascular development and maintenance by regulating key vascular molecules necessary for angiogenesis. Consequently, loss of *Hoxa13* leads to a dramatically altered phenotype, visible in both the tissues and cells where it is required, and this correlates with changes in vascular-specific molecular markers. Furthermore, we propose that perturbations in the placenta cause secondary defects in the heart, and the concomitant cardiovascular and placental defects cause the mid-gestation lethality of $Hoxa13^{GFP}$ mutant mice. To test these hypotheses, the following specific aims were addressed.

Specific Aim One: Characterize the expression pattern of *Hoxa13* in the formation of the chorioallantoic placenta and vasculature

Specific Aim Two: Analyze the placental and cardiovascular phenotypes of *Hoxa13*-deficient mice using detailed histological analyses and molecular markers

Specific Aim Three: Identify changes in the gene expression profile due to *Hoxa13* insufficiency in affected tissues

To demonstrate the comprehensive experimental analyses I performed in to address these aims, each specific aim is addressed within individual chapters of my thesis.

Chapter Three

Novel expression of *Hoxa13* in the developing placental vasculature

Specific Aim 1: Characterize the expression pattern of Hoxa13 *in the formation of the chorioallantoic placenta and vasculature*

3A. Introduction

HOXA13 is a transcription factor that is important for the development and patterning of the embryonic limb, urogenital (UG) system, and the umbilical arteries (UA) (Stadler et al., 2001). *Hoxa13* expression supports the *Hox* gene rule of colinearity: since the *Hoxa13* gene is located in the 5′ end of the *HoxA* cluster on mouse chromosome 6, it is appropriately expressed in the posterior of the embryo (urogenital system and umbilical arteries) and in the developing limbs. As a transcription factor, HOXA13 functions cell-autonomously, and therefore the loss of *Hoxa13* leads to phenotypic abnormalities within the tissues where it is expressed.

While previous studies recognized *Hoxa13* expression in the UA and placenta, we sought to determine the exact spatio-temporal expression of *Hoxa13* during mouse cardiovascular and placental development (Warot et al., 1997; Stadler et al., 2001). From this primary characterization, we hoped to shed light on additional defects caused by the loss of *Hoxa13*. We hypothesized that *Hoxa13*-associated defects of the cardiovascular system and placenta would present as a phenotype that does not support life, thus explaining the mid-gestational lethality observed in *Hoxa13* mutant mice.

3B. *Hoxa13* is expressed in discrete regions of the developing placenta and umbilical arteries

Utilizing the *Hoxa13*^{GFP} mutant allele as a fluorescent marker for gene expression (Stadler et al., 2001), we explored the *Hoxa13* expression pattern from E7.75 to E14.5 using immunohistochemistry (IHC) and fluorescence confocal microscopy. *Hoxa13* expression begins at E7.75 in the allantoic bud, a mesodermal outgrowth from the posterior hindgut (Figure 3.1-A), and expression increases within the growing allantois through fusion with the distal chorion (3.1-B-D). This stage marks the initation of the chorio-allantoic placenta. During placenta labyrinth initiation and vascularization (E10.5-E11.5), *Hoxa13* is strongly expressed in both the *Hoxa13* heterozygous and homozygous mutant labyrinths (Figure 3.1-E, Figure 3.2). To note, the timing of allantoic-chorion fusion is indistinguishable between wildtype, *Hoxa13* heterozygous, and homozygous mutant embryos, and the size of the labyrinth remains comparable at E10.5. However, at E11.0, differences between heterozygous and homozygous mutant tissues become noticeable. The mutant labyrinth layer becomes reduced in size and thickness compared to the heterozygous or wildtype labyrinths, as evident by the distal expansion of the PECAM-expressing, *Hoxa13*-positive vascular layer (Figure 3.2) and by the spongiotrophoblast marker *Tpbp* which defines the border of the embryonic labyrinth (Figure 4.2). Furthermore, *in situ* hybridization (ISH) using a *Hoxa13*-specific probe confirmed expression within the labyrinth region from E10.5 to E11.5 (Figure 3.2).

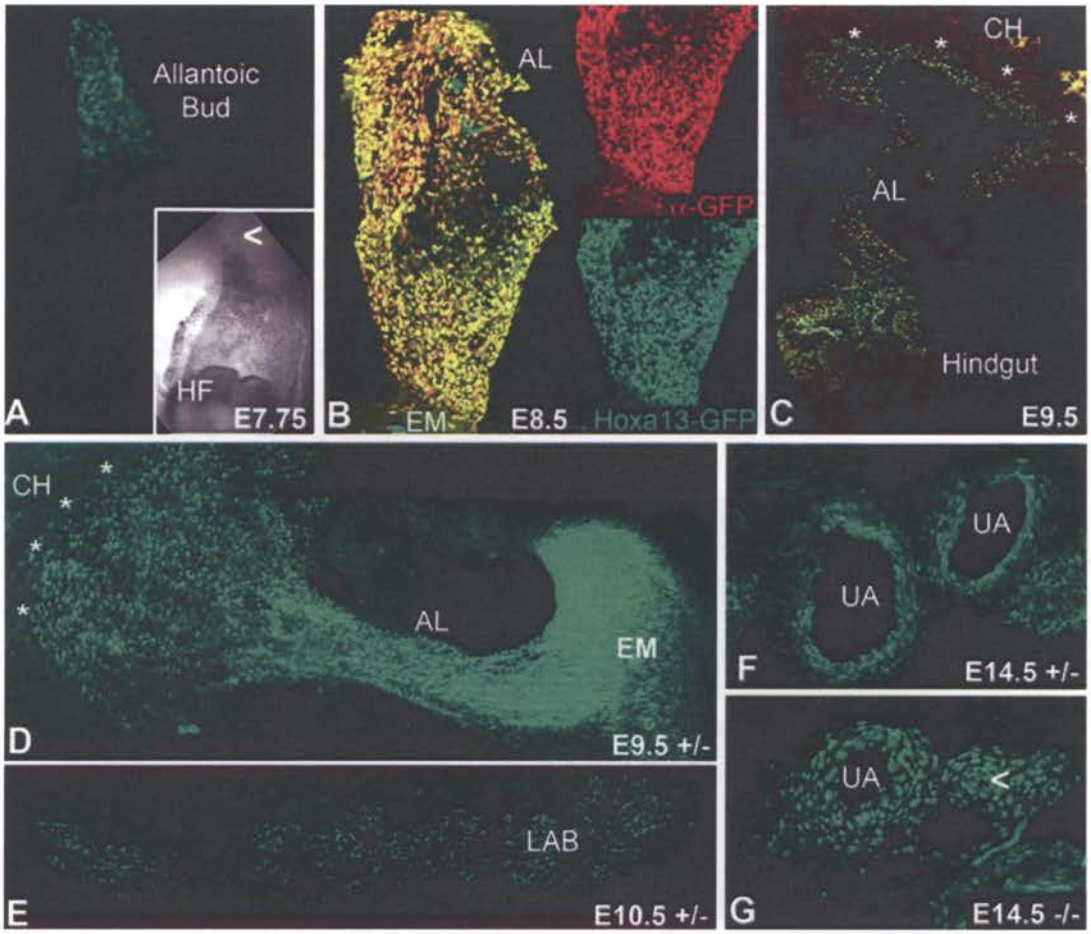

Figure 3.1: *Hoxa13* expression during placental initiation and maturation

As shown by the *Hoxa13*^{GFP} allele (green nuclei), *Hoxa13* is expressed in the pre-fusion allantois at stages E7.75 (**A**) and E8.5 (**B**), and in the branching chorioallantoic placenta from initial formation at E9.5 (**C-D**, asterisks identify the chorion-allantoic fusion point) through maturation to a vascularized tissue at E10.5 (**E**). To clarify and confirm the GFP marker, immunohistochemistry was performed using an anti-GFP antibody (B-C). *Hoxa13* is strongly expressed in the UA endothelium and smooth muscle layer (**F-G**). The arrowhead identifies the UA stenosis in the *Hoxa13* mutant (G). Chorion (CH), allantois (AL), labyrinth (LAB), embryo (EM), head fold (HF), umbilical arteries (UA).

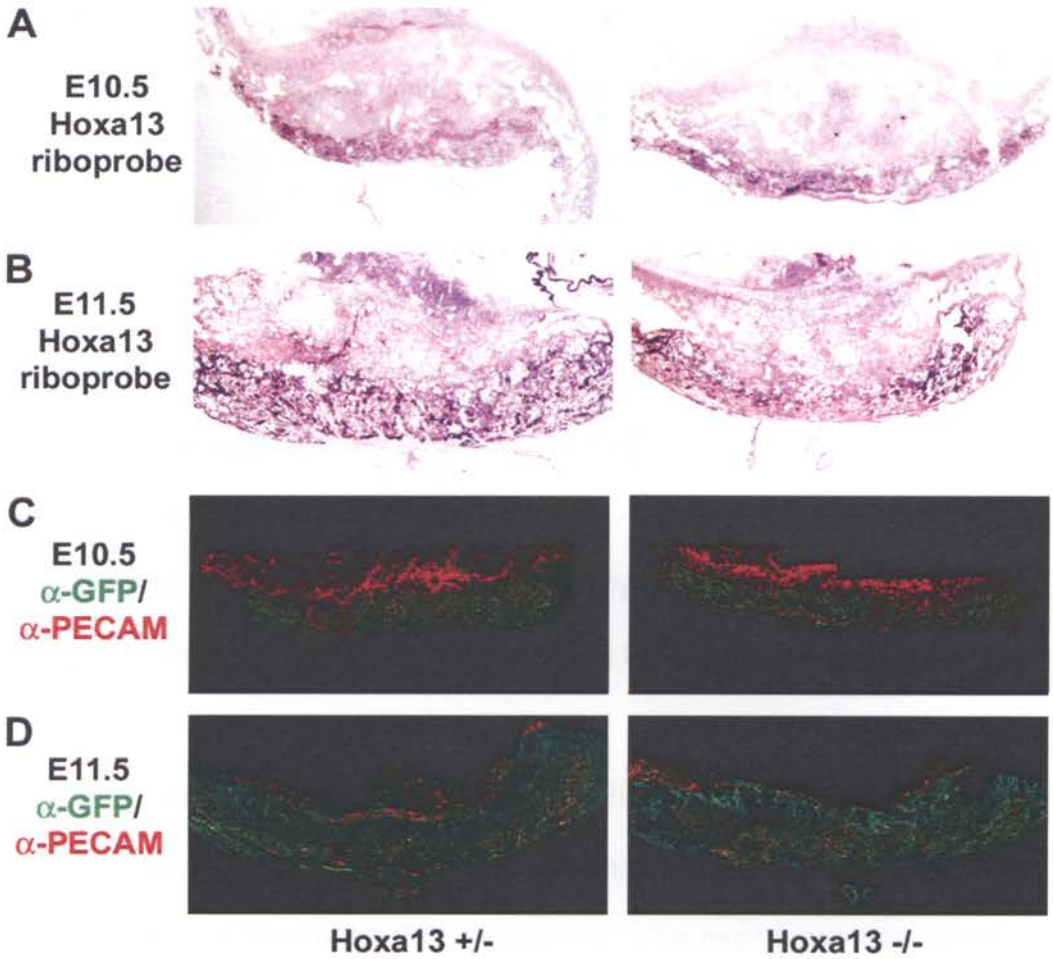

Figure 3.2: *Hoxa13* is expressed in the emerging placenta labyrinth

At E10.5 (A, C) and E11.5 (B, D), the expression of *Hoxa13* was localized to the placental labyrinth layer. *In situ* hybridization identifies *Hoxa13* transcription within the labyrinth at E10.5 (A) and E11.5 (B). Immunohistochemistry using antibodies against GFP and PECAM confirm the co-localization of HOXA13 and the labyrinth endothelial cells (C-D). To note, ISH studies of older placentas proved difficult due to increased background signal, but the IHC imaging at older ages was achieved with good results (Figures 3.3-3.4).

3C. *Hoxa13* is localized to the placental labyrinth endothelial cells

In the developing placental labyrinth, which cells express *Hoxa13*? To fully appreciate the precise tissue localization of HOXA13, immunohistochemistry using the EC-specific PECAM-1 antibody revealed that HOXA13 is localized to the ECs of the labyrinth vasculature, beginning at E10.5, and expression is maintained throughout placental maturation (Figure 3.2-3.3). Importantly, higher magnification images showed that HOXA13-GFP is restricted to the PECAM-1-positive ECs in the placental labyrinth (Figure 3.4). Furthermore, *Hoxa13* was not expressed in trophoblasts or the yolk sac by our analysis. The finding that *Hoxa13* is expressed within placental labyrinth ECs defines a previously unrecognized expression profile.

Additionally, *Hoxa13* was expressed in the umbilical arteries (UA), specifically within the EC layer and the surrounding supportive smooth muscle and mesenchyme (Figure 3.1 F-G, Figure 3.5). This expression was observed throughout the length of the UA, from the placenta to the embryonic body wall and through the internal organs to the trigone (Figure 3.5). While the UAs of heterozygous embryos displayed a smooth cellular morphology and large, well developed lumens (Figure 3.1F), there was stenosis of one of the two UAs in the *Hoxa13* mutant embryos and a persistently rounded cellular phenotype of the vessel wall (Figure 3.1G). We observed partial to full single UA stenosis in most mutant UAs by stage E13.5 to E14.5.

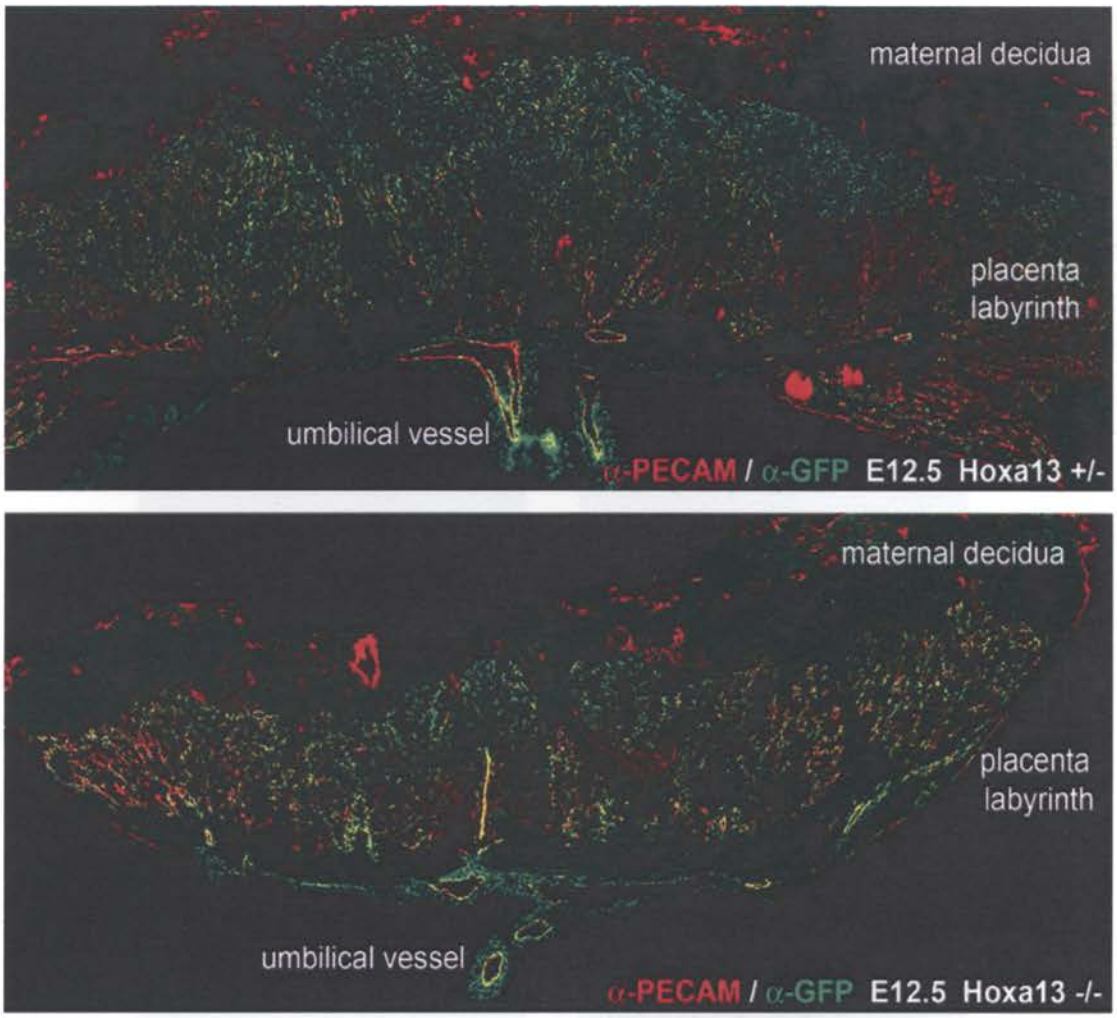

Figure 3.3: Expression of *Hoxa13*^{GFP} in placental labyrinth vasculature

Immunohistochemistry on placenta sections using antibodies to the EC-specific molecule PECAM (red) and to GFP (green) reveals HOXA13 expression within the labyrinth layer of the developing placenta. Shown at E12.5, there is colocalization in the larger and well developed *Hoxa13* heterozygous placentas (above) and in the smaller homozygous mutant placentas (below). Images were obtained by confocal microscopy at 20x magnification and compiled into a montage image of the full placenta.

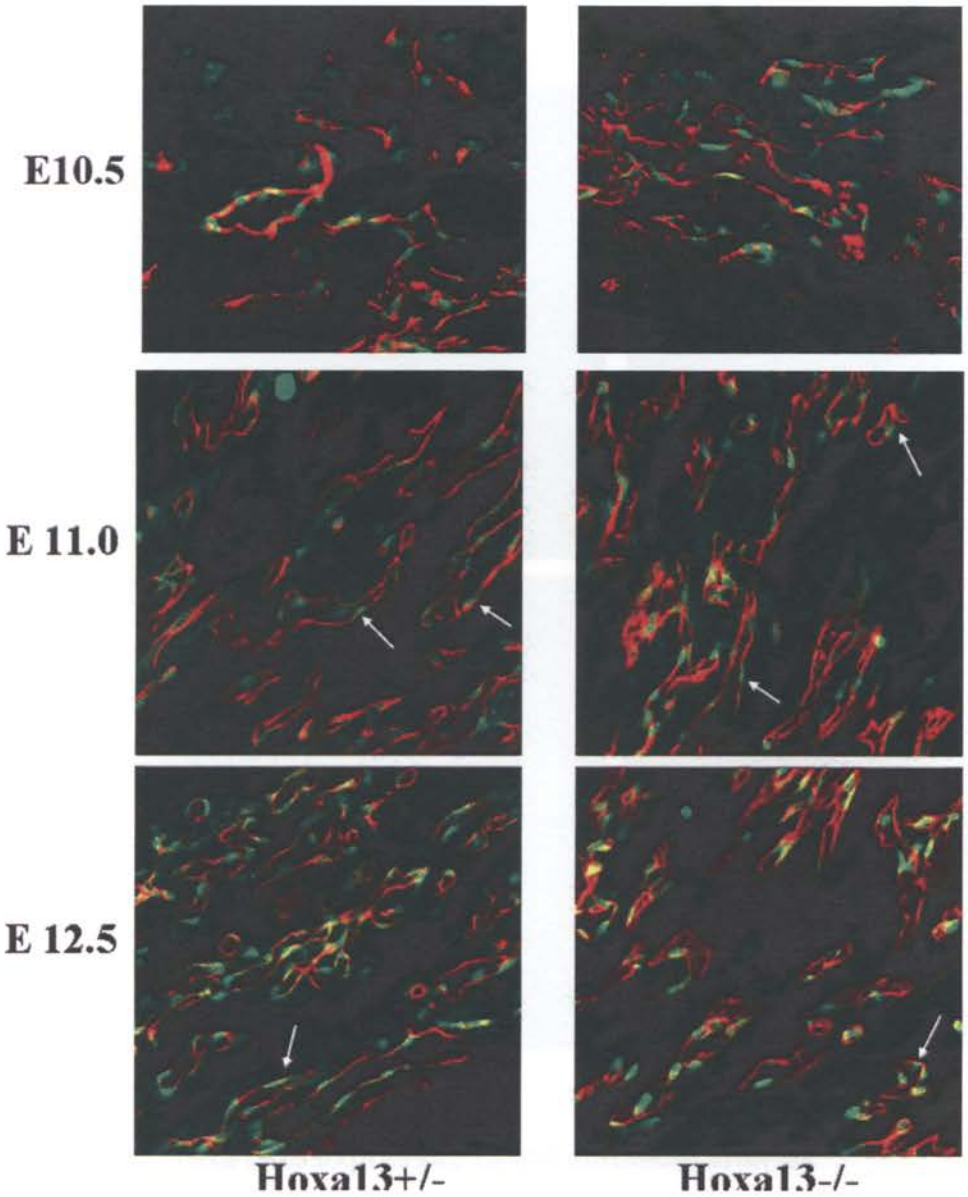

Figure 3.4: *Hoxa13* is expressed in placental endothelial cells

Higher magnification of the placental labyrinths show that GFP-positive nuclei (green) colocalize with the endothelial marker PECAM-1 (red), revealing that *Hoxa13* is specifically expressed in fetal placental ECs. Arrows denote areas of precise colocalization. This colocalization was observed in all ages studied, from E10.5 to E14.5. Images were obtained at 40x magnification.

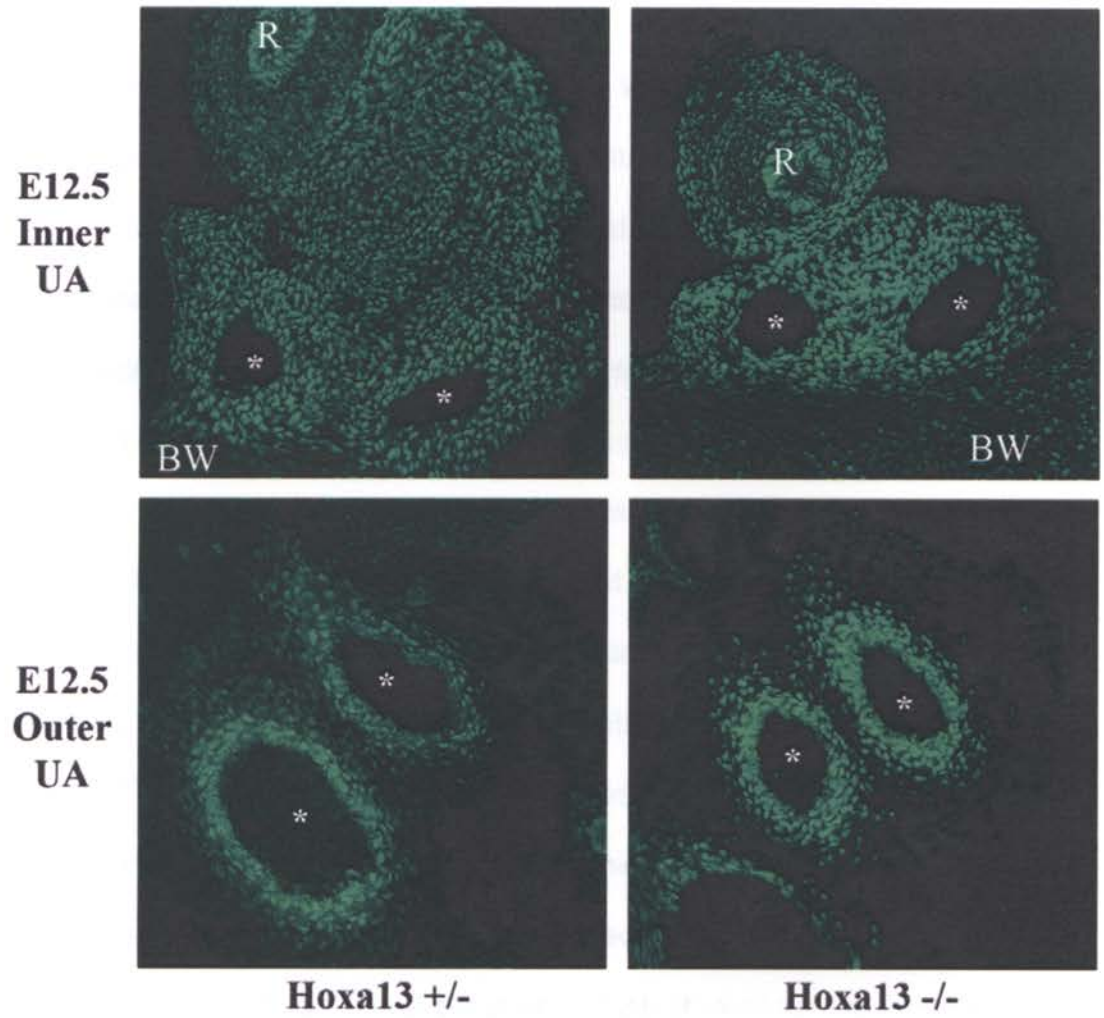

Figure 3.5: *Hoxa13* is expressed in the umbilical arteries

The *Hoxa13*^{GFP} allele marks *Hoxa13* expression in the umbilical arteries (asterisks) and surrounding mesenchyme at E12.5. *Hoxa13* expression was observed in the UAs upon their formation at E11.0 and throughout development, and it was maintained from the placenta to the body wall and through to the trigone. Images were obtained by confocal microscopy at 20x magnification. Body wall (BW), rectum (R).

3D. Summary

Our characterization presents a novel *Hoxa13* expression pattern within a specific cell type of the developing placenta. While previous research noted weak expression of *Hoxa13* within the placenta (Warot et al., 1997), there has been no further characterization or associated defects reported in the literature. Furthermore, while *Hoxa13* expression was noted in the umbilical arteries and surrounding urogenital system, the onset of *Hoxa13* expression was never identified (Stadler et al., 2001).

My initial studies of the umbilical arteries led me to consider the question: When is the earliest developmental time point for *Hoxa13* expression? More importantly, what is the UA ontogeny, what tissues also arise from this early structure, and where is *Hoxa13* expressed within these structures? The $Hoxa13^{GFP}$ mutant allele made it possible to identify *Hoxa13*-expressing cells at different developmental time points. Using this tool, we discovered that *Hoxa13* is expressed much earlier than previously predicted or reported, at E7.75 in the emerging allantoic bud. This expression persists throughout the formation of the umbilical arteries, which arise by vasculogenesis within the allantois. Also, *Hoxa13* is expressed during the initiation of the chorio-allantoic placenta at E9.0, and it's expression persists within the placental labyrinth as it increases in size and complexity from E10.5 to E14.5. To note, the placenta is one of the first organs to form during embryonic development, and it is an essential organ for embryonic health and survival.

In addition to determining when *Hoxa13* is expressed in the developing placenta and vasculature, we also wanted to address the question: Which placenta cells express *Hoxa13*? Using vascular specific antibodies, we showed that fetal endothelial cells exclusively express *Hoxa13* within the placenta labyrinth. This discovery was essential in narrowing our subsequent phenotypic characterizations and molecular analyses, and it allowed us to form clear hypotheses about the function of HOXA13 in the placenta ECs. What is the phenotypic effect of *Hoxa13* loss within placenta ECs? Does HOXA13 regulate EC-specific genes within the placenta vasculature? We address these questions in the following chapters.

Chapter Four

Hoxa13-deficient mice display defects of placental angiogenesis and endothelial cell morphology

Specific Aim 2: Analyze the placental and cardiovascular phenotypes of Hoxa13*-deficient mice using detailed histological analyses and molecular markers*

4A. Mice lacking *Hoxa13* display significant placental defects

Since *Hoxa13* is clearly expressed within the developing placenta and umbilical arteries, we wanted to ascertain the associated phenotypes due to *Hoxa13* loss. Initial studies of the gross morphology showed that embryos lacking *Hoxa13* appear to have reduced blood flow through their UAs and bodies (Figure 4.1). By dissecting out and weighing the fetal component of the placenta, we determined that *Hoxa13*^{GFP} mutant placentas are significantly smaller than normal placentas (Figure 4.2-B). By sectioning placentas at various developmental stages and performing ISH using the spongiotrophoblast- specific riboprobe for *Tpbp*, a reduced placenta size and thickness was clearly observed in *Hoxa13* mutant placentas (Figure 4.2-A). Importantly, the mutant and wildtype embryos remain similar in size (Figure 4.1), suggesting that these defects are not simply a reflection of general growth delay.

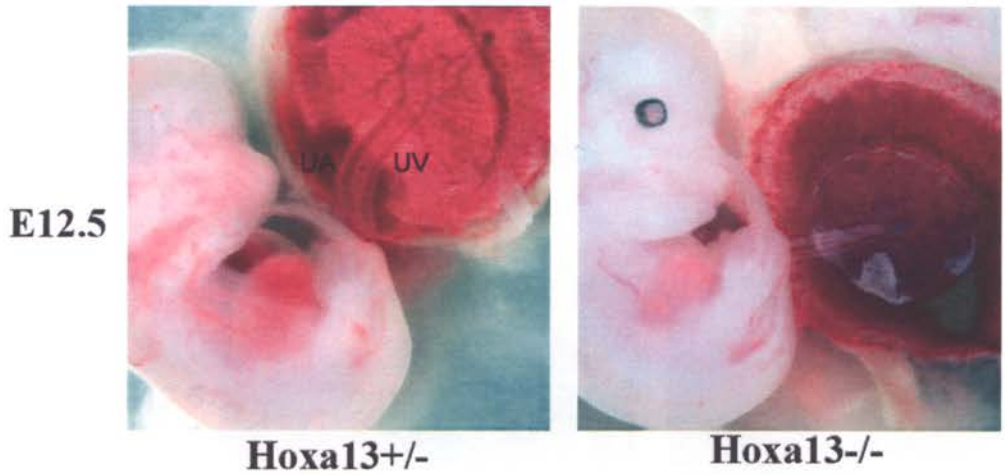

Figure 4.1: *Hoxa13* deficient mice display reduced blood flow

Hoxa13^{GFP} mutant mice often have weaker blood flow through the umbilical cord and the embryo, as evidenced by a pale body. Embryos are E12.5 littermates.

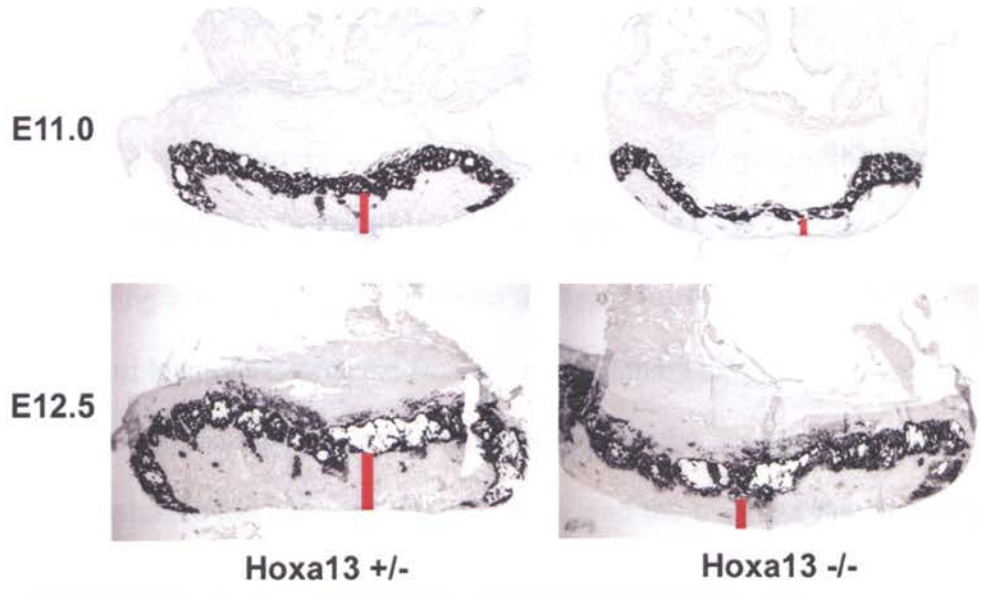

A.

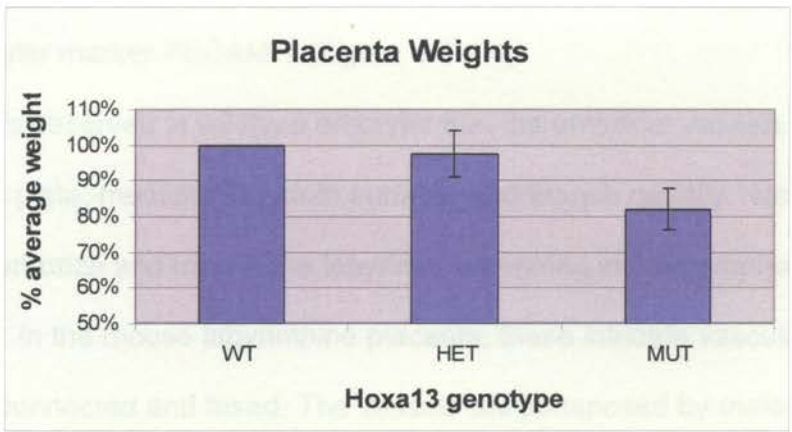

B.

Figure 4.2: Mutant placental labyrinths are reduced in thickness

(A) *Tpbp* expression within the placental spongiotrophoblast layer (black) outlines the fetal labyrinth border (below). The reduction of the labyrinth layer is visible in *Hoxa13* mutant placentas. Labyrinth thickness is denoted with red bars. The decidua and spongiotrophoblast layers appear unaffected.

(B) By weighing dissected labyrinths from 7 litters of embryos (E12.5-E13.5), the percent difference in labyrinth weight from wildtype was calculated. (T-test comparing HET and MUT: $p < 0.004$)

4B. *Hoxa13*-deficient placentas display incomplete vascularization due to vascular branching defects

While we have shown a *Hoxa13*-dependent reduction in labyrinth size and *Hoxa13*-specific expression in placental ECs, the effect of *Hoxa13* loss on vascular patterning and integration remained unclear. Furthermore, we hypothesized that loss of EC-specific *Hoxa13* would inhibit proper angiogenic vascularization of the placenta. To address this hypothesis, we used several techniques to visualize the labyrinth vascular tree, and the clearest view arose by a novel technique of bisecting the placenta and performing whole-tissue IHC with the vascular marker PECAM-1 (Figure 4.3-4.4).

We observed in wildtype embryos that the umbilical vessels cross the chorionic plate, meet the labyrinth surface, and branch radially. Next, these stem vessels arborize and invade the labyrinth, branching into a complex vascular network. In the mouse labyrinthine placenta, these intricate vascular branches are interconnected and fused. The vessels are juxtaposed by maternal blood space, as observed by histological sectioning and TEM imaging (Figure 4.7). The individual vascular stems first sprout into defined lobes which, by angiogenic branching and remodeling, gain higher complexity and continuity as they develop from E11.5 to E14.5 (Figure 4.4). This increase in fetal vasculature maximizes the surface area for efficient maternal-fetal exchange (Faber and Thornburg, 1977). This structure is analogous to the chorionic villous placenta in humans (Rossant and Cross, 2001).

In our mouse model, the initial vascularization of the placenta appears normal until E10.5 (Figure 4.3-A-B). This is soon followed by a visibly reduced numbers of vascular branches within each lobe of the mutant labyrinth, beginning at E11.5 (Figure 4.3-C-H). As the labyrinth matures, several observations can be made about the placental vascularization of the *Hoxa13* mutant. The vasculature is reduced in size and number of fine vessels, often presenting as distinct lobes of vessels (Figure 4.4-F). When the vasculature does fill in laterally, there is incomplete invasion of the vascular network distally toward the maternal deciduae, thereby creating a thinner vascular labyrinth zone than that observed in wildtype or heterozygous placentas (Figure 4.4-E). This defect is initiated at E11.5 and persists through E13.5, and the mutant vascular layer never catches up in size, suggesting that this is not due to growth delay nor a progressive assault on the endothelial cell integrity, but rather, there are intrinsic EC-specific defects that cause the EC phenotype.

Upon closer examination of the placental vasculature branching, it appears that angiogenic intussusception plays an important role in the mouse placenta. As noted by previous studies, the vessels within the mouse placenta are interconnected laterally (Charnock-Jones et al., 2004). This occurs by intussusceptive microvascular growth (IMG), a mechanism of non-branching angiogenic remodeling which effectively increases vascular complexity by increasing the number of vessels through dividing current vessels (Djonov et al., 2000; Djonov et al., 2002). While typical studies of IMG rely on vascular casts and electron microscopy of serial sections, our images from whole tissue PECAM

IHC clearly show the interconnected vasculature typical of IMG (Figure 4.3-4.4). While the normal placental vasculature is comprised of thin, interconnected vessels, we consistently observed thicker vessels that more resemble a vascular plexus within the *Hoxa13* mutant placentas (Figure 4.5). Therefore, our data suggests that IMG is an important mechanism for expanding the labyrinthine vasculature, and *Hoxa13*-deficient placentas appear defective in IMG angiogenesis.

Complementary to these experiments, we utilized the *Tie2-LacZ* transgenic mouse line to identify and evaluate *Tie2*-expressing vessels within the maternal- and fetal-specific vasculature. When the maternal tissue was *Tie2-LacZ*-positive but the fetus was negative, the Tie2+ maternal vessels were restricted to the decidua and the distal spongiotrophoblast tissue (Figure 4.6). This is consistent with the labyrinth morphology where the maternal blood space is lined with fetal trophoblast cells rather than maternal EC. Next, when the embryo was *Tie2-LacZ*-positive but the maternal tissue was negative, the fetal vessels could be clearly identified by their expression of *Tie2* (Figure 4.6), which is consistent with IHC analysis (Figure 5.5). Overall, this analysis supports the finding that mutant labyrinths have restricted vascular trees and thicker vessels with fewer intricate branches.

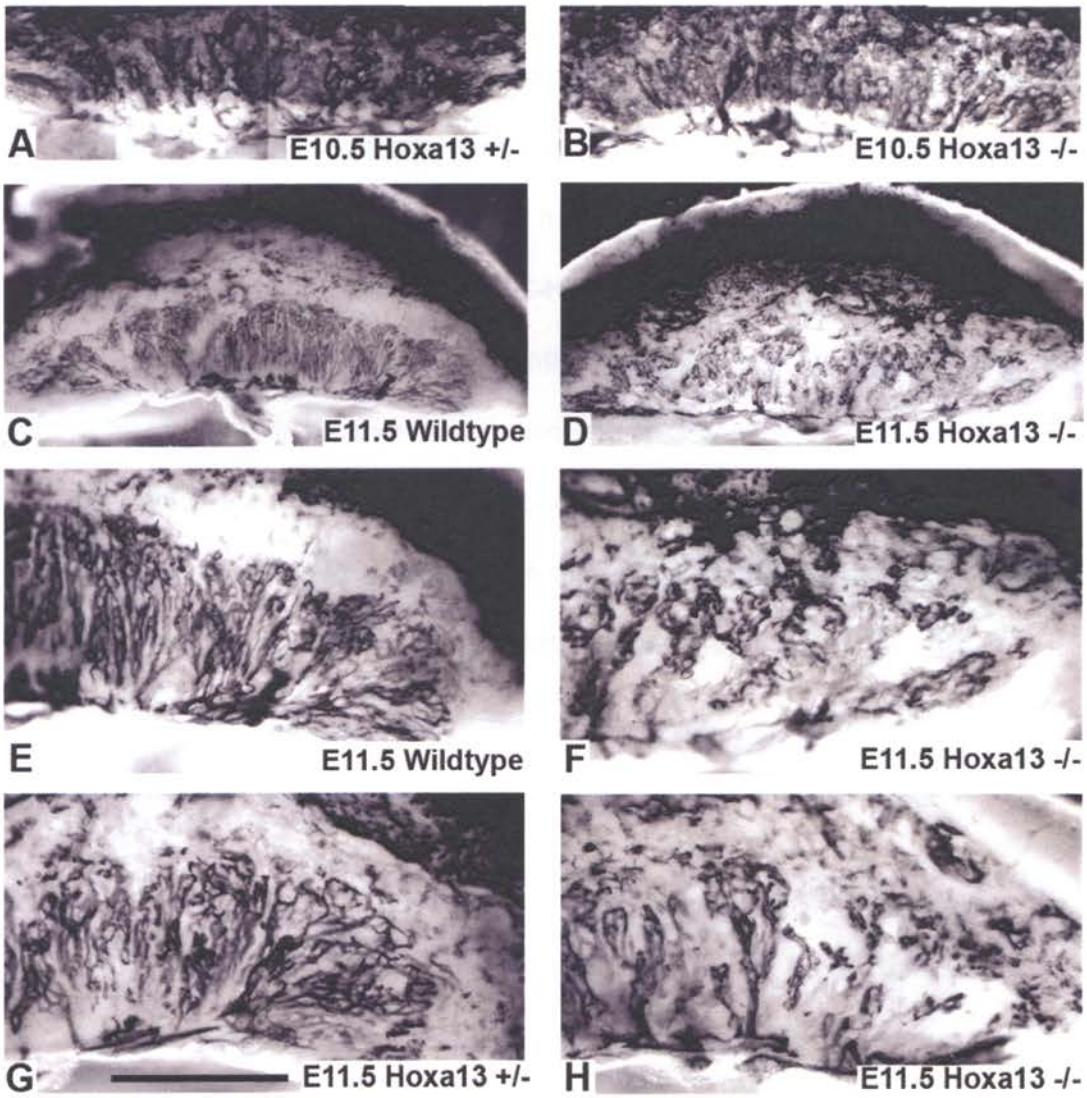
A
E10.5 Hoxa13 +/-
B
E10.5 Hoxa13 -/-
C
E11.5 Wildtype
D
E11.5 Hoxa13 -/-
E
E11.5 Wildtype
F
E11.5 Hoxa13 -/-
G
E11.5 Hoxa13 +/-
H
E11.5 Hoxa13 -/-

Figure 4.3

Figure 4.3: Placental vascular patterning defects emerge at E11.5

To visualize the developing vascular branching within the labyrinth, whole-tissue immunohistochemistry was performed using the PECAM vascular marker. **(A-B)** At E10.5, the nascent labyrinth vascular tree structure is similar between *Hoxa13* heterozygous and mutant placentas. **(C-H)** Vascular branching defects are apparent by E11.5. While normal labyrinths are highly vascularized (C), the *Hoxa13* mutant labyrinths show a reduced and spotty vascular tree (D). Higher magnification images reveal the highly branched structure of the *Hoxa13* heterozygous labyrinths (E, G), while the mutant vasculature is incomplete and misshapen, displaying thicker vessels that are less branched (F, H). Bar in G represents ~1 mm.

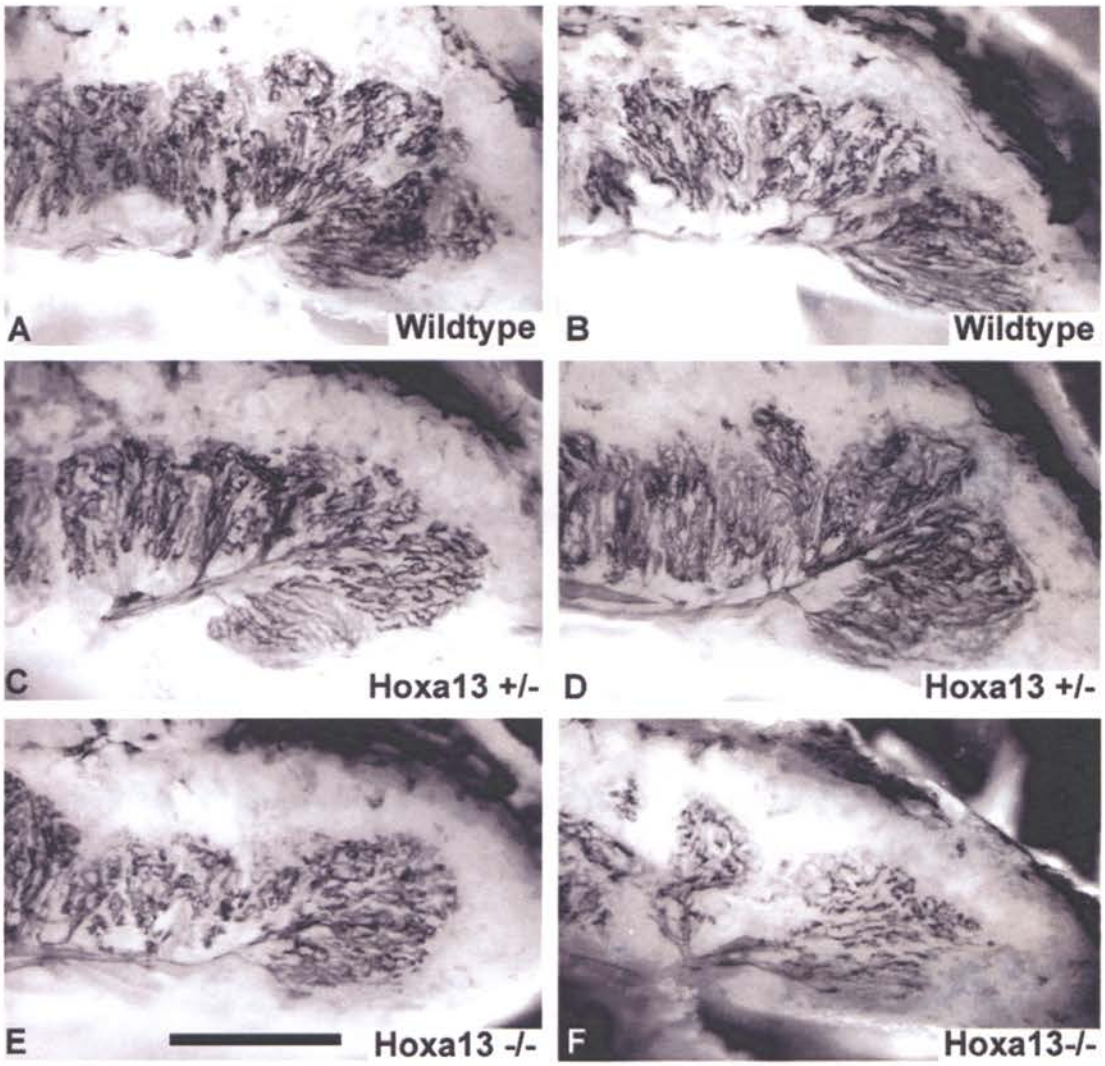

Figure 4.4

Figure 4.4: Loss of *Hoxa13* prevents complete labyrinth vascularization

To best view the extent of branching within the placental labyrinth vascular tree, whole-tissue immunohistochemistry was performed on E12.5 placentas using the PECAM vascular marker.

(A-D) Wildtype (A-B) and *Hoxa13* heterozygous (C-D, +/-) placentas display a complex vascular tree that is highly branched and that completely fills the labyrinth layer of the placenta.

(E-F) *Hoxa13* mutant placentas consistently display incomplete vascular branching, as seen by reduced vascular area (E-F) and by the presence of separate vascular lobes (F). The *Hoxa13* mutant vessel phenotype suggests reduced intussusceptive angiogenesis and vascular tree complexity.

Images were obtained using a dissecting microscopy and a 2x objective. Bar in E represents ~1 mm.

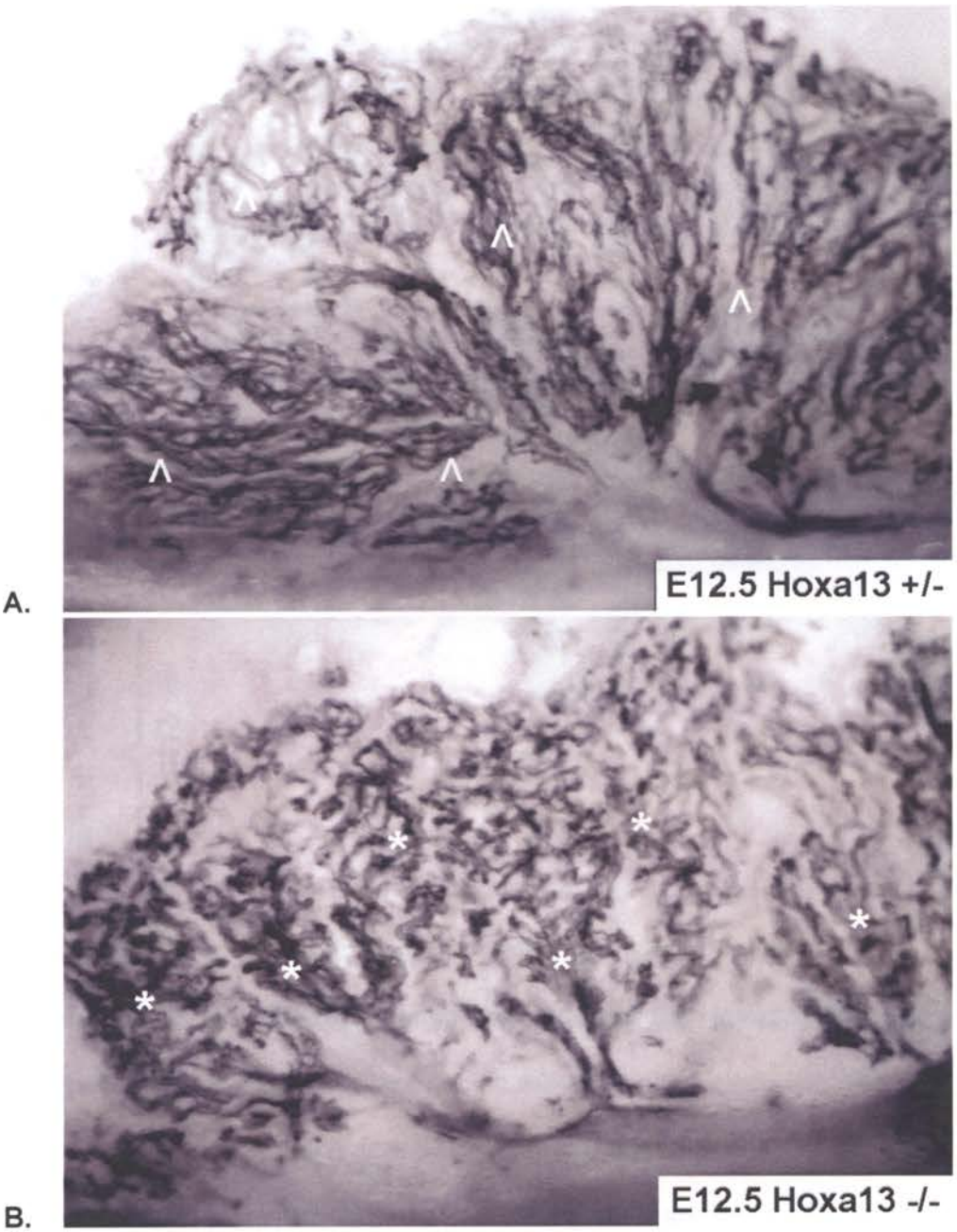

Figure 4.5: Phenotype suggests defective IA in *Hoxa13* -/- vessels

While the *Hoxa13* heterozygous vessels develop radially from the chorionic plate into a complex network of thin, interconnected vessels (arrowhead, **A**), the *Hoxa13* mutant vessels retain a thick, bulky phenotype (asterisk, **B**). Images were obtained using a dissecting microscopy and the 8x objective.

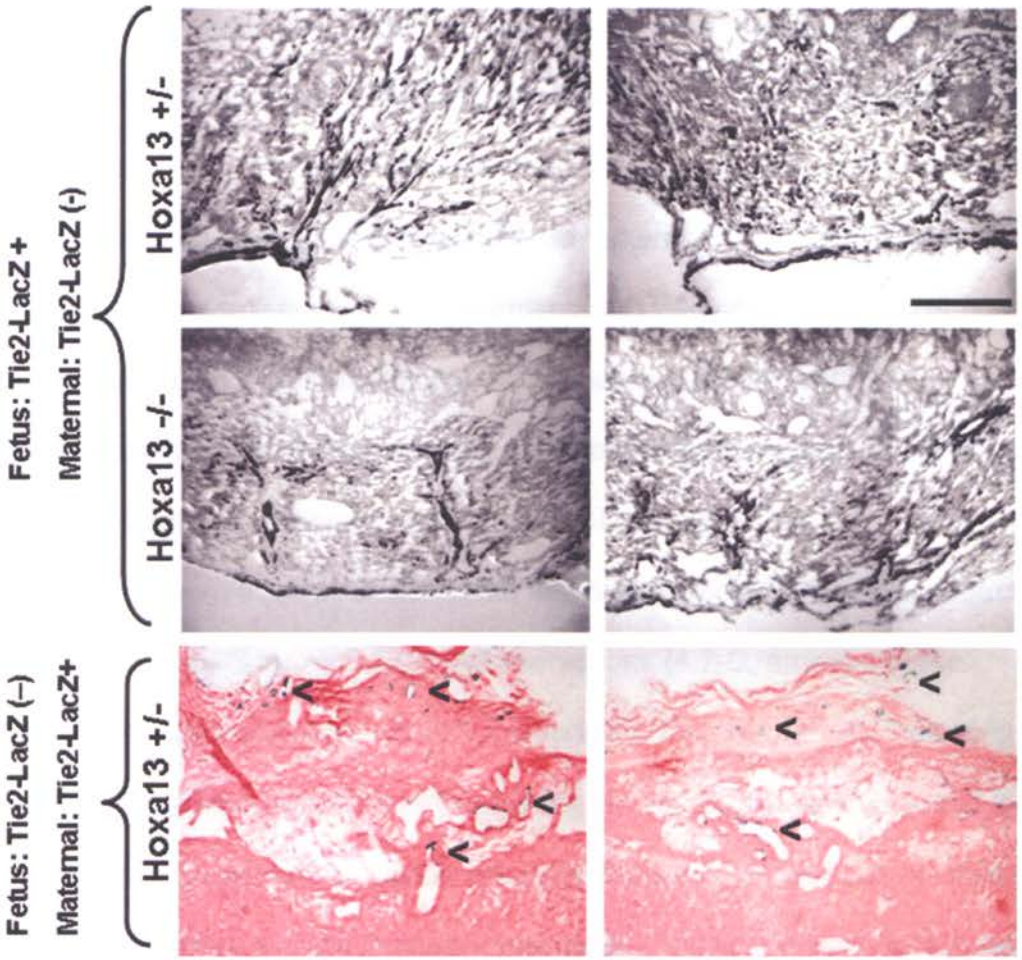

Figure 4.6: Fetal-specific vascular patterning defects

By introducing the *Tie2-LacZ* transgenic allele into the *Hoxa13*^{GFP} mouse line, we can assay for the *Tie2* vascular-specific receptor in the placental labyrinth. While normal placentas display a dense and complex vascular network (above), *Hoxa13* mutant placentas have thicker vessels that are less branched (middle). Furthermore, we can distinguish between maternally and fetal-expressed *Tie2*, revealing that the fetal expression of *Tie2* is restricted to the labyrinth vessels, while the maternal *Tie2* is expressed by the spiral arterioles and ends at the spongiotrophoblast layer (blue staining, below). Bar represents 1 mm.

4C. Lack of *Hoxa13* causes a dramatic loss of proper EC morphology

Since *Hoxa13* was expressed specifically in the ECs of the placenta labyrinth, and loss of *Hoxa13* prevented full placental growth and vascularization, we hypothesized that *Hoxa13* loss causes an altered EC morphological phenotype. Transmission electron microscopy (TEM) of the labyrinth presented a clear view of the ECs morphology and associated defects. At E13.5, ECs lacking *Hoxa13* displayed severe loss of cell body and cytoplasm accentuated by rounded nuclei and a thinned cell (Figure 4.7-D, arrows). Furthermore, breaks in the EC lining were often apparent in the labyrinth vessels, indicating a breach in the EC barrier and loss of EC cell-cell interactions (4.7-D, arrow). These observations were also made in E11.5 labyrinths (Figure 4.7-A-B), indicating that the mutant EC phenotype occurs throughout placental vascularization and is not a product of EC damage over time. Regions of edema, or extracellular fluid accumulation, were evident in mutant placentas, including striking detachment of the ECs from the underlying syncytiotrophoblast layers (Figure 4.7-B, D arrowhead). Since we did not observe these defects in the wildtype or *Hoxa13* heterozygous placentas which were treated in the same manner (Figure 4.7-A, C) and care was taken to preserve vascular labyrinth structure, we believe that these are *Hoxa13*-specific effects on the ECs. Furthermore, the EC basement membrane remained intact, eliminating this as the direct cause of the mutant ECs morphology or edema (Figure 4.8). Importantly, the three layers of syncytiotrophoblasts were present in mutant placentas, signifying that *Hoxa13* loss does not affect trophoblast differentiation or patterning. Finally, in a few

mutant cells, we observed large, open vacuoles within the EC body, indicative of further cell damage (Figure 4.7-D). To note, neither TUNEL staining (not shown) nor EC nuclei analysis by TEM suggested that apoptosis was a factor of the mutant phenotype. In summary, the placenta ECs lacking *Hoxa13* display a dramatically altered morphological phenotype, which often includes reduced cell body (reduced cytoplasm and cell thickness), breaks in the cell layer, and edema with detachment of the EC from the underlying cell layer.

To quantify the alteration in EC morphology, a cell scoring system was developed to score the EC phenotype within labyrinth cross-sections (Figure 4.9-A). Cells were scored as normal, intermediate (cell rounding or irregular shape), or abnormal (cell detachment, edema, diminished cell body). While the wildtype and *Hoxa13* heterozygous vessels displayed ~82% normal cells and very few (<3%) abnormal cells, the mutant vessels displayed only 50% normal cells and nearly 20% abnormal cells (Figure 4.9-B). In the mutant placentas, the abnormal cells corresponded to regions of severe edema. Overall, the mutant EC morphology suggests a defect in EC structure and patterning required for proper blood flow and efficient placental function.

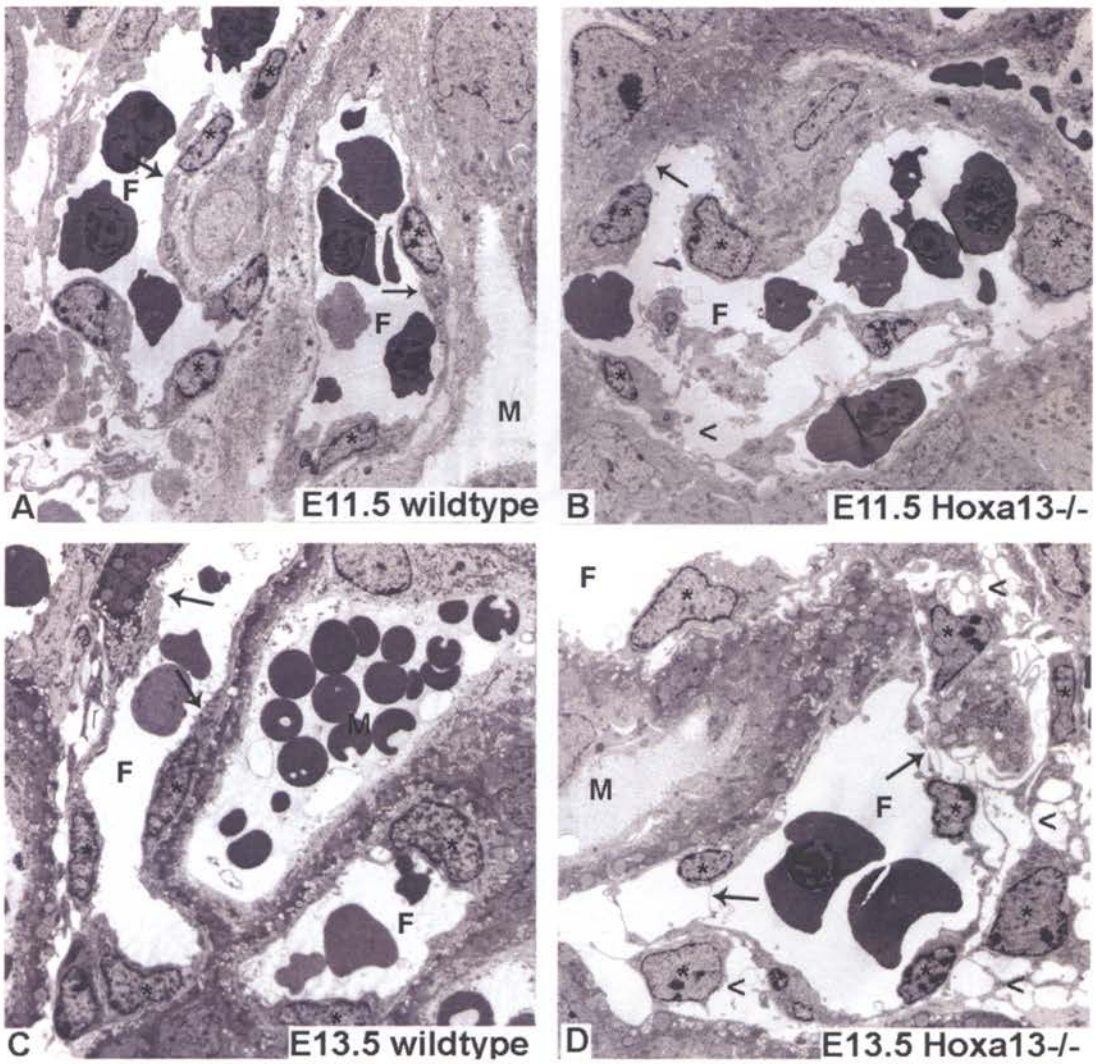

Figure 4.7: TEM of the placental labyrinth reveals abnormal EC morphology

TEM of the placental labyrinth revealed changes in *Hoxa13* mutant EC morphology from E11.5 (A-B) to E13.5 (C-D). While the ECs (denoted by asterisks) lining the fetal vessels display a smooth epithelial morphology against the underlying trophoblasts in the wildtype placentas (A,C), the mutant ECs display a reduced cell thickness, extracellular edema, and delamination at E11.5 (B) and E13.5 (D). Fetal vessel (F), maternal sinuses (M), EC nucleus (*), trophoblasts (TR). Images shown are from 55x TEM photographs.

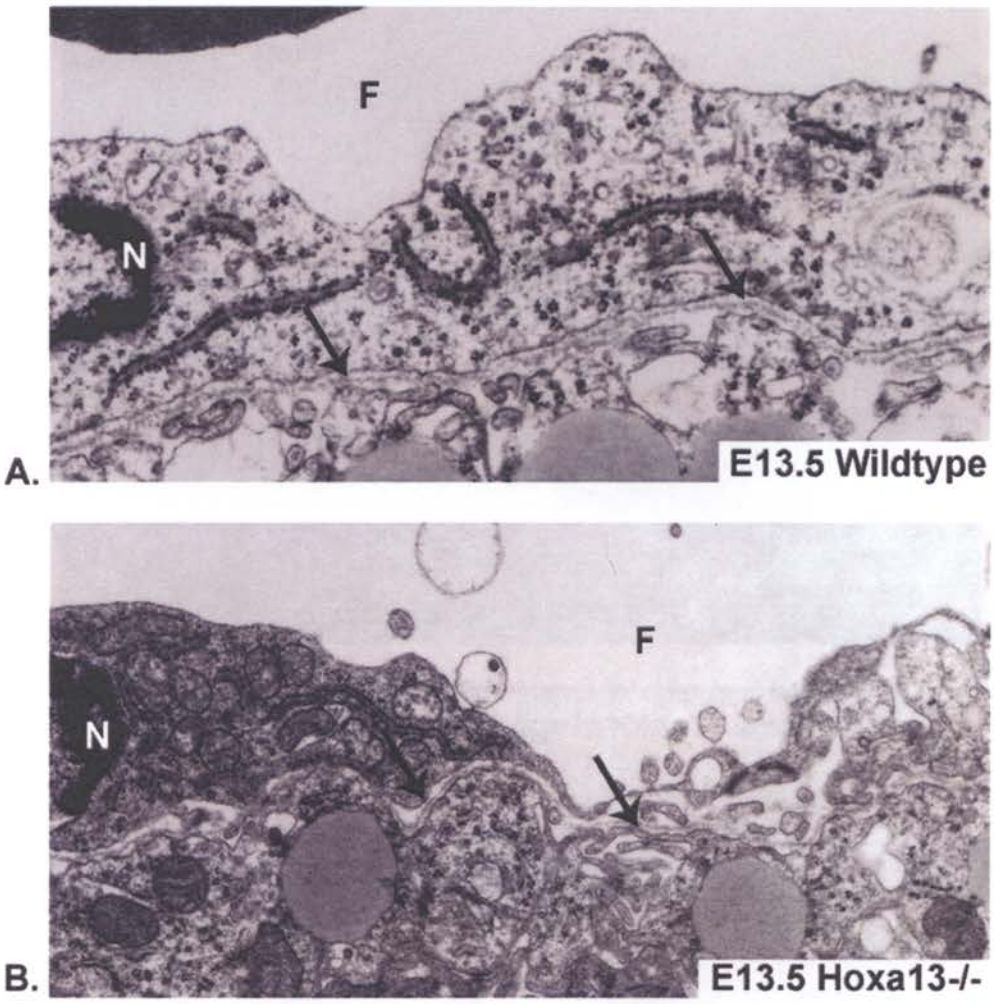

Figure 4.8: Higher magnification TEM shows retention of the ECM

Higher magnification of the endothelial cells illustrates the loss of structure and cell body thickness in the mutant placenta (B). However, the basement membrane is retained in both the wildtype and mutant endothelial cells (arrows). Fetal lumen (F), EC nucleus (N). Images shown are from 90x photographs.

A.

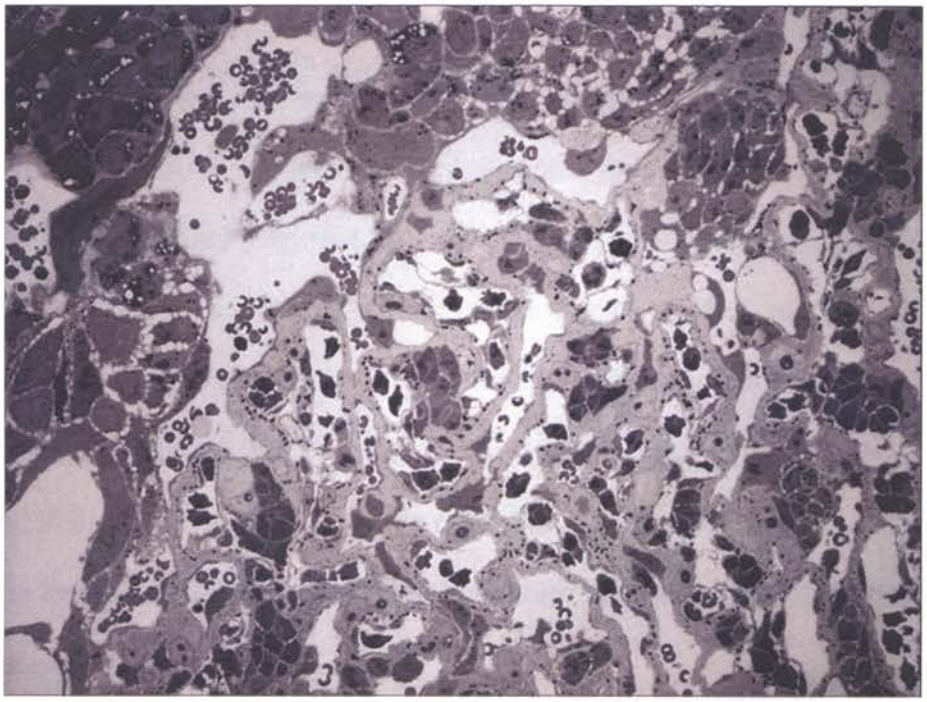

B.

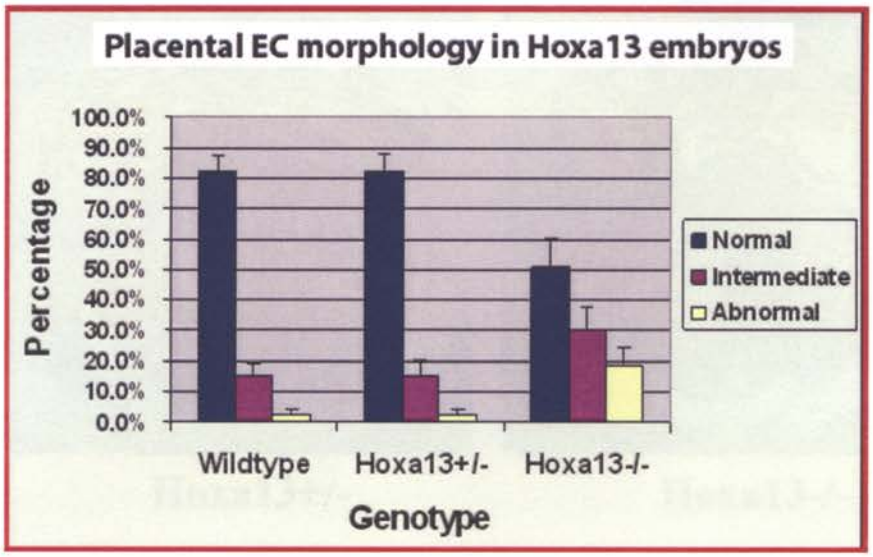

Figure 4.9: Mutant labyrinths contain a high percentage of abnormal ECs

By counting and scoring the shape of the placental ECs from 10x photographs (*Hoxa13* heterozygote shown in **A**), we observed that while the wildtype and *Hoxa13* heterozygous placenta have <3% 'abnormal' ECs, the mutant placentas display ~20% 'abnormal' ECs and only ~50% normal ECs **(B).**

4D. Loss of *Hoxa13* leads to secondary cardiac defects

While *Hoxa13* is never expressed in the cardiac field or in the heart (data not shown), mice lacking *Hoxa13* exhibit a dramatic reduction in the thickness of the myocardial heart wall (Figure 4.10). A closer analysis of the myocardial tissue layer revealed that *Hoxa13* mutant hearts display a ~45% reduction in the number of cells spanning the left ventricle (3.6±1.1 cells) compared to wildtype or *Hoxa13* heterozygotes (6.3±0.8 cells) (Figure 4.11). Similar figures were calculated in the right ventricle wall. To note, this was the only cardiac defect we observe in the *Hoxa13*^{GFP} mutant mice; there were no observable outflow tract or septal defects in the heart.

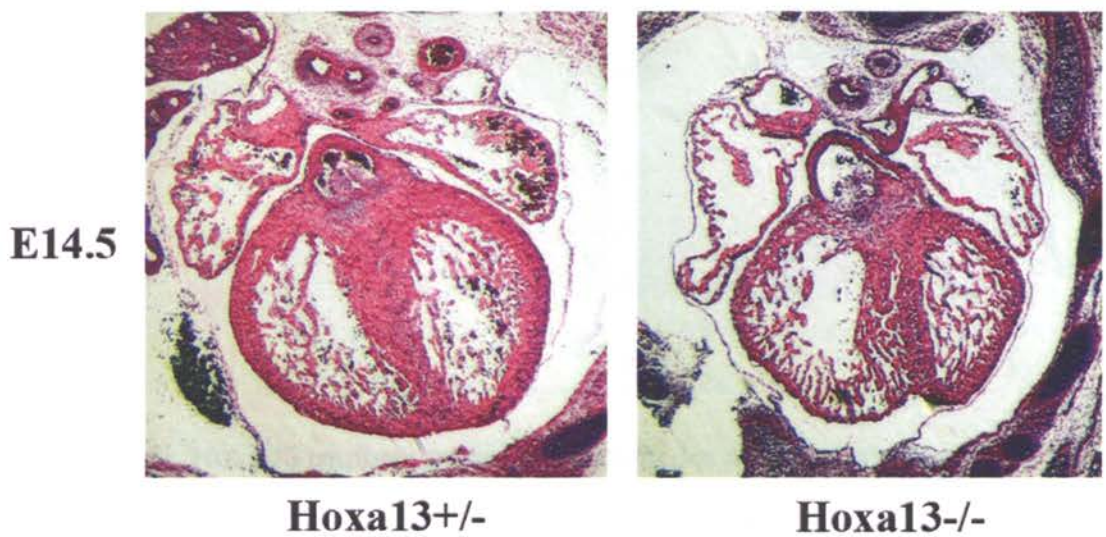

Figure 4.10: Loss of *Hoxa13* causes secondary heart defects

While normal heart development includes formation and differentiation of a thick myocardial wall, the *Hoxa13*^{GFP} mutant embryos displayed a thinner heart wall. Importantly, no other heart defects are observed in these mice, and *Hoxa13* is never expressed within the developing heart.

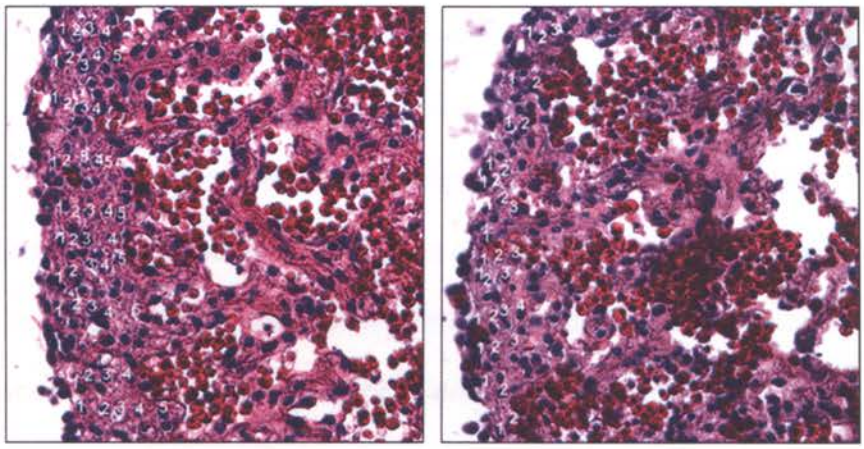

A.

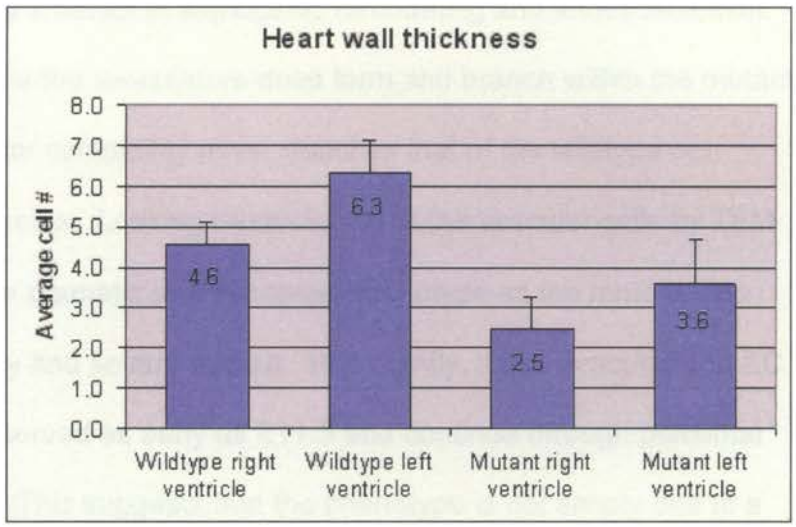

B.

Figure 4.11: *Hoxa13* mutant embryos suffer from a thinner heart wall

(A) As shown in E13.5 right ventricles, wildtype embryos display a thick heart wall of ~4-6 cells thick, while the *Hoxa13*^{GFP} mutant ventricles are reduced in thickness to ~55% of normal.

(B) The bar graph shows the average cell number across the myocardial wall of both ventricles. This was tested at E13.5 from 3 separate heart samples per genotype.

4E. Summary

Since we have shown that *Hoxa13* is expressed within endothelial cells of the placenta labyrinth, we predicted that these would be the cells most affected by *Hoxa13* loss. To test this hypothesis, the histology of the placenta and its vasculature was observed at all stages of placenta labyrinth development and maturation (E10.5 to E13.5). We have shown that *Hoxa13*-deficient placental labyrinths are reduced in thickness and weight. Furthermore, the density and complexity of the fetal vasculature was greatly reduced in $Hoxa13^{GFP}$ mutant placentas, suggesting a defect in angiogenic remodeling and intussusception. It is interesting that while the vasculature does form and branch within the mutant placentas, the vascular complexity never matches that of the wildtype or $Hoxa13^{GFP}$ heterozygotes. Looking more closely at the vascular cells by TEM reveals an even more dramatic and abnormal phenotype as the mutant ECs show loss of cell body and severe edema. Importantly, these vascular and EC phenotypes were observed as early as E11.5 and continue through placental maturation at E13.5. This suggests that the phenotype is not simply due to a progressive loss of vascular function and integrity stemming from an earlier hit to their function, but rather *Hoxa13* is required throughout placental vascularization to maintain EC morphology and vascular patterning. Furthermore, the lethality in Hoxa13-deficient mice occurs at the exact time when the placental labyrinth is expanding and differentiating (e12.5 to E14.5), consistent with the requirement for a dynamically developing placental vasculature.

Finally, the reduction in placental vasculature leading to reduced blood flow return to the embryo may cause changes in embryonic blood pressure. These harsh stresses on the embryo have been linked to secondary cardiac defects in the "placenta-heart axis" theory proposed by Hemburger and Cross (2001). Interestingly, *Hoxa13*^{GFP}-deficient embryos are afflicted by additional heart defects, even though *Hoxa13* is never expressed in the heart. We suggest that the dramatic loss of placental vascular patterning and endothelial cell integrity prevents proper blood flow between the embryo and the placenta, leading to changes in blood flow, stress on the heart, and secondary heart defects. However, beyond the obvious heart defects, we propose that the placental vascular defects do not support life or placental function, and therefore, loss of *Hoxa13* in the placenta leads to placental insufficiency and mid-gestational lethality. Overall, *Hoxa13* is required for placental vascular integrity and function.

The dramatic vascular phenotype and EC morphology due to loss of *Hoxa13* strongly implicates HOXA13 in the regulation of placental vascular patterning and the overall expansion and differentiation of the vascular tree. Therefore, we asked how HOXA13 directly affects vascular identity and gene regulation. Does HOXA13 directly regulate the transcription of vascular- and placenta-specific genes? What molecular markers are perturbed by the loss of HOXA13? These questions are addressed in the following chapter.

Chapter Five

The HOXA13 transcription factor directly regulates expression of *Tie2* and *Foxf1*

Specific Aim 3: Identify changes in the gene expression profile due to HOXA13 insufficiency in affected tissues

5A. Introduction

While a direct role for HOXA13 in placenta formation remained elusive, the unique reduction in placenta size and vascularization led us to hypothesize that HOXA13 plays an important molecular role in regulating and specifying the placenta vasculature. Our goal was to identify genes that were misexpressed in the placenta due to the loss of *Hoxa13*, relate their importance in ECs, and determine whether the HOXA13 transcription factor directly regulates the transcription of these candidate genes. Our approach included identifying candidate genes by microarray technology and testing candidate gene expression by immunohistochemistry, *in situ* hybridization, and qRT-PCR.

In previous studies of HOXA13 function, HOXA13 binds to unique regulatory sequences of candidate genes both *in vitro* and *in vivo* (Knosp et al., 2004; Knosp et al., 2006). Through biochemical analysis of HOXA13 DNA binding affinity performed in our lab, a HOXA13 high-affinity binding sequence "AAATAAAAA" was identified (Knosp et al., 2006). Since we detected significant changes in candidate gene expression within *Hoxa13*-deficient ECs, we hypothesized that the HOXA13 transcription factor directly regulates some of these genes by binding to preferred HOXA13-binding sites within their upstream promoter sequences. To test this hypothesis, we employed several complementary methods of analysis: electrophoretic mobility shift assay (EMSA) to determine whether a HOXA13 DNA binding domain (A13-DBD) peptide could

bind to gene-specific sequences, chromatin immunoprecipitation (ChIP) and luciferase assays to identify if HOXA13 binds to these sites *in vivo* and *in vitro,* and fluorescence anisotropy to quantitate the affinity of HOXA13 for each potential binding site.

5B. Loss of *Hoxa13* leads to down-regulation of placental and vascular genes

To begin our molecular analysis, we performed microarray assays on E13.5 placental labyrinths to identify gene expression changes due to *Hoxa13* loss. E13.5 placentas were used since there is a visible phenotype at this stage and Hoxa13 is expressed strongly. Six replicate microarrays were performed for each genotype, revealing more genes were down-regulated (86 genes) from loss of *Hoxa13* than there were genes up-regulated (8 genes) (FDR p-value < 0.1) (Figure 5.1, Figure 5.2, Appendix 2 contains the full list of genes). In fact, only 3 genes were up-regulated while 31 genes were down-regulated when comparing mutant and wildtype placentas and using a FDR p-value of <0.05 (Appendix 2). Furthermore, there were no significant differences in gene expression between sex-specific microarrays, which primarily identified X and Y-linked genes (Figure 5.1). With this statistical information on gene expression, we focused our subsequent characterizations on genes down-regulated in *Hoxa13*^{GFP} mutant placentas and that were statistically signficant (FDR p-value <0.5 and FC < -1.5). Furthermore, we began with genes required for angiogenesis and vascular function or with a role in development, growth, and differentiation. Microarray fold changes of characterized genes are presented in Figure 5.3 and in Table A.

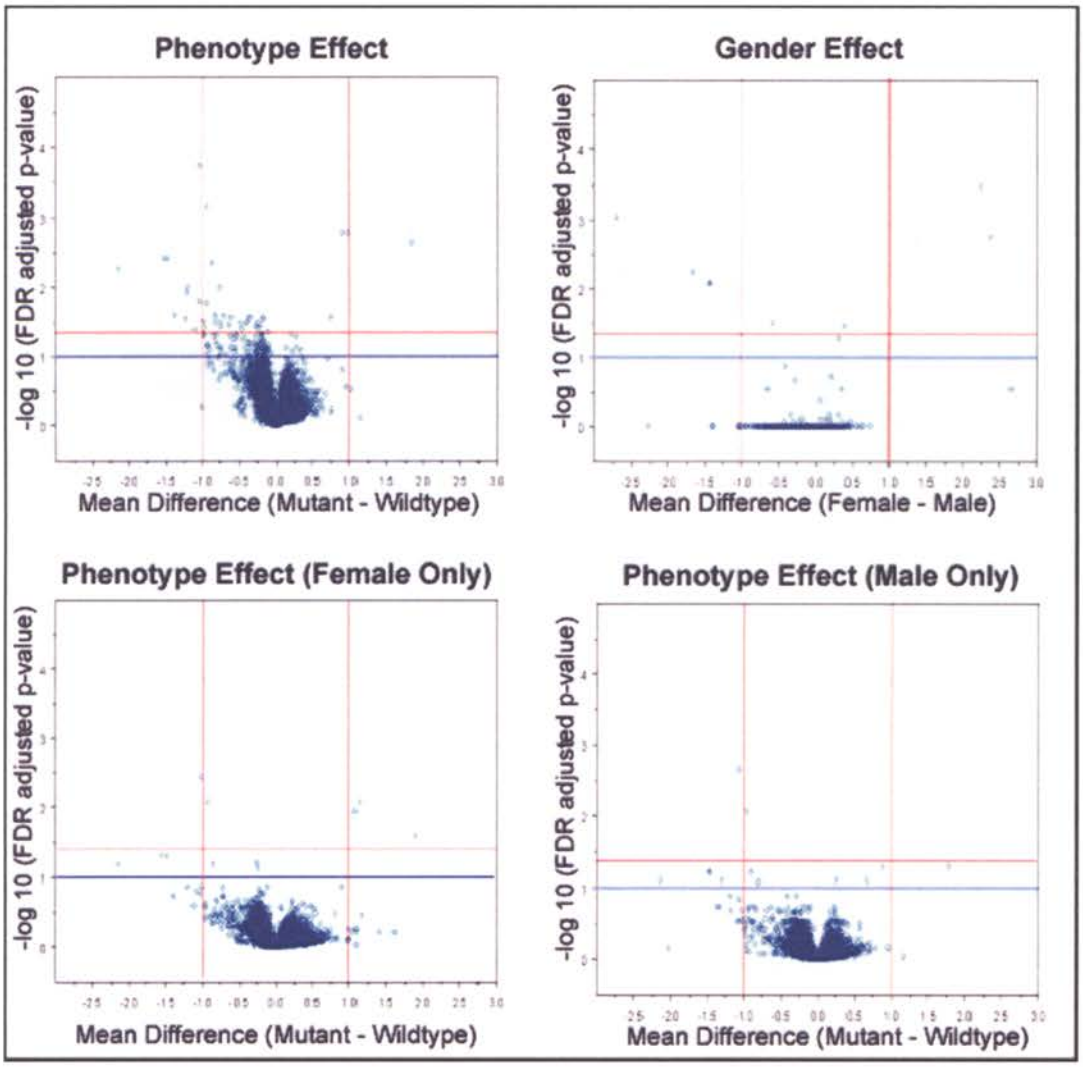

Figure 5.1: Volcano plot of microarray data

To evaluate the microarray data, a volcano plot was used to identify significantly differentially-expressed genes. The x-axis shows the fold change, while the y-axis shows the statistical significance. Therefore, the upper left and right regions of the plot encompass genes that have greater than 2 fold difference and are statistically significant. From these graphs, the most candidate genes arise when focusing on the phenotypic effect (mutant versus wildtype) and including both male and female samples (upper left graph).

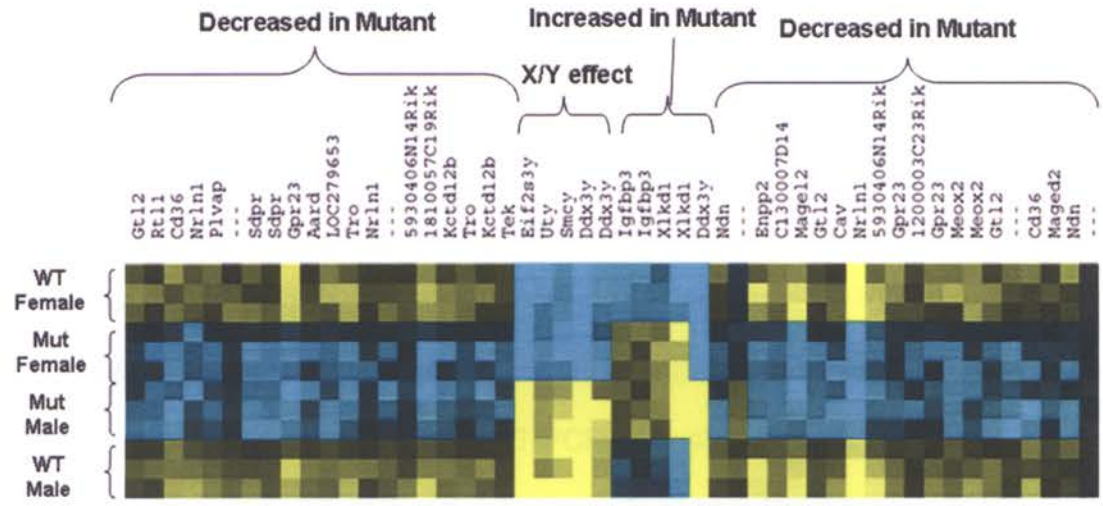

Figure 5.2: Hierarchical clustering of differential gene expression

Three microarrays were performed on individual samples with the genotypes wildtype female, *Hoxa13* mutant female, wildtype male, and *Hoxa13* mutant male (labeled on left, each row represents a unique microarray). Few sex-specific genes were identified (center), allowing us to combine the female and male data sets for each *Hoxa13* genotype. Many genes were significantly reduced in the *Hoxa13* mutant placentas, including *cd36, tek (tie2), trophinin, caveolin-1, necdin,* and *mageL2*. Blue squares represent genes that are expressed at lower levels, while the yellow squares indicate highly expressed genes.

Confirming the misexpression of candidate genes

Candidate genes identified by microarray were tested to confirm their expression in the placenta, to identify their precise expression within EC, and to confirm their misexpression in *Hoxa13*^{GFP} mutant tissue *in vivo*. Quantitative real-time PCR (qRT-PCR) provided a clear way to confirm the microarray results while also quantifying EC-specific expression. Preliminary RT-PCR experiments using whole placental RNA showed that the changes in gene expression were consistent between microarray and RT-PCR analysis (data not shown). However, we hypothesized that the decrease in gene expression would be amplified by performing qRT-PCR on cDNA derived from purified *Hoxa13*-expressing placenta ECs. To test this hypothesis, we isolated E13.5 placental ECs using Dynabead-PECAM-1 beads, collected RNA, and produced cDNA for qRT-PCR experiments. For all genes tested, the fold change by qRT-PCR was more dramatic than the fold change by microarray analysis (Figure 5.3, Table A). Also, the expression levels of some genes in the mutant PECAM+ tissue were equal to the expression levels in the PECAM (-) cells (which don't express *Hoxa13)*. This is exemplified by the genes *mageL-2* and *enpp2*, where the mutant expression levels are decreased over ten fold more by EC-specific qRT-PCR than the fold change by whole-placenta microarray (Table A). This analysis suggests that *Hoxa13*-expressing ECs are the primary placental cells to express these genes, and a loss of *Hoxa13* results in reduced expression of these genes.

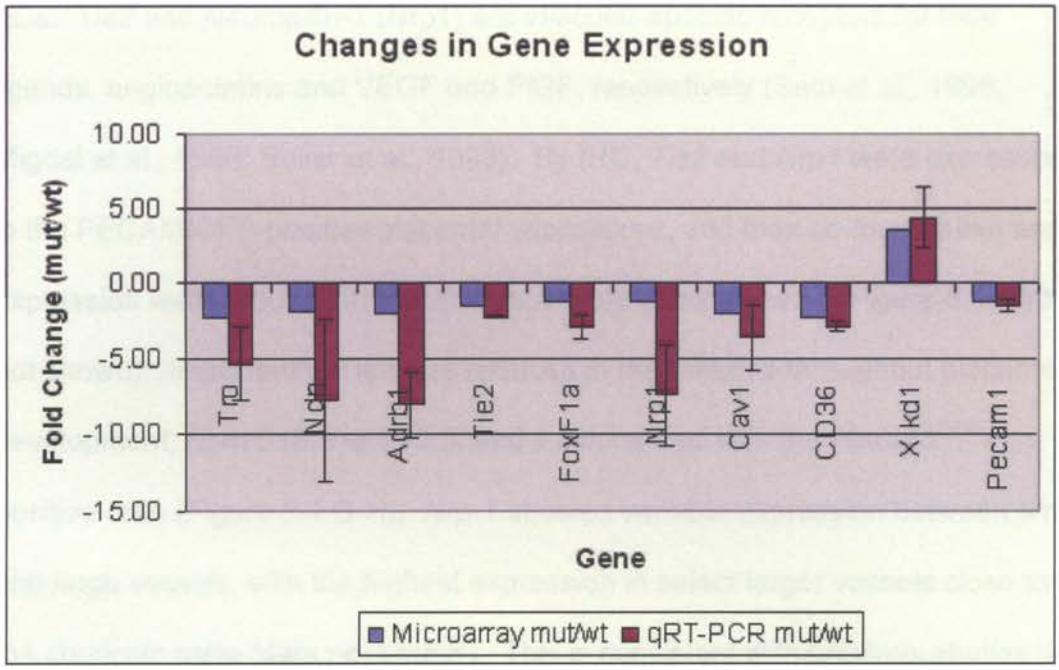

Figure 5.3: Changes in gene expression by microarray and qRT-PCR

Candidate genes were identified by microarray assays and the changes in gene expression were confirmed by qRT-PCR on endothelial cells. Since the qRT-PCR used isolated ECs, a more dramatic fold change was observed when comparing mutant to wildtype gene expression.

In situ hybridization and IHC

To confirm the candidate genes expression in the labyrinth and mis-regulation in mutant placentas, we used *in situ* hybridization (ISH) and immunohistochemistry (IHC) on frozen placenta sections. When a high-affinity antibody was available, IHC proved to be a powerful method of confirming the microarray data while testing for molecular co-localization with PECAM-positive

ECs. Tie2 and Neuropilin-1 (Nrp1) are vascular-specific receptors for their ligands, angiopoietins and VEGF and PlGF, respectively (Sato et al., 1995; Migdal et al., 1998; Soker et al., 1998). By IHC, *Tie2* and *Nrp1* were expressed in the PECAM/GFP-positive placental vasculature, and their co-localization and expression were reduced in mutant vasculature (Tie2 shown in Figure 5.4, Nrp1 not shown). Importantly, Tie2 was reduced in the mutants throughout placenta development, from E10.5 to E13.5, and it colocalized with the *Hoxa13*^{GFP}-positive cells (Figure 5.4 G-H). *Nrp-1* showed variable expression between small and large vessels, with the highest expression in select larger vessels close to the chorionic plate (data not shown). This is consistent with previous studies that show differential expression of *Nrp1* between arteries and veins (Herzog et al., 2001).

One vascular marker that was highly over-expressed in the mutant placenta vasculature was Lyve1 (lymphatic vessel endothelial receptor-1; extra-cellular-link domain containing 1, Xlkd1). Microarray analysis revealed Lyve1 overexpression (Xlkd1, Figure 5.2-5.3), and qRT-PCR confirmed this expression pattern in endothelial cells (Figure 5.4). Using a Lyve-1 specific antibody, Lyve1 was found to be modestly expressed in wildtype placenta vasculature, whereas it was dramatically over-expressed in the mutant PECAM-positive placenta vessels at all stages observed, from E10.5 to E13.5 (Figure 5.5). Furthermore, normal Lyve1 expression was strongest in the distal microvessels near the spongiotrophoblast layer and reduced in the larger vessels at the chorionic plate. *Hoxa13* mutant labyrinths did not follow this trend; rather Lyve1 was strongly and

consistently expressed throughout the labyrinth vasculature. We wondered if the increase in Lyve1 affected the levels or localization of hyaluronan. However, our attempts to identify hyaluronan through it's binding with hyaluronan-binding protein (HABP) were inconclusive. While Lyve1 function in the placenta is unclear, our finding supports recent research that identified *Lyve1* expression in human placenta endothelium (Gu et al., 2006).

Three members of the MAGE (Melanoma Antigen-encoding Gene) family, which encode proteins with roles in cell growth, differentiation, and adhesion, were down-regulated by microarray and ISH. *Trophinin*, a protein expressed in the endometrium and the blastocyst embryo and involved in implantation (Nadano et al., 2002), was expressed in a punctuated pattern within the heterozygous labyrinth, while *trophinin* expression was effectively lost in the mutant labyrinth. Likewise, other MAGE family members *mageL-2* and *necdin* were expressed in a similar pattern within the heterozygous placenta and were nearly completely absent in the mutant placenta. (Figure 5.6). Importantly, none of these proteins have been previously identified or characterized in the placenta labyrinth or in the vasculature.

Finally, expression of Adrenergic receptor beta-1 *(adrb1)*, a receptor with a role in vaso-constriction and relaxation, was also normally expressed in the labyrinth yet absent in the mutant placenta (Figure 5.6). *Adrb1* expression was previously identified in the placenta, although a full characterization of placental expression and function has not been established (Hellgren et al., 2000).

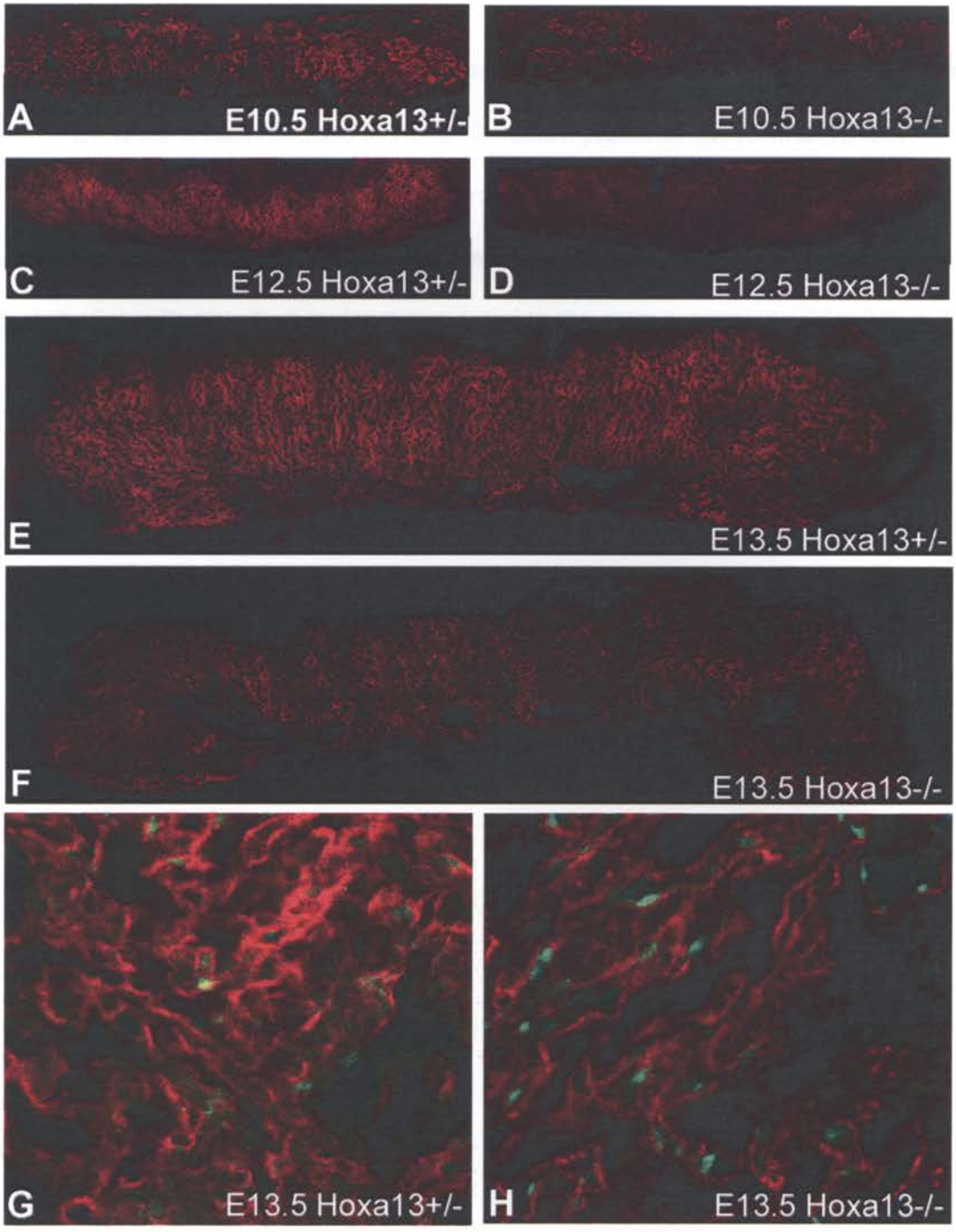
A
E10.5 Hoxa13+/-
B
E10.5 Hoxa13-/-
C
E12.5 Hoxa13+/-
D
E12.5 Hoxa13-/-
E
E13.5 Hoxa13+/-
F
E13.5 Hoxa13-/-
G
E13.5 Hoxa13+/-
H
E13.5 Hoxa13-/-

Figure 5.4

Figure 5.4: Tie2 in the developing placental vasculature

The Tie2 receptor was consistently expressed in *Hoxa13* heterozygous labyrinths (A, C, E), while it was reduced in *Hoxa13* mutant placental labyrinths (B, D, F). (G-H) Higher magnification of the labyrinth reveals Tie2 (red) colocalization with the Hoxa13^{GFP}+ nuclei (green). While Tie2 is strongly localized to the Hoxa13+/- endothelial cells (G), Tie2 is down-regulated in the mutant placenta ECs (H).

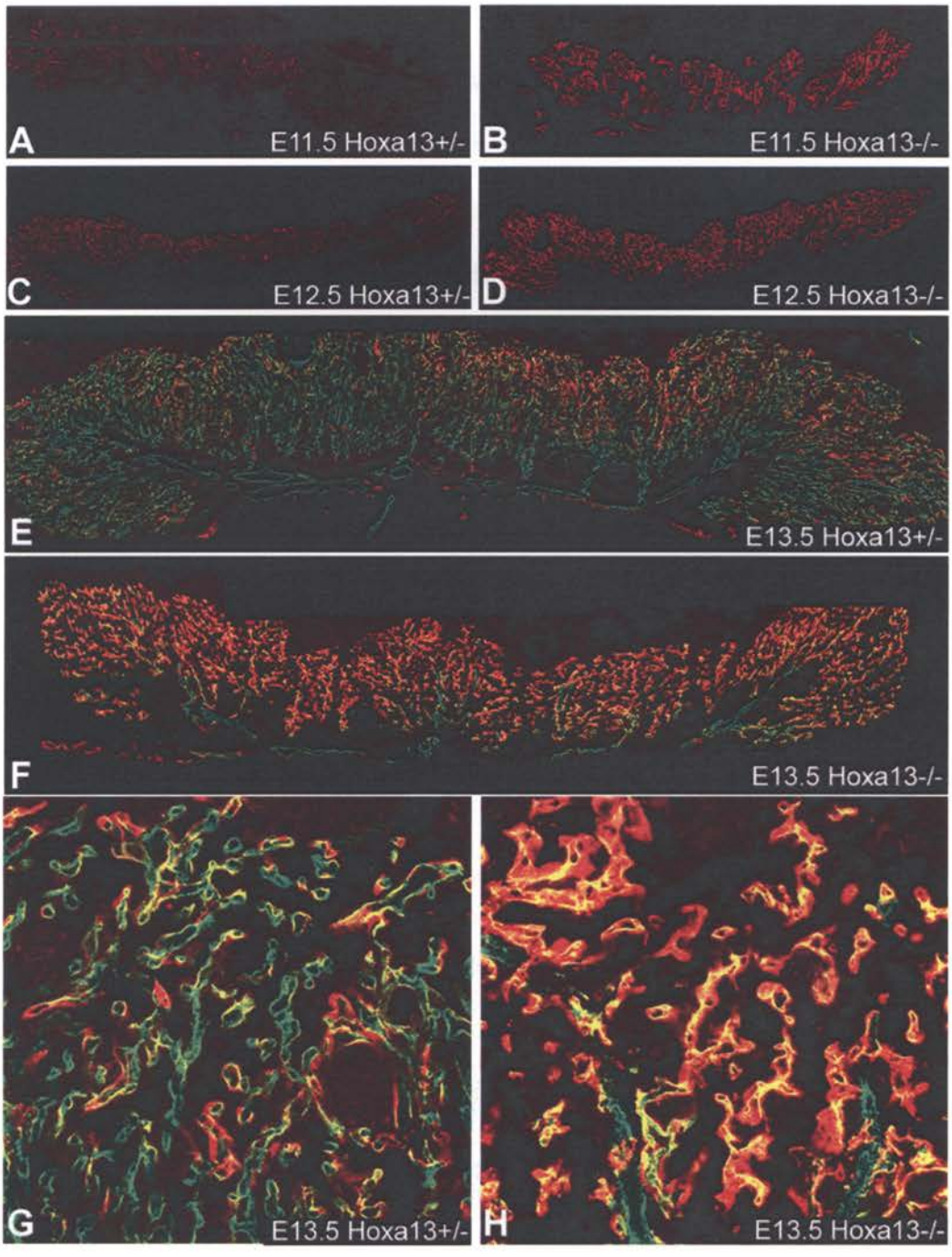
A
E11.5 Hoxa13+/-
B
E11.5 Hoxa13-/-
C
E12.5 Hoxa13+/-
D
E12.5 Hoxa13-/-
E
E13.5 Hoxa13+/-
F
E13.5 Hoxa13-/-
G
E13.5 Hoxa13+/-
H
E13.5 Hoxa13-/-

Figure 5.5

Figure 5.5: Lyve1 in the developing placental labyrinth

Immunohistochemistry using a Lyve1 antibody (red) and a PECAM-1 antibody (green) revealed colocalization within the placental blood vessels. At E11.5 (A-B), E12.5 (C-D), and E13.5 (E-H), Lyve1 is expressed at moderate levels within the *Hoxa13* heterozygous blood vessels (A, C, E, G), while it is highly over-expressed in the *Hoxa13* mutant vessels (B, D, F, H).

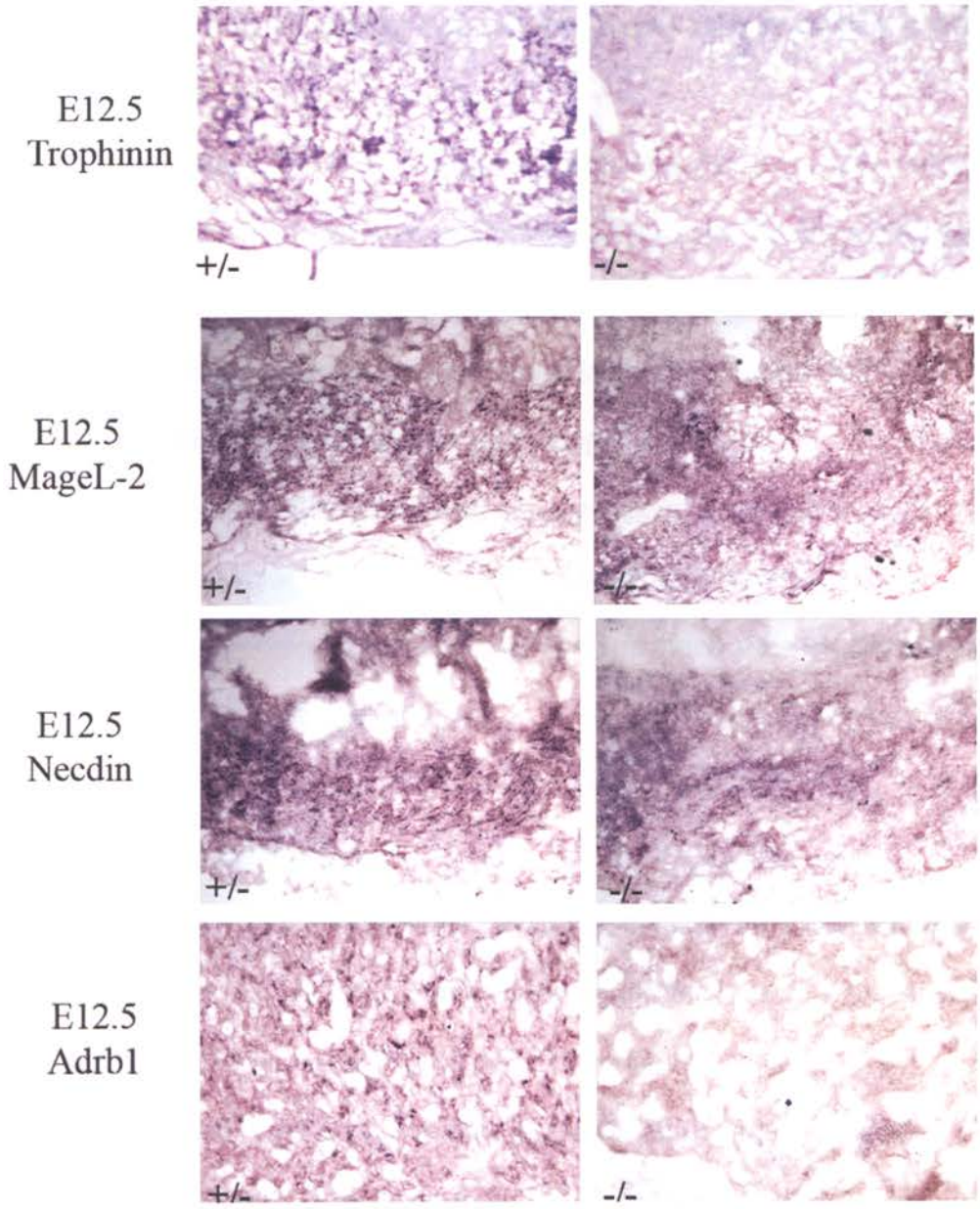

Figure 5.6: *In situ* hybridization on placental labyrinth sections

In situ hybridization (ISH) was performed on *Hoxa13* heterozygous and mutant E12.5 placental sections. While *trophinin*, *mageL-2, necdin,* and *adrb1* are expressed at moderate levels in the *Hoxa13* heterozygous placental labyrinths, the signal is absent or greatly reduced in the *Hoxa13* mutant placental labyrinths. Sections were counterstained with BC-50 to reveal tissue structure.

5C. HOXA13 directly regulates the transcriptional activation of important angiogenic factors

We hypothesized that HOXA13 directly regulates the transcription of some candidate target genes by binding to preferred HOXA13-binding site within the upstream promoter sequence. The following sections highlight the results from several complementary analyses we performed to identify whether HOXA13 binds to the promoters of candidate genes. Using the Ensembl Genome Browser (www.ensembl.org), the HOXA13 binding site was represented within regions from -3000 to -1 base pairs upstream of the transcriptional start sites of our candidate genes, and primers were designed to flank these sites for cloning and PCR amplification (Table B, see methods).

Chromatin Immunoprecipitation

To test our hypothesis that HOXA13 directly binds to the candidate gene promoter sequences *in vivo,* ChIP assays were performed on E13.5 placental labyrinths using an N-terminal HOXA13-specific antibody. As a result, we successfully amplified the *foxf1a* promoter region #2 and *tie2* promoter region #1 from HOXA13-ChIP DNA, while these regions were not amplified from the negative control samples (no antibody or pre-immune sera) (Figure 5.7-C). Importantly, while HOXA13 bound to these promoters in the heterozygous placentas, there was no binding in the mutant placentas since the mutant allele does not encode the C-terminus DNA-binding domain (Stadler et al., 2001). Therefore, regulation of gene expression by HOXA13 is dependent on direct

binding of the HOXA13 homeodomain (the 3rd alpha-helix) to DNA. Furthermore, HOXA13 directly binds to the promoters of *Tie2* and *Foxf1 in vivo*, and these promoters contain our defined HOXA13 DNA binding sites (Figure 5.7-A). To note, the Foxf1#2 promoter sequence is 85% conserved among mouse, human, and chimpanzee (*Pan troglodytes*), while the Tie2#1 promoter site is 50% conserved between mouse and human (Figure 5.7-B).

We were not able to amplify the *cd36* or *caveolin-1* promoters containing putative HOXA13 binding sites, and the *nrp1* ChIP PCR was indeterminate due to high background in the negative controls, presumably from PCR amplification of the salmon-sperm DNA blocking agent (data not shown). Since both Tie2 and Foxf1 are important molecules for angiogenic patterning and early development, we focused on these essential genes in our luciferase and anisotropy experiments to validate their regulation by HOXA13.

Foxf1 Promoter region#2 -1284bp to -1163bp

cgcgggcttctctact**cttattattaaagg**atcccccggaac
gtgtttacgttgagccttgtaaacttcctgccccggactttg
ccatctctcaggaaatcagaacctgcgcttgtaaaagg

Tie2 Promoter region #1 -2413bp to -2273bp

gggaaggggagtggataacaaactctgggagcagggacgggg
aaggagggcaacatt**tgtaattaaata**ataaaata**atttaa**
taaaaaaaatgaagaaacaggataacttgggaatggttacag
cagggctgggattag

A.

Foxf1

Tie2

B.

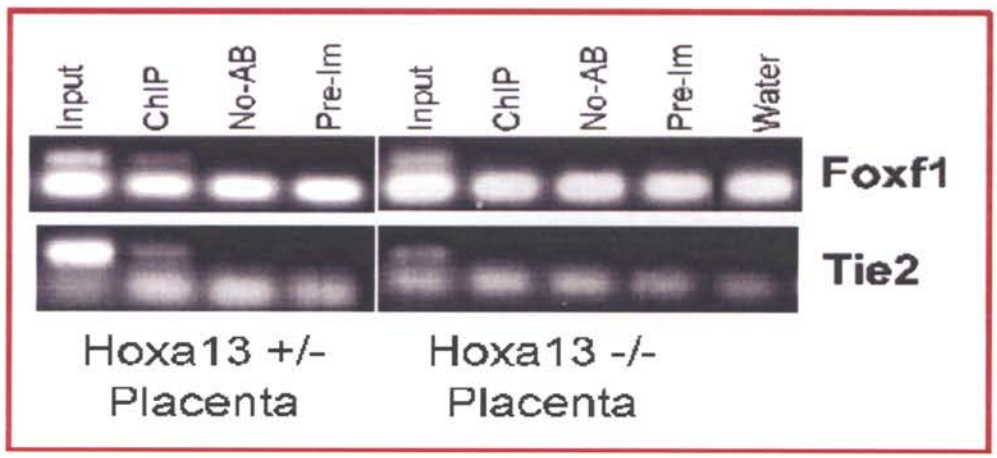

C.

Figure 5.7

Figure 5.7: ChIP assays show that HOXA13 directly binds to the promoters of *Foxf1* and *Tie2*

(A) The promoter sequences upstream of *Foxf1* and *Tie2* were tested by EMSA (Figure 5.9), luciferase assays (Figure 5.8), and ChIP assays (C), and these regions were chosen due to the presence of TA-rich HOXA13 binding sites. Key binding sites (red) were tested by fluorescence anisotropy (Figure 5.10)

(B) The promoter sequences of *Tie2* and *Foxf1* are conserved between mouse and other species. *Foxf1* region #2 is 85% conserved between mouse, human, and chimpanzee. *Tie2* region #1 is 50% conserved between mouse and human.

(C) Chromatin immunoprecipitation of HOXA13 from labyrinth tissue revealed that HOXA13 binds to the upstream regulatory regions of *Tie2* and *Foxf1*. Using PCR primers to flank key HOXA13 binding sites, promoter regions were amplified from *Hoxa13* heterozygous placentas, while they could not be amplified from *Hoxa13* mutant tissue or in ChIP experiments without antibody (No-AB) or with pre-immune sera (Pre-Im).

Luciferase assays

Complementary to the ChIP data, luciferase assays showed that HOXA13 can transcriptionally activate these promoters. pGL3-Basic vectors containing either the Tie2#1 (140bp) or Foxf1#2B (346bp) promoter regions were activated 3.2 fold and 3.6 fold, respectively, when co-transfected with HOXA13, while these vectors were not activated in the absence of HOXA13 (Figure 5.8). Removal of HOXA13 binding sites from the Foxf1 vector (Fox-del, 213bp) resulted in a loss of HOXA13-directed expression (Figure 5.8, Figure 6.2). A comparable deletion of the HOXA13 binding sites from the Tie2#1 vector could not be performed due to the small initial length of the promoter element.

Electrophoretic mobility shift assays (EMSA)

To confirm whether HOXA13 can bind to candidate gene promoters, we performed EMSA with the HOXA13 DNA-binding domain (A13-DBD) peptide and radio-labeled, PCR-amplified promoter regions. One to five nanograms of A13-DBD peptide was sufficient to shift two unique promoter fragments from both *tie2* (region #1: -2413bp to -2273bp) and *foxf1a* (region #2: -1284bp to -1163bp), as well as promoter regions from the genes *nrp1, enpp2, cd36, caveolin1, trophinin*, and *mageL-2* (Figure 5.9, and data not shown).

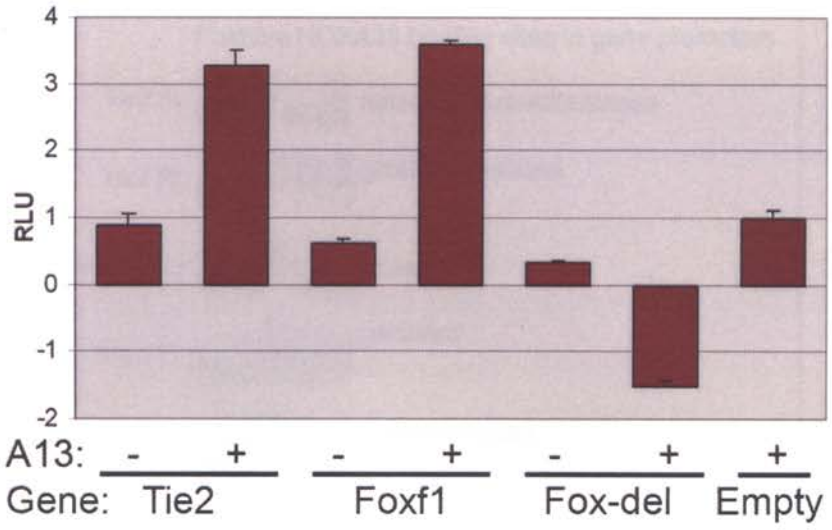

Figure 5.8: Luciferase assays test HOXA13's activation of *Tie2* and *Foxf1* gene promoters

Luciferase assays show that the co-expression of HOXA13 is sufficient to activate pGL3-Basic vectors containing either *Tie2* or *Foxf1* promoter regions. When HOXA13 binding sites are deleted from the Foxf1 vector, the ability of HOXA13 to activate the vector is lost. Each bar graph represents data from 3 replicate luciferase assays, and error bars represent the standard deviation.

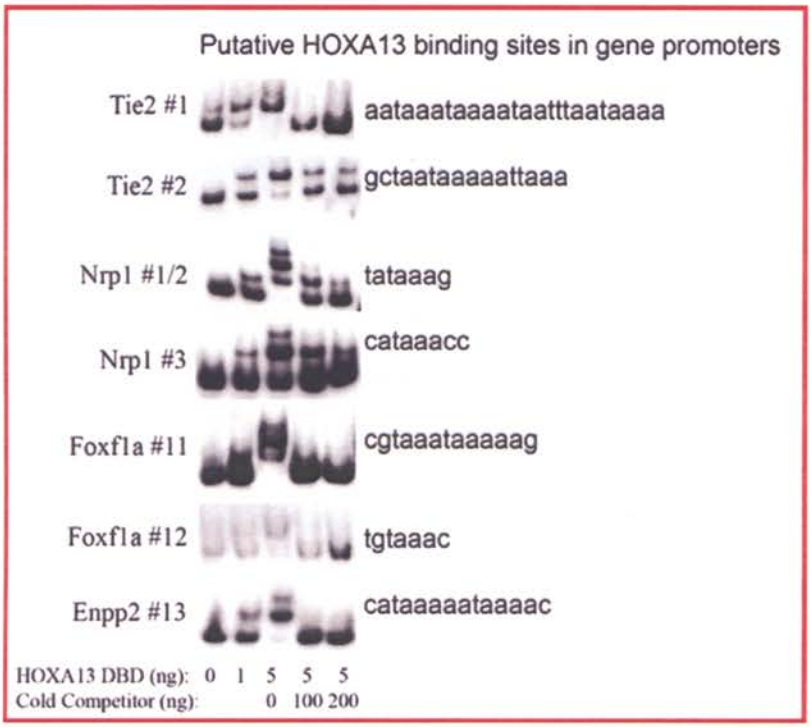

Figure 5.9: The HOXA13-DBD can bind to gene-specific promoter sequences

Electrophoretic mobility shift assays showed that the HOXA13 DNA-binding domain (A13-DBD) can bind to *Foxf1, Tie2, Enpp2,* and *Nrp1* promoter-specific DNA sequences. With 5ng of A13-DBD added to radio-labeled promoter-specific oligonucleotides, there was a complete up-shift of the oligo, while the addition of 'cold' non-radio-labeled oligos prevented the up-shift of the labeled oligo.

Fluorescence Anisotropy

Since we have shown than the A13-DBD can bind to the *Foxf1a* and *Tie2* promoters by EMSA, and HOXA13 specifically binds these promoters *in vivo* and *in vitro*, we used fluorescence anisotropy assays to quantify the binding affinity of the A13-DBD to putative HOXA13 binding sites represented within these promoter regions. Two consensus binding sites were analyzed from the *Tie2* promoter while one *Foxf1* site was analyzed (highlighted in red, Figure 5.7-A). A13-DBD bound to the Foxf1 site with a K_d of 42.6nM, while the D13-DBD bound with less affinity and a K_d of 105nM (n = 5). The A13-DBD bound to the Tie2-site#1 oligo giving a K_d of 27.8nM, while the D13-DBD bound with less affinity and a K_d of 72.5nM (n = 4). The Tie2-site#2 oligo was bound by the A13-DBD with a K_d of 31.6, while the D13-DBD bound with a K_d of 270.3nM (n = 3). (Figure 5.10) Overall, the A13-DBD peptide bound to the gene-specific sites with a much higher affinity (lower K_d) when compared to the D13-DBD. Control oligonucleotides consisting of TGAC repeats were tested, and neither the A13-DBD nor the D13-DBD showed binding to the control DNA (data not shown).

Overall, the anisotropy data will be helpful for future comparisons of the gene-specific binding affinity between HOXA13 and other transcription factors, as well as identifying the preferred binding sites of transcription factors. For example, our data shows differential binding of HOXA13 to HOXD13, and it proved to be an effective way to compare gene-specific binding sequences.

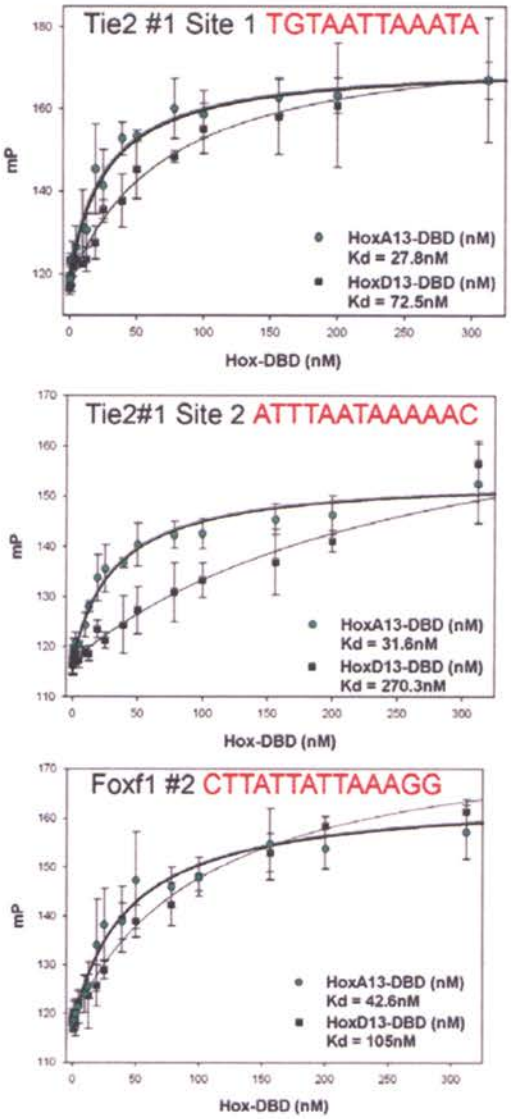

Figure 5.10: Fluorescence anisotropy quantitates the binding affinity of HOXA13-DBD to its target sites

The affinity of the HOXA13-DBD peptide (green circles) and HOXD13-DBD peptide (black squares) for unique potential HOXA13 binding sites (in red) was tested by fluorescence anisotropy. One Foxf1-#2 promoter site and two Tie2-#1 promoter sites were tested. Data curves and error bars represent averaged data from 4-5 separate experiments.

5D. Summary

My characterizations of the cellular and histological changes within the placenta due to loss of *Hoxa13* led to subsequent questions concerning the molecular mechanisms behind the observed phenotypes. What genes are misexpressed within the placenta and the endothelial cells due to the loss of *Hoxa13*? Does HOXA13 directly regulate the transcription of some of these genes? We began answering these questions using microarray technology and other methods to identify mis-regulated genes. Next, we tested the ability of HOXA13 to act on the promoters of these genes to affect their transcription. This approach proved successful in identifying multiple candidate genes, including two important EC-specific genes *Foxf1* and *Tie2* which are directly regulated by HOXA13.

Foxf1 is a transcription factor that is strongly expressed in the lung and placenta. While Foxf1-deficient mice have lung and early embryonic patterning defects, a placental phenotype has not been identified (Mahlapuu et al., 2001). Tie2 is an essential receptor on ECs, and mutant mice exhibit severe defects in vasculogenesis (see discussion) (Sato et al., 1995). Since Foxf1 and Tie2 are known to play a role in vascular formation and development, including vascular phenotypes in knockout mouse models, we primarily focused on testing the promoters of these genes. While the ultimate experiment would be to mutate the exact HOXA13-binding sites of these promoters *in vivo* or *in vitro*, this was not within the scope of my graduate research work. Furthermore, we believe that the positive complementary results from ChIP, luciferase assays, EMSA, and

fluorescence anisotropy strongly implicate HOXA13 as a direct regulator of *Tie2* and *Foxf1* in placental endothelial cells during their development and maturation.

Beyond the genes directly regulated by HOXA13, it is equally important to consider the global changes in EC gene expression due to the loss of *Hoxa13*. In HOXA13-deficient placentas, there is a dramatic change in vascular patterning and EC morphology, and this correlates with mis-expression of genes involved in cell adhesion, vascular growth factor binding, and EC signaling. The loss of *Hoxa13* alters EC patterning to such a degree that multiple genes are affected and can be observed through their gene expression profiles. Overall, *Hoxa13* deficiency in the placenta vasculature causes a change in the cells ability to properly differentiate and retain its cellular integrity, and this correlates with a loss of important angiogenic regulators and receptors, cell adhesion molecules, and other essential cellular components.

Chapter Six

Materials and Methods

Mouse model and placenta dissection

Mice used in this study were from the *Hoxa13*^{GFP} line, and mouse breeding strategies and genotyping techniques were previously described (Stadler et al., 2001). Proper mouse handling protocols and standard practices were followed. Gestational ages were defined by the detection of vaginal plugs at embryonic day (E) 0.5. To support our detailed analyses, only placentas from embryos that appeared healthy and with a strong heart beat were used for study. Placentas were dissected in cold PBS and fixed 3 hours to overnight in 4% PFA/PBS at 4°C on a rocker. For frozen sections, placentas were treated with a 10-30% sucrose/PBS gradient, embedding in OCT, and stored at -80°C.

Immunohistochemistry

OCT-embedded tissues were sectioned at 17-20μm on a Leitz Kryo-Stat 1740, mounted on Superfrost slides (Fisher), and stored at 4°C. All immunohistochemistry (IHC) washes were performed in 4-slide pap tubes and at room temperature. Slides were rehydrated in 1XPBS for 5 minutes, followed by a 45 minute pre-block in PBSTM+D [4% powdered milk, 5% normal donkey serum (Jackson ImmunoResearch, #017-000-121), 0.5% Triton-X100, in PBS]. Primary and secondary antibodies were diluted in blocking buffer, tissue on the slides were isolated using a Super Pap Pen (The Binding Site, Inc). Tissue slides were treated with primary antibody overnight at 4°C and with secondary antibody for 2-3 hours at room temperature, all within a humidity chamber. After each antibody treatment, the slides were washed with wash buffer (4% powdered

milk, 0.5% Triton-X100, in PBS) for 2 x 1 hour on a rocking stage. After the secondary antibody treatment and washes, slides were given 2 x 30 minute washes in PBS. Slides were analyzed using a Leica DMR confocal microscope with a Bio-Rad MRC 1024 laser and software, typically using a 20x objective.

The following antibodies and dilutions were used for IHC: PECAM-1 for sections (#550274, BD Pharmingen, 1:200), GFP (AB3080, Chemicon, 1:100), Lyve1 (ab14917, Abcam, 1:500), Tie2 (MAB1148, Chemicon, 1:200), Foxf1 (AB4128, Chemicon, 1:500), VEGF (Abcam, 1:50). The anti-rabbit neuropilin-1 polyclonal antibody was generously provided by Dr. David Ginty (1:500). Cy5 and Texas Red fluorescence-tagged secondary antibodies were used for most IHC experiments [Jackson ImmunoResearch: Texas Red AffiniPure Donkey anti-rabbit IgG (#711-075-152) or Donkey anti-rat IgG (#712-075-150); Cy5 AffiniPure Donkey anti-rabbit IgG (#711-175-152) or Donkey anti-rat IgG (#712-175-150)].

Section *In situ* hybridization

In situ hybridization (ISH) and riboprobe synthesis experiments were carried out as previously described (Manley and Capecchi, 1995; Schweitzer et al., 2001; Morgan et al., 2003). OCT-embedded tissues were sectioned at 17-20μm on a Leitz Kryo-Stat 1740, mounted on Superfrost slides (Fisher), and stored at -20°C. Wax-embedded tissues were sectioned at 7-10μm on a Leica BM2135 microtome and mounted on slides as above. During *in situ* hybridization experiments, all reagents were treated with DEPC.

Section *in situ* hybridization was performed as previously published (Schweitzer et al., 1993) with few modifications. OCT-embedded placenta tissue sections were typically used, and the sections were rehydrated in PBS. The steps to ISH are as follows.

Day 1: fix in 4% PFA/PBS 10 minutes, rinse in PBST (1XPBS, 0.1% Tween-20), and wash 2 x 5 min in PBST. Treat with Proteinase-K 5 min (1ug/mL in PBS), wash 2 x 5 min in PBST, re-fix in 4% PFA/PBS 5 min, and wash 2 x 5 min in PBST. Next, treat with acetylation buffer 15 min (2.5% acetic anhydride, 0.1M triethanolamine in water) and wash 2 x 5 min in PBST. Air dry the slides 10 min on bench top, then treat each slide with 100λ pre-warmed hybe solution and a coverslip with plastic for 2-4 hours at 65°C, and finally treat with hybe solution containing 1% riboprobe overnight at 65°C in a humidity chamber. The hybe solution contains 100mM Tris pH7.5, 600mM NaCl, 1mM EDTA, 0.25% SDS, 10% Dextran sulfate, 1X Denhardt's buffer, 200ug/mL yeast tRNA, 50% formamide, and it is stored at -20*C.

Day 2: Rinse slides in 5x SSC, treat with 1x SSC/ 50% formamide for 30 min at 65°C, then TNE for 10 min at 37°C, TNE with 20ug/mL RNaseA for 30 min at 37°C, and TNE for 10 min at 37°C. Wash in 2x SSC for 20 min at 65°C and 2x SSC for 2 x 20 min at 65°C. Next, wash slides 2 x 5 min in MABT (100mM Maleic acid, 150mM NaCl, 0.1% Tween-20, pH 7.5), pre-block 2 hours with 20% fetal lamb serum in MABT, and incubate with alkaline phosphatase-conjugated anti-DIG antibodies in 5% serum/ MABT overnight at 4°C in humidity chamber.

Day 3: After 3 x 5 min. washes in MABT and a 10 min pre-soak in color reaction buffer (100mM NaCl, 100mM Tris pH 9.5, 50mM $MgCl_2$), the color reaction was induced with BCIP/NBT in color reaction buffer. Color reactions were monitored under the microscope and quenched by 2 x 5 min washed in PBS when the color reaction was strong and when little background was observed. The color reactions were fixed for 30 minutes in 4% PFA/PBS, followed by 2 x 5 min washes in PBS.

To detect the spongiotrophoblasts and cytotrophoblasts, *Tpbp* and *Gcm1* riboprobes were generated from plasmids which were generously provided by Dr. James Cross (University of Calgary), and ISH with these riboprobes utilized wax-embedded placentas. *Trophinin*, *mageL-2, necdin*, and *adrb1* riboprobe clones were synthesized by PCR amplification using the following primers: *Trophinin*: 5′-TTTTGGTGGTGCACCTTGTA-3′ and 5′-CCACCGAAGTTGGTACTCGA-3′ (NM0195481, 837 bp amplicon); *MageL-2*: 5′-GCTCTGCAGGATCCTTATGC-3′ and 5′- CACTGAGGGTACGCCATCTT-3′ (NM013779, 797 bp amplicon); *Necdin*: 5′-CCCGAAGAACGGATAGAAGA-3′ and 5′-GCCCCTGGACCTTTTTAGTC-3′ (NM010882, 809 bp amplicon); *Adrb1*: 5′-CTTCTGCGAGCTCTGGACTT-3′ and 5′-CCCAGCCAGTTGAAGAAGAC-3′ (NM007419, 678 bp amplicon).

Whole placenta immunohistochemistry

For whole placenta IHC, placentas were bisected with a double-edge razor before fixation in 4% PFA/PBS, 3-4 hours at 4°C. All steps were performed

in 12-well Costar dishes on ice or the in 4°C cold room on a rocker. Placentas were washed in PBS, methanol dehydrated (10, 20, 30, 50, 75%), treated for 4 hours with 4:1:1 methanol/30% H_2O_2/DMSO, and rehydrated in a methanol/PBS series (50%, 40%, 30%, 20%, 10%, PBS, PBS). Next, placentas were pre-treated with PBSTM (2% powdered milk, 0.5% Triton-X100, in PBS) for 45 minutes, blocked for 45 minutes with PBSTM + 2% heat-inactivated donkey serum (Jackson Immuno), then treated overnight with anti-rat PECAM-1 primary antibody (MEC13.3, #553369 BD Pharmingen, 1:200) in blocking buffer. Following extensive PBSTM washes (5 x 45 minutes) at room temperature, samples were treated overnight with Donkey anti-rat peroxidase-conjugated secondary antibody (Jackson Immuno #712-035-153, 1:400) in blocking buffer. The next day, color reactions were performed as follows, all steps at room temperature: wash placentas 4 x 30 minutes with PBSTM, wash for 30 minutes in PBT (PBS, 0.2% BSA, 0.5% Triton-X 100), pre-incubate for 30 minutes in 1 part PBT and 2 parts DAB solution (1 Sigma Fast DAB tablet in 15 mL water), and treat with 2 mL of color reaction solution [Sigma Fast DAB tablet system (#D4418) and 10mg nickel chloride in water, filter sterilized], monitoring carefully the color reaction progression under a dissecting microscope. Placentas were washed 4 x 5 minutes in PBT, stored in PBS, and photographed while in PBS. Placentas were photographed at 1x to 8x magnification using a digital camera mounted on a dissecting light microscopy.

LacZ staining of placenta sections

The *Tie2-LacZ* mouse strain (Jackson Laboratory; FVB/N-TgN(TIE2LacZ) 182Sato) was crossed with *Hoxa13*^{GFP} heterozygous mice to create *Hoxa13+/-; Tie2-LacZ+* mice for breeding (Sato et al., 1995; Sato et al., 1997). LacZ staining of whole tissues and cryosections was performed as previously published (Sato et al., 1995). Slide mounted placenta cross-sections were rinsed with PBS, post-fixed for 20 minutes in 2% PFA/ Pipes, rinsed with PBS, and washed 2 x 20 minutes in wash buffer (2mM $MgCl_2$, 0.02% NP-40, 0.01% sodium deoxycholate, PBS). Slides were treated overnight in staining buffer (1 mg/mL X-gal, 5 mM potassium ferricyanide, 5 mM potassium ferrocyanide, in wash buffer), rinsed in wash buffer and PBS, counterstained with BC-50 Red Counterstain (M11, Biomeda), and treated with Situ/Mount (M04, Biomeda). Placentas sections were photographed at 2x to 8x magnification using a digital camera mounted on a Leica DM-LB2 light microscopy.

Transmission Electron Microscopy (TEM)

The placenta labyrinths were analyzed by the Shriner's Research Center Core EM lab. After placenta dissection in PBS, placentas were bisected and fixed for two hours in 1.5% glutaraldehyde/ 1.5% formaldehyde/ 5% sucrose/ 0.05% tannic acid in DMEM. After fixation, samples were post-fixed in 1% osmium tetroxide, dehydrated in ethanol, and embedded in spurrs epoxy. Samples were post-stained in 2% ethanolic uranyl acetate and Reynold's lead

citrate. Samples were examined using a Philips 410 transmission electron microscope.

EC counting and morphological scoring

E13.5 placentas were sectioned at 1 um, mounted on slides, and counterstained with toluidine blue with basic fushin. For each placenta sample, the section with the largest surface area was chosen for photography and cell counting and scoring. Therefore, 7-10 photos were scored per placenta, representing the complete labyrinth surface area. Multiple placentas and sections were analyzed: 3 wildtype placentas (25 photos; 1510 endothelial cells), 5 *Hoxa13* heterozygous placentas (38 photos; 1938 ECs), and 5 *Hoxa13* mutant placentas (39 photos; 1301 ECs). Within each photo, fetal labyrinth lumens were identified, and all ECs with a visible nucleus were counted and their morphology scored as either normal (smooth EC layer and lumen), intermediate (cell rounding or irregular shape), or abnormal (cell detachment, edema, diminished cell body). The average percentage of each cell morphology type was calculated.

Microarray and statistical analysis

E13.5 mouse placentas were dissected to isolate the umbilical vasculature, labyrinth placenta, and spongiotrophoblast tissues. Tissues were dissected in RNAlater (Ambion), flash-frozen in liquid nitrogen, and stored at -80°C. The RNA STAT-60 (Tel-Test, Inc.) and RNeasy Micro Kit (Qiagen)

systems were employed for RNA extraction, following manufacturer's protocol. Briefly, within 1.5 mL tubes, tissues were homogenized in 1 mL RNA STAT-60 using a 1.5 mL-tube dowel, treated with 0.2 mL chloroform for nucleic acid extraction, followed by isopropanol precipitation on ice and resuspension in RNase-free water. The RNA was cleaned and isolated using the RNeasy Micro Kit (Qiagen), following manufacturers protocol. For representative microarray RNA samples, three RNA samples of like genotype were pooled. Placental samples comprised the following genotypes: wildtype female, wildtype male, *Hoxa13* mutant female, and *Hoxa13* mutant male.

Microarray analyses were performed by the Affymetrix Microarray Core of the OHSU Gene Microarray Shared Resource using the GeneChip Mouse Expression Set 430 gene chip arrays. Since individual male and female arrays were nearly indistinguishable in genotype comparisons, and there was no sex-specific placenta phenotype, we combined the male and female array data sets to give 6 total array data sets to compare mutant and wildtype placentas. Two-Factor Analysis of Variance (ANOVA) statistical analysis was used to define the False Discovery Rate (FDR) and Fold Change when factoring in genotype and sex, as performed by the Biostatistics and Bioinformatics Shared Resources (OHSU).

Collection of placenta endothelial cells for cDNA synthesis

The extraction and isolation of EC was achieved by adapting previously published methods (Silverman et al., 2001) and by the kind support of Dr. David Zamora, OHSU Ophthalmology. Furthermore, this method was utilized in our

studies of blood vessels of the external genitalia (Shaut et al., 2006, submitted manuscript, see Appendix 3).

E13.5 placenta ECs were dissected from fresh placentas as for the microarray. Two to three placentas of similar *Hoxa13* genotype were combined. Samples were treated with 0.2% Collagenase Type IV (Gibco) at 37°C for 30 minutes. Tissue was then transferred to individual Netwells in 12-well dishes (Costar) and treated with digestion media (0.1% Trypsin/EDTA, 0.2% Collagenase IV, in PBS) for 30 minutes at 37°C, pipeting to break up the tissue every 10 minutes. Magnetic Dynabeads (M450, Dynal Inc.) were coated with an anti-mouse PECAM-1 antibody (MEC 13.3, #553369 BD Pharmingen) as described by the manufacturer. In 0.7 mL micro-tubes, 2.5 x 10^6 cells were combined with 1 x 10^7 beads PECAM1-coated Dynabeads (4x more beads than cells), incubated for 1 hour at 4°C on rotating platform, followed by the addition of 200 μL 1x PBS to prevent trapping of unbound cells. The bead-antibody-cell complexes were isolated using a magnet and the remaining cell supernatant was collected as a PECAM (-) control. The cell complexes were gently washed 4 times with 0.1% BSA/PBS and collected for RNA extraction.

RNA was extracted from both the PECAM (+) and PECAM (-) cell samples as with the microarray samples, and treated with DNase (#79254, Qiagen) to remove genomic DNA. One μg of RNA was used for cDNA synthesis using the Superscript First-Strand Synthesis system (#12371-019, Invitrogen). For qRT-PCR, cDNA was diluted 1:10 with water to make a 200 λ working solution.

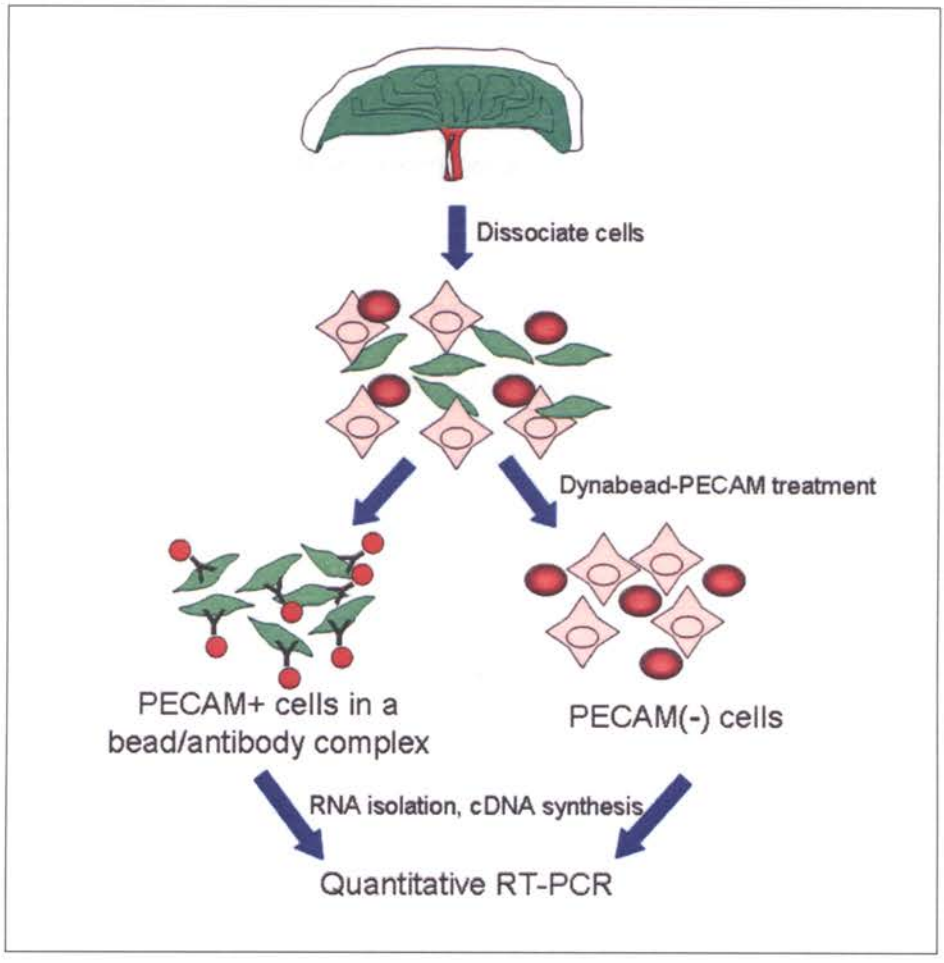

Figure 6.1: Isolation of placental ECs by PECAM-bead purification

After dissociation of cells from E13.5 placental labyrinths, the cells were treated with PECAM-coated magnetic beads and the PECAM+ endothelial cells were isolated from other cells such as trophoblasts. RNA was purified from each cell fraction for cDNA synthesis and qRT-PCR comparisons of gene expression.

Quantitative Real-time PCR (qRT-PCR):

qRT-PCR was used to detect gene expression levels within cell-specific cDNAs. Samples included: PECAM (+) wildtype cDNA, PECAM (+) *Hoxa13* mutant cDNA, PECAM (-) wildtype cDNA, and PECAM (-) *Hoxa13* mutant cDNA.

qRT-PCR reactions were performed in triplicate, and each gene primer set was tested against 4-5 separate cDNA samples using the SYBR Green PCR Master Mix (Applied Biosciences). Each reaction contained 1x SYBR Green PCR Master Mix (#4309155, Applied Biosciences), 0.15 U Uracil DNA glycosylase (#18054-015, Invitrogen), 0.80 μM forward and reverse primers, and 1.2 μL of the 200 μL qRT-PCR data was normalized to a control gene expression (gapdh or actin). All qRT-PCR reactions were performed using an Applied Biosystems Model 7700 Sequence Detector, a shared resource of the Dermatology Division and the Department of Cellular and Developmental Biology at OHSU. The candidate gene primer sequences are listed in Table A, and their amplicon size and gene location are as follows: *trophinin,* 136 bp, exon 3-4; *mageL-2,* 132 bp, exon 1; *necdin,* 134 bp, exon 1; *adrb1*, 100 bp, exon 1; *enpp2*, 120 bp, exon 24-25; *tie2*, 104 bp, exon 13-14; *foxf1*, 126 bp, exon 1-2; *neuropilin-1,* 115 bp, exon 12-13; *caveolin-1,* 136 bp, exon 1; *CD36,* 143 bp, exon 3; *lyve-1*, 150 bp, exon 2-3. The primer sequences for the control genes (*gapdh*, *actin*, and *pecam-1*) are as follows: *pecam-1*, For-5′-CCAGTGCAGAGCGGATAAT-3′, Rev-5′-GCACCGAAGTACCATTTCAC-3′ (148 bp, exon 7-8); *actin,* For-5′-CCTGCCATGTATGTGGCTAT-3′, Rev-5′-CTCATAGATGGGCACGTTGT-3′ (114 bp, exon 3-4); *gapdh* For-5′-CACTGCCACCCAGAAGACTGT-3′, Rev-5′-GGAAGGCCATGCCAGTGA-3′ (147 bp).

Table A: Microarray and qRT-PCR analysis of gene transcription comparing mutant and wildtype tissue

Affymetrix array probe ID	Gene	GO: Molecular Function/ Biological Process	qRT-PCR Primers (5' - 3')	MUT/WT Fold Change	
				Whole placenta microarray	Endothelial cell-specific qRT-PCR
1421201a_at	*Trophinin*	Cell adhesion / Cell growth and organization	GAACCCACGACCAGAACC – For GCAAAATGGCCACATCTC – Rev	-2.16	-5.4
1448136_at	*Enpp2*	Hydrolase and nucleotide diphosphatase activity / Chemotaxis; cell motility	CCGACCTGACAATGATGAGA – For AAATCCAAACCGGTGAGATG – Rev	-2.33	-23.1
1417217_at	*Magel-2*	Protein binding / Regulation of transcription	AACGCTTTGGTGCAGTTTCT – For CTTAGTGTTGGCACGGTTGA – Rev	-2.87	-98.9
1449145a_at	*Caveolin-1*	Protein binding / Vasoconstriction; vasodilation; EC proliferation	GGGAACAGGGCAACATCTAC – For AACACGTCGTCGTTGAGAT – Rev	-1.92	-3.6
1423420_at	*Adrb1*	Receptor activity / Blood pressure regulation; vasodilation	GCTGATCTGGTCATGGGATT – For AAGTCCAGAGCTCGCAGAAG – Rev	-1.93	-8.0
1418788_at	*Tie2 (Tek)*	Receptor activity / Regulation of angiogenesis and cell migration; cell adhesion	TGAGGACGCTTCCACATTC – For CAACAGCACGGTATGCAAGT – Rev	-1.55	-2.2
1429379_at	*Lyve1 (Xlkd1)*	Receptor activity; hyaluronic acid binding / Cell adhesion	AGCCAACGAGGCCTGTAA – For CACCTGGGGTTTGAGAAAAT – Rev	+3.58	+4.4
1450883a_at	*CD36*	Receptor activity / Cell adhesion; fatty acid and lipid metabolism and transport	GAGTTGGCGAGAAAACCAGT – For GTCTCCGACTGGCATGAGA – Rev	-2.28	-2.9
1418084_at	*Neuropilin-1*	Receptor activity; VEGF receptor activity / Angiogenesis; cell migration	TGTCCTGGCCACAGAGAAG – For CCAGTGGCAGAATGTCTTGT – Rev	-1.29	-7.4
1435382_at	*Necdin*	Transcription factor / Cell growth and migration	TGGTACGTGTTGGTGAAGGA – For AACACTCTGGCGAGGATGAC – Rev	-1.81	-7.7
1434939_at	*FoxF1*	Transcription factor / Vasculogenesis; organ development; ECM organization	GCAGCCATACCTTCACCAA – For GCCATGGCATTGAAAGAGA – Rev	-1.3	-2.9

Electrophoretic mobility shift assay

Electrophoretic mobility shift assays (EMSA) with the A13-DBD were performed as previously described (Knosp et al., 2004). Gene promoter regions of 100-150 bp, spanning potential HOXA13 binding sites from 1000-3000 bp upstream of the transcriptional start site, were amplified by PCR. PCR products were isolated by agarose gel extraction using the QIAquick Gel Extraction Kit (#28704, Qiagen), quantified by UV spectroscopy, and sequenced to confirm the correct gene promoter sequence. The candidate gene promoter regions and PCR primers are listed in Table B. PCR amplicons were labeled with [γ-^{32}P]-ATP (3,000 Ci/ mmol) using the T4 polynucleotide kinase system (Promega), followed by purification over sepharose bead columns to remove unincorporated ATP. Gel shifts were performed using the Promega Gel Shift Binding System (#E3050), following the manufacturers protocol. DNA-peptide binding reactions were run on 4-6% gels, dried on gel dryers, and exposed to film for 30 minutes to overnight at -80°C.

Table B: PCR primers and promoter gene regions tested by EMSA and ChIP

Gene	Region #	Forward primer 5'-3'	Reverse primer 5'-3'	Product size (bp)	RefSeq	Bases from translational start site (Ensembl)
Enpp2	1	AAGGCTATCCTCCTGACTGC	ATGTCTCCACCCCCAACAG	100	NM_015744	-2456 to -2555
Enpp2	2	TCCACACATGGAAAGCACAT	CTAAATGCATACACACCATCTAGC	103	NM_015744	-2240 to -2138
Enpp2	3	GTGACCAACTTGCTCTCACG	ATACAGCTCAGAAACTGAAGATCA	112	NM_015744	-1864 to -1753
Foxf1a	1	TGAGGTACAGCCCAGAGTCC	CACACCCCCAAGTTTTCTTC	138	NM_010426	-2368 to -2231
Foxf1a	2	CGCGGGCTTCTCTACTCTTA	CCTTTTACAAGCGCAGGTTC	122	NM_010426	-1284 to -1163
MageL-2	1	AACGAGCCTGTTTTCCTCAA	GGGGGAATACAATCCTTTGG	120	NM_013779	-3910 to -3791
MageL-2	2	GGATTGTATTCCCCCGATTT	TGCAAAACAAGGTTGCCTTC	144	NM_013779	-3809 to -3666
MageL-2	3	ACTGCCCTAGGCTGCAAAC	TTGGTATTCTTTCTCCCCAAAA	120	NM_013779	-3389 to -3270
Meox2	1	AACACTTGAAAAACAAAACATCC	TTGCACAACTTTCAAAAACTTCA	92	NM_008584	-3252 to -3161
Meox2	2	GCTTTCAGTCGAGGGATCTT	ACCCTGGGTTCTGAAAGCAT	123	NM_008584	-2550 to -2428
Meox2	3	TTTGGAAGTTCCTTTTCTGGA	CCAAGGCAGAACCCTTCTCT	98	NM_008584	-1863 to -1766
Nrp1	1	TGTCTCCTAGGCAGATCTGTGA	GCAAGTGTGAGACAGAGGAAGA	106	NM_008737	-3239 to -3134
Nrp1	1-2	TGTCTCCTAGGCAGATCTGTGA	TACTTCTCCACCCAGGGAAA	146	NM_008737	-3239 to -3094
Nrp1	3	TTGATCAGAAGCCTCAACCA	TGTAGTCCGGTTCCATCCTC	109	NM_008737	-1716 to -1608
Tie2	1	GGGAAGGGGAGTGGATAACA	CTAATCCCAGCCCTGCTGTA	141	NM_013690	-2413 to -2273
Tie2	2	CTTCCTGTGCCAAGTTCTCC	GACCAGATTCCACAGCCATT	158	NM_013690	-859 to -702
Cav1	1	ATAGCACGCCGTTCCCATTA	CGGCTGATAGGGAAGCAAT	151	NM_007616	-2849 to -2699
Cav2	1-2	GTGTCACACCCTGATAAAAATAAA	CGGCTGATAGGGAAGCAAT	124	NM_007616	-2822 to -2699
CD36	1	CCAAACATATGCAGCCTGAC	TCCCTATTCTGGAGGGATCTT	117	NM_007643	-2576 to -2460
CD36	2	CGGAATGCCCATAGTGTTCT	TGCCCATCATTTAGATGAAAAA	105	NM_007643	-1892 to -1788
CD36	3	GGGGGAAGATTTCTATGCTTTC	GTTATTCTATGAGCAATTCCAACA	102	NM_007643	-1423 to -1319

Luciferase Assays

The promoter regions tested by gel shifts (Table B) were cloned into the pGL3-Basic vector (Promega) in the forward and reverse orientation, as determined by direct sequencing from the RVprimer3 site. Luciferase assays, fluorescence detection, and NG108-15 cell culture were performed as previously described (Knosp et al., 2004) including luciferase transfection standardization to a Renilla control plasmid (Promega). NG108-15 cells were cultured in HAT media: 10% fetal bovine sera (Gibco), 2x HAT media (MP Biomedicals), 1% HyQ penicillin-strepomycin, in 1x DMEM without sodium pyruvate (Cell Gro 10-017-CV). Transfections were performed using the Superfect reagents and following manufacturer's protocols (Qiagen), and the cells lysates were collect in 100 μL M-PER lysis reagent (Pierce) 48-hours post-transfection. To detect fluorescence, the Dual-Glo Luciferase Assay system (Promega) and a Packard Fusion Universal Microplate Analyzer (Perkin-Elmer) were utilized in these assays. For each experimental condition, 3 replicate assays were performed consisting of 4 replicate cell treatments per assay.

A larger Foxf1 promoter #2 construct (Foxf#2B) was created containing the sequences –1315 to –970 (346bp) from the transcriptional start site, and a Foxf1#2 deletion construct (Foxf#2-Δ, 213bp) lacked the Hoxa13 binding sites (del -1283 to -1152) and was created using two *SstII* sites (Figure 6.2)

Foxf1#2B promoter construct (346 bp)

ataggggcatcaggccaactccccccgcgccgcgggcttctctactcttattat
taaaggatccccggaacgtgtttacgttgagccttgtaaacttcctgccccggactttg
ccatctctcaggaaatcagaacctgcgcttgtaaaaggggacacggggccgcgggccaa
ctaagcggatttcagagttaagcgtgggggggaggggctccgaggagactttgctctgtg
aattcagatctgagagtggcagcttcccgggggaccctggggaacgtgagtggggagcgc
actggtgcaagcctgcgcgtctaagttggtgattagaggattcgcttgggg

Foxf1#2-del promoter construct (213 bp)

ataggggcatcaggccaactccccccgcgccgcgggccaa
ctaagcggatttcagagttaagcgtgggggggaggggctccgaggagactttgctctgtg
aattcagatctgagagtggcagcttcccgggggaccctggggaacgtgagtggggagcgc
actggtgcaagcctgcgcgtctaagttggtgattagaggattcgcttgggg

Figure 6.2: Luciferase assay constructs of the *Foxf1* promoter region #2

Putative HOXA13 binding sites are red, while SstII sites are green. Primers are underlined text, showing forward primers F13 and reverse primer R14.

Chromatin Immunoprecipitation (ChIP)

Whole placentas were cut into 2 mm portions and fixed in 1% formaldehyde solution for 2 minutes, followed by treatment with 1M glycine/PBS/protease inhibitors. Tissue was digested in cell lysis buffer for 10 minutes on ice, followed by ten minute incubation in SDS Lysis buffer (Upstate Biotech) and homogenization using microcentrifuge tube dowels. Sonication was performed in a Biorupter sonicator (CosmoBio) for 15 minutes for 30 seconds on/ 1 minute off cycles in an ice bath. DNA shearing (100-500 bp) was confirmed by running sonicated chromatin on an agarose gel along with a DNA ladder. The HOXA13 protein was detected by Western-immunoblot using the polyclonal rabbit anti-Hoxa13 antibody (1:200). ChIP was performed using the methods and solutions of the Upstate ChIP Assay Kit (Cat #17-295), followed by DNA purification using the Qiaquick PCR Purification kit (Qiagen). PCR primers used in the Chip PCR were the same as those used for gel shift promoter analysis

(Table B), and PCR was performed using minimal cycle times in order to obtain data in the linear range of amplification. The ChIP assay was performed in triplicate using unique placenta samples.

Fluorescence Anisotropy

Following published protocols (Knosp et al., 2004), fluorescence anisotropy was performed using A13-DBD and D13-DBD peptides and gene promoter-specific oligonucleotides comprised of double-stranded DNA and 5 cytosine residues for the loop (shown in lower case below). Each gene-specific oligonucleotide displayed 14 base-pairs of double-stranded DNA in an annealed hairpin loop (shown in uppercase below). The DBD peptides were tested in concentrations from 0.22 nM to 400 nM. The HPLC-purified, fluorescein-labeled (5′ 6-FAM) oligonucleotides were purchased from Integrated DNA Technologies:

Tie2#1: 5′- CTGTAATTAAATACccccGTATTTAATTACAG -3′

Tie2#2: 5′- CATTTAATAAAAACccccGTTTTTATTAAATG -3′

Foxf1: 5′- CTTATTATTAAAGGccccCCTTTAATAATAAG -3′

TGAC control: 5′- TGACTGACTGACTGccccCAGTCAGTCAGTCA -3′

The HOXD13-DBD peptide was used as a control comparison of HOX transcription factor binding capabilities. Millipolarization was counted using the Beacon 2000 Fluorescence Polarization System (Panvera Corp.). This was shown graphically by plotting the peptide concentration and the millipolarization (mP), and stronger interactions are indicated by a steeper binding curve. Each plot represents the average mP from three separate replicate experiments for each condition with error bars showing statistical significance.

Chapter Seven

Conclusions and Discussion

Conclusions and Discussion

7A. Summary of our discoveries

As a member of a highly conserved family of homeodomain-containing HOX transcription factors, HOXA13 plays an important role in patterning the developing limb autopod, urogenital system, and the UA (Stadler et al., 2001; Morgan et al., 2003; Knosp et al., 2004). To study HOXA13 function, we use a mouse model of *Hoxa13* that replaces the conserved DNA-binding homeodomain with a cassette for *GFP*, effectively deleting functional HOXA13 while creating a fusion protein that marks *Hoxa13*-expressing cells with detectable fluorescence (Stadler et al., 2001). Important to this study, loss of *Hoxa13* in knockout mice leads to patterning defects in the tissues where it is expressed, along with mid-gestation lethality around E13.5 to E14.5. Previous studies have noted the expression of *Hoxa13* in the placenta and umbilical arteries (Warot et al., 1997; Stadler et al., 2001), but a full characterization and analysis of associated *Hoxa13* mutant phenotypes were unpublished.

Due to the intriguing initial phenotypes in the heart and UA due to loss of *Hoxa13*, we chose to elucidate additional cardiovascular developmental defects, beginning with a full characterization of extra-embryonic *Hoxa13* expression. Surprisingly, we found that *Hoxa13* is expressed much earlier than predicted or previously reported, at E7.75 in the emerging allantois, the mesenchymal tissue budding from the posterior hindgut into the extra-embryonic coelom. Expression of *Hoxa13* persists in the E8.5 allantois as it fuses to the chorion and establishes

the nascent chorio-allantoic placenta at E10 (Hemberger and Cross, 2001). By E11.5, the three placental layers are well established: the proximal labyrinth layer, the outer giant trophoblast decidua, and the middle spongiotrophoblast layer (Rossant and Cross, 2001). *Hoxa13* was expressed exclusively within the ECs of the placental labyrinth layer and not within any trophoblast cells. The fetal and maternal blood spaces become denser and more integrated via the angiogenic remodeling of the fetal vascular tree, leading to maximum surface area for maternal-fetal exchange (Hemberger and Cross, 2001; Adamson et al., 2002). While many molecular markers are essential for placental initiation and chorio-allantoic formation, the molecular regulation of placenta size and vascularization is unclear.

The *Hoxa13* mutant vascular phenotype and expression led us to consider the changes in general EC morphology, vascular patterning and integrity, and molecular identity due to this mutation. While $Hoxa13^{GFP}$ mutant labyrinths do become vascularized, the *Hoxa13* placental phenotype suggests a loss of angiogenic patterning and branching of the embryonic vasculature that persists throughout placental maturation. While some may simply attribute this to growth delay, no overall growth delay was observed in the developing *Hoxa13* mutant mice. Overall, the severe loss of EC morphology, reduced blood vessel patterning, and subsequent reduction of important molecular markers revealed a larger placental vascular defect due to the loss of *Hoxa13*.

Wildtype and *Hoxa13* heterozygous placental ECs display classic cell morphology: ECs fully line the vessel lumens while retaining secure attachments

to the underlying trophoblasts. In contrast, mutant ECs have a distinctly dysmorphic appearance: the cells lack a robust cell body, often being reduced to a thin wall comprised mostly of membrane, leading to severe edema behind the ECs. The trophoblast layer is unperturbed and the expression of trophoblast markers such as *Gcm1, Esx1*, and *Vhlh* are not altered in the mutant placentas (Appendix 1 shows *Gcm1*, data not shown for others). Careful examination of the ECM reveal no changes in it's presence or localization; this is an important finding because the changes in EC morphology and loss of cell body can not be attributed to a loss in ECM (Stupack and Cheresh, 2002; Davis and Senger, 2005). In all, the *Hoxa13* mutant EC morphology does not support proper EC or placental function, and we believe that this dramatic loss in EC structure and integrity leads to placental insufficiency and lethality in this mouse model. Specifically, the disturbed EC-trophoblast interaction and edema would not support proper placental function, leading to fetal demise. Proper endothelial structure and overall vascular branching and patterning is attributed to key EC-specific angiogenic and adhesion molecules, and a global EC defect due to the loss of functional HOXA13 leads to aberrant gene regulation and cell function.

7B. HOXA13 modulates EC patterning and function via key molecules

Microarray and expression analyses identified several genes important for placental EC function and patterning. Several genes were significantly down-regulated in *Hoxa13* mutant placentas, including genes encoding for EC-specific receptors (*tie2*, *neuropilin-1*), transcription factors (*foxf1, necdin*), cell adhesion

molecules (*mageL-2, trophinin*), and cell transport/caveolae-specific molecules (*caveolin-1, CD36*) (Table A). Significantly, we identified *Enpp2* (ectonucleotide pyrophosphatase/phosphodiesterase-2, aka autotaxin) as a gene strongly down-regulated in the *Hoxa13*-deficient placenta and EC. *Enpp2* has been reported in other studies as a direct target of HOXA13 (Williams et al., 2005; McCabe and Innis, 2005). Enpp2 promotes angiogenesis and cell migration, and loss of *Enpp2* by mouse knockout studies reveal it's requirement in proper development of the yolk sac and embryonic vasculature, and of the allantois (Nam et al., 2001; van Meeteren et al., 2006).

CD36 and caveolin-1 were both down-regulated in mutant placenta ECs (CD36 down -2.9X, Cav1 down -3.6X), and these interacting proteins are both essential components of cell surface invaginations called caveolae which are abundant on endothelial cells (Frank et al., 2002; Sbaa et al., 2005). CD36 and caveolin-1 are known to be important in EC intracellular trafficking of essential fatty acids and cholesterols (Lyden et al., 2002; Williams and Lisanti, 2004). Caveolae are implicated in many diverse cellular and vascular processes including cell mobility, cell permeability, and tyrosine kinase signaling (Bauer et al., 2005; Sbaa et al., 2005; Vihanto et al., 2006). Furthermore, caveolin-1 interacts with and negatively regulates eNOS activity within caveolae (Garcia-Cardena et al., 1996; Sbaa et al., 2005), and caveolin-1 knockout mice lack distinct caveolae and exhibit increased eNOS activity and decreased vascular tone (Razani et al., 2001). While the electron micrographs did not reveal a reduction in EC caveolae within the placenta, molecular and physiological

defects may be present, thus the reduction in *caveolin-1* and *CD36* expression merits further study.

Another molecule which has an important role in vascular signaling is the receptor Neuropilin-1 (Nrp1). *Nrp1* is down-regulated in the mutant placental vasculature, as shown by microarray, qRT-PCR, and IHC. In the vasculature, NRP1 is a receptor for VEGF165, PlGF-2, and VEGF-B, and its activation leads to cell proliferation and migration (Migdal et al., 1998; Soker et al., 1998; Whitaker et al., 2001). These interactions and downstream effects are enhanced by NRP1 interaction with the receptors VEGFR-1 and VEGFR-2 (Giraudo et al., 1998; Neufeld et al., 2002). Interestingly, *Nrp1* knockout mice die at mid-gestation (E10.5 to E12.5) from defects of the heart, vasculature, and nervous system, while *Nrp1/Nrp2* double knockout mice die earlier at E8 from severe defects in placental and embryonic vascularization (Kawasaki et al., 1999; Takashima et al., 2002). While we have shown that VEGF levels are unperturbed by the loss of *Hoxa13* (Appendix 1), the significant reduction of a receptor would be sufficient to reduce the VEGF effect on vascular remodeling and patterning. We propose that the loss of Nrp1 promotes the loss of vascular maintenance and morphology.

Several molecules important for cell adhesion and proliferation were reduced in the placentas, including members of the MAGE family of proteins: Necdin, Trophinin, and MageL-2. While their cellular function in ECs and the placenta is not clear, we confirmed their normal expression in the placenta which was not previously reported (Uetsuki et al., 1996; Suzuki et al., 1999; Lee et al.,

2000; Matsumoto et al., 2001; Nadano et al., 2002). Due to their role in cell adhesion, we predict that loss of the MAGE proteins promotes the alteration in the EC morphology and integrity.

One vascular specific gene that was upregulated in *Hoxa13* mutant placentas was *lyve1* (Lymphatic vessel endothelium-1, Xlkd1), a homolog of the hyaluronan-binding protein CD44. While *lyve1* expression is typically associated with lymphatic vasculature (Jackson et al., 2001; Prevo et al., 2001; Huang et al., 2006, in press), new studies have revealed *lyve1* expression within blood vessels of the sinusoidal endothelium of liver and spleen, and in a unique subset of macrophages (Mouta Carreira et al., 2001; Martinez-Pomares et al., 2005; Schledzewski et al., 2006). Our data supports previous human expression studies which show *lyve1* within the placental endothelium, and we have shown a significant increase in vascular *lyve1* with the loss of *Hoxa13* (Gu et al., 2006). The degradation and uptake of hyaluronan, a glycosaminoglycan in the ECM, has been associated with angiogenesis and cell adhesion (Goshen et al., 1996; Savani et al., 2001), and hyaluronan is found in the human placenta villi (mouse labyrinth) and umbilical cord (Wasserman et al., 1979; Ponting and Kumar, 1995). As a receptor for hyaluronan, Lyve1 may promote angiogenic cues in the placenta vasculature, possibly affecting the extracellular matrix composition and endothelial-matrix adhesion properties.

7C. HOXA13 is necessary for proper EC activation and expression of *Tie2* and *Foxf1*

To elucidate the direct targets of the HOXA13 transcription factor, our lab is interested in determining the bona fide *in vivo* HOXA13 binding sites. On-going research has defined a TA-rich HOXA13 DNA-binding consensus sequence (Knosp et al., 2006). Our multi-faceted approach to identifying HOXA13 targets (expression analysis, biochemical testing, *in vivo* and *in vitro* binding assays) proved successful in parsing out a unique regulatory role for HOXA13 in placental vascular patterning. For example, we found that HOXA13 directly binds to the *Tie2* and *Foxf1* upstream sequences within placental tissue. Due to the clear reduction in the expression of *Tie2* and *Foxf1* within placental ECs (qRT-PCR and IHC), we propose that HOXA13 promotes the transcriptional activation of these genes during placental vascular development.

The receptor tyrosine-kinase Tie2 mediates the activation of ECs toward angiogenic sprouting and branching by promoting cell proliferation, destruction of the underlying basement membrane, and cell motility (Folkman and D'Amore, 1996). Loss of *Tie2* leads to embryonic lethality in mice at E11.0 due to severe lack of angiogenic patterning of the primary vascular network (Dumont et al., 1994; Sato et al., 1995). As in the *Tie2* knockout mouse models, the placenta vasculature in *Hoxa13* mutants is structurally weak and lacks proper angiogenic remodeling, including a reduction in intussusceptive microvascular remodeling that normally adds to the complexity and density of the vascular tree (Patan, 1998). Within the placenta, angiopoietin-2 is the primary Ang ligand that is

strongly expressed, and ANG2-TIE2 signaling promotes angiogenic remodeling of vasculature (Zhang et al., 2001; Geva et al., 2002; Geva et al., 2005). Due to its significant role in vascular integrity and maintenance, a moderate reduction in *Tie2* would be sufficient to cause alterations in vascular remodeling and integrity as seen in *Hoxa13* mutant placentas.

In the same manner as *Tie2*, *Foxf1* is down-regulated in the ECs of the mutant placenta, and HOXA13 directly binds to a unique site on the promoter of Foxf1 *in vivo*. *Foxf1* (Forkhead box protein-F1, *FREAC-1*), a member of the Forkhead family of transcriptional regulators, is expressed embryonically within mesodermal tissues such as the allantois, placenta, lung mesenchyme, and lateral plate mesoderm (Pierrou et al., 1994; Hellqvist et al., 1996; Peterson et al., 1997; Mahlapuu et al., 2001; Ormestad et al., 2004). *Foxf1* knockout mice die by E10 due to defects in extra-embryonic patterning, vascularization, and mesoderm proliferation (Mahlapuu et al. 2001a), while mice haploinsufficent for *Foxf1* die peri-natally due to lung hemorrhaging and foregut defects (Mahlapuu et al., 2001b). Previous studies have shown the importance of the highly conserved *Foxf1* upstream sequence, suggestive of the conserved regulation of *Foxf1* by HOXA13 (Kim et al., 2005). While the molecular mechanism behind the link between *Foxf1* and vascular integrity remains unclear, we suggest that the direct regulation of *Foxf1* by HOXA13 is required for proper placenta vascularization and patterning.

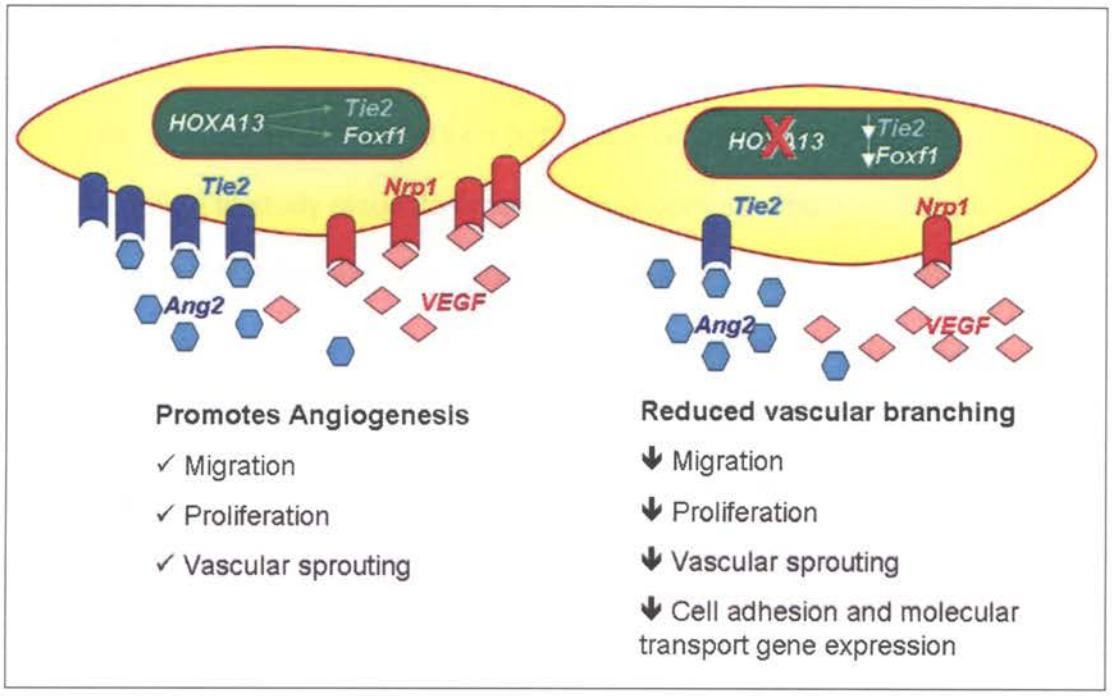

Figure 7.1 - Loss of *Hoxa13* in placenta ECs leads to reduced vascular branching by the mis-expression of important vascular cues

HOXA13 transcriptionally activates *Tie2* and *Foxf1* within the placenta ECs, and loss of *Hoxa13* leads to a reduction the vascular receptors Tie2 and Nrp1 and reduced vascular branching and intussusception.

7D. Placenta regulation: what we can learn from Hoxa13

Human and mouse placentas share a similar ultra-structure, vasculature, cell types, and molecular expression patterns, making the mouse placenta a relevant model to study placenta function, development, and genetics (Rossant and Cross, 2001; Adamson et al., 2002; Coultas et al., 2005). The development of the hemochorial placenta shared by humans and rodents is an intricate process of cell-cell regulation and invasion, trophoblast stem cell differentiation, and complex tissue branching morphogenesis. While the morphology and genetics of many of these steps is understood, many questions remain regarding its molecular regulation. Within the labyrinth, the interactions of the allantoic mesoderm, chorionic trophoblasts, and vascular branches are very complex and not yet understood at the molecular level (Kingdom et al., 2000; Adamson et al., 2002). For example, it is not clear whether one cell type regulates the branching and size of the vascular villous tree within the labyrinth. While trophoblast-specific genes such as *gcm1* and *esx1* are required for vascular integration within the labyrinth (Li and Behringer, 1998; Anson-Cartwright et al., 2000; Rinkenberger and Werb, 2000), our data suggests that trophoblast differentiation and villous branching are not sufficient to regulate the patterning and maintenance of the fetal vasculature. Essentially, the *Hoxa13* mutant is the first reported mouse model to display an EC-specific placental defect. Retention of the ECM and trophoblast layers underlying the ECs negates these as possible origins of the EC dysmorphology. Rather, there is a fundamental change in EC morphology resulting in a thinner labyrinth with a reduced vascular villous tree

and reduced vascular integrity, a combination that is fatal to embryos lacking HOXA13.

How did *Hoxa13* become restricted to placenta ECs, while HOXA13 is not required in other placental cells or ECs throughout the body? It is interesting to speculate that HOXA13 function in the posterior urogenital system was co-opted by the placental vasculature as an important regulatory and developmental gene (Godwin and Capecchi, 1998). To note, several other Hox genes are expressed in both endothelial cells and in other organs during development, signifying that a Hox gene can play unique roles in various tissue types (see introduction for genes and references). While HOXA13 plays an important role in patterning the nearby external genitalia (Morgan et al., 2003), we suggest that HOXA13 function has been recruited in the patterning and differentiation of the placenta and umbilical vasculature. Comparative embryology studies would be interesting to ascertain if *Hoxa13* is expressed in homologous vascular structures in other eutherian mammals such as humans and lagomorphs, or more importantly, whether *Hoxa13* is absent in the amniotic stalk and vessels in non-placental amniotes such as the birds and reptiles, which rely on the vitelline vasculature for support.

The 'placenta-heart axis theory' proposed by Hemburger and Cross (2001) states that changes in placental blood flow and patterning will cause secondary defects in the heart due to changes in blood pressure. This theory is supported by studies of cardiovascular and placental defects and by these studies of $Hoxa13^{GFP}$ mutant mouse (Sapin et al., 1997a; Sapin et al., 1997b).

While the placental vascular phenotype can be attributed to the loss of *Hoxa13* within these ECs, at no time during development is *Hoxa13* expressed in the heart (data not shown). While our current methods of analysis are insufficient to study blood pressure and flow of the mouse embryo *in vivo*, future research and gains in technology will help address this question. Meanwhile, we propose that defects in *Hoxa13*^{GFP} mutant placentas affect embryonic blood pressure and place stress on the cardiovascular system, leading to secondary cardiac defects.

In summary, the dramatically altered vascular and EC morphology within the placenta leads us to propose that placental insufficiency prevents Hoxa13-deficient mice from surviving past mid-gestation. We have characterized the expression of *Hoxa13* in placental labyrinth ECs and the EC-specific requirement for HOXA13 in proper placental vascularization and EC morphology. Within placental ECs, HOXA13 is necessary for full activation of the genes *Tie2* and *Foxf1*, and ECs lacking HOXA13 show reduced expression of important angiogenic receptors (*Tie2, Nrp1*), transcription factors (*foxf1, necdin*), and cell adhesion molecules. With this shift in EC gene expression, the *Hoxa13*^{GFP} -deficient ECs lose proper morphology leading to the pronounced vascular phenotype in the placenta. Furthermore, we hypothesize that this placental defect results in changes in blood flow and pressure, thereby inducing the secondary cardiac defects in the *Hoxa13* mutant mice.

7E. Future Directions

The successful identification of molecular and morphological changes due to the loss of *Hoxa13* within the placenta has opened up a new direction of basic research in the lab and new avenues of research on placental vascularization. Importantly, *Hoxa13* is the first gene to play an essential role in patterning the placental vasculature. Since these discoveries have developed into a project rich in new ideas, this naturally leads to more and more unresolved yet fascinating questions. How is the size and level of vascularization within the placenta molecularly regulated? What is the functional mechanism behind the HOXA13 effect on EC integrity? There is still much work to be done.

Therefore, a few of the fascinating potential projects that could stem from my new discoveries have been outlined. My wish is that a new student or post-doc might find ideas or inspiration to pick up where I left off, taking this research to a new level of understanding and complexity.

Identification of common direct targets of HOXA13

- Compare microarray results from the placenta, limb, and bladder to identify common target pathways and genes regulated by HOXA13.
- Perform microarray analysis on bead-purified placental ECs and compare these results with the whole placenta arrays.
    - Which genes are similar? Are there more dramatic changes in gene expression?

Explore the functional interactions of FOXF1 and HOXA13

- Determine whether the FOXF1 and HOXA13 transcription factors interact and/or work in combination to activate EC-specific genes such as Tie2.
    - Do they work together? Do they have opposing effects? Do they have redundant effects?
- Since HOXA13 and FOXF1 share similar T/A-rich core binding sites, compare the binding affinity of these transcription factors for gene-specific binding sites by fluorescence anisotropy.
- Investigate whether there are any placenta vascular defects in *Foxf1* knockout mice and compare them to the *Hoxa13* phenotype.

Identity the direct function of HOXA13 in placenta ECs

- Create a conditional knockout mouse that lacks *Hoxa13* in endothelial cells (using a Tie2-Cre transgenic mouse)
    - Does this recapitulate the umbilical artery and placenta defects?
    - Do these mice survive or live longer than the *Hoxa13* mutant mice?
- Perform cell motility and migration experiments to determine whether *Hoxa13* is required for EC movement and angiogenic patterning.
- Identify whether loss of the MAGE proteins such as trophinin affect cell-cell and cell-matrix interactions of ECs
- Delete HOXA13 binding sites with candidate gene promoters (for luciferase assays or knockout mice) to inhibit direct activation by HOXA13

Characterize *hoxa13* expression in other species

- Identify whether *hoxa13* is expressed in human placenta endothelial cells and in HUVEC and other cell lines.
- Compare the expression of *hoxa13* in mammalian chorio-allantoic placentas to those from non-placental amniotes such as chick

In the past 12 years, the molecular characterization of the placenta has identified over 100 genes that are essential for placenta development (Cross, 2005). Interestingly, the vascular expression and associated defects of the *Hoxa13* mouse represent the first known model of a gene essential and specific to the developing placental vasculature. Therefore, further examination of HOXA13s role in placenta vascularization will reveal the significance of the regulation of placenta size and vascular patterning to embryonic suvival and health. Furthermore, a better understanding of endothelial-specific and placental-specific genes is imperative to identifying the molecular regulation of the placenta system, as well as identifying genes controlling a healthy pregnancy and fetal survival.

References

Adamson, S. L., Lu, Y., Whiteley, K. J., Holmyard, D., Hemberger, M., Pfarrer, C., and Cross, J. C. (2002). Interactions between trophoblast cells and the maternal and fetal circulation in the mouse placenta. Dev Biol 250, 358-373.

Adelman, D. M., Gertsenstein, M., Nagy, A., Simon, M. C., and Maltepe, E. (2000). Placental cell fates are regulated in vivo by HIF-mediated hypoxia responses. Genes Dev 14, 3191-3203.

Ahmed, A., Dunk, C., Ahmad, S., and Khaliq, A. (2000). Regulation of placental vascular endothelial growth factor (VEGF) and placenta growth factor (PlGF) and soluble Flt-1 by oxygen--a review. Placenta 21 Suppl A, S16-24.

Amesse, L. S., Moulton, R., Zhang, Y. M., and Pfaff-Amesse, T. (2003). Expression of HOX gene products in normal and abnormal trophoblastic tissue. Gynecol Oncol 90, 512-518.

Anson-Cartwright, L., Dawson, K., Holmyard, D., Fisher, S. J., Lazzarini, R. A., and Cross, J. C. (2000). The glial cells missing-1 protein is essential for branching morphogenesis in the chorioallantoic placenta. Nat Genet 25, 311-314.

Baldwin, H. S., Shen, H. M., Yan, H. C., DeLisser, H. M., Chung, A., Mickanin, C., Trask, T., Kirschbaum, N. E., Newman, P. J., Albelda, S. M., and et al. (1994). Platelet endothelial cell adhesion molecule-1 (PECAM-1/CD31): alternatively spliced, functionally distinct isoforms expressed during mammalian cardiovascular development. Development 120, 2539-2553.

Bauer, P. M., Yu, J., Chen, Y., Hickey, R., Bernatchez, P. N., Looft-Wilson, R., Huang, Y., Giordano, F., Stan, R. V., and Sessa, W. C. (2005). Endothelial-specific expression of caveolin-1 impairs microvascular permeability and angiogenesis. Proc Natl Acad Sci U S A 102, 204-209.

Beck, L., Jr., and D'Amore, P. A. (1997). Vascular development: cellular and molecular regulation. Faseb J 11, 365-373.

Bjarnegard, M., Enge, M., Norlin, J., Gustafsdottir, S., Fredriksson, S., Abramsson, A., Takemoto, M., Gustafsson, E., Fassler, R., and Betsholtz, C. (2004). Endothelium-specific ablation of PDGFB leads to pericyte loss and glomerular, cardiac and placental abnormalities. Development 131, 1847-1857.

Boudreau, N., Andrews, C., Srebrow, A., Ravanpay, A., and Cheresh, D. A. (1997). Induction of the angiogenic phenotype by Hox D3. J Cell Biol 139, 257-264.

Burri, P. H., Hlushchuk, R., and Djonov, V. (2004). Intussusceptive angiogenesis: its emergence, its characteristics, and its significance. Dev Dyn 231, 474-488.

Carmeliet, P., Ferreira, V., Breier, G., Pollefeyt, S., Kieckens, L., Gertsenstein, M., Fahrig, M., Vandenhoeck, A., Harpal, K., Eberhardt, C., et al. (1996). Abnormal blood vessel development and lethality in embryos lacking a single VEGF allele. Nature 380, 435-439.

Cetin, I., Foidart, J. M., Miozzo, M., Raun, T., Jansson, T., Tsatsaris, V., Reik, W., Cross, J., Hauguel-de-Mouzon, S., Illsley, N., et al. (2004). Fetal growth restriction: a workshop report. Placenta 25, 753-757.

Charnock-Jones, D. S., Kaufmann, P., and Mayhew, T. M. (2004). Aspects of human fetoplacental vasculogenesis and angiogenesis. I. Molecular regulation. Placenta 25, 103-113.

Clark, D. E., Smith, S. K., Sharkey, A. M., and Charnock-Jones, D. S. (1996). Localization of VEGF and expression of its receptors flt and KDR in human placenta throughout pregnancy. Hum Reprod 11, 1090-1098.

Connolly, D. T., Heuvelman, D. M., Nelson, R., Olander, J. V., Eppley, B. L., Delfino, J. J., Siegel, N. R., Leimgruber, R. M., and Feder, J. (1989). Tumor

vascular permeability factor stimulates endothelial cell growth and angiogenesis. J Clin Invest 84, 1470-1478.

Coultas, L., Chawengsaksophak, K., and Rossant, J. (2005). Endothelial cells and VEGF in vascular development. Nature 438, 937-945.

Craven, C., and Ward, K. Embryo, Fetus, and Placenta: Normal and Abnormal, in Scott, J., et al.: Danforth's Obstetrics and Gynecology, Eighth Edition, Philadelphia, Lippincott Williams & Wilkins, 1999, pages 29-45.

Cross, J. C. (2005). How to make a placenta: mechanisms of trophoblast cell differentiation in mice--a review. Placenta 26 Suppl A, S3-9.

Cross, J. C., Nakano, H., Natale, D. R., Simmons, D. G., and Watson, E. D. (2006). Branching morphogenesis during development of placental villi. Differentiation 74, 393-401.

Darland, D. C., and D'Amore, P. A. (1999). Blood vessel maturation: vascular development comes of age. J Clin Invest 103, 157-158.

Davis, G. E., and Senger, D. R. (2005). Endothelial extracellular matrix: biosynthesis, remodeling, and functions during vascular morphogenesis and neovessel stabilization. Circ Res 97, 1093-1107.

Demir, R., Kayisli, U. A., Cayli, S., and Huppertz, B. (2006). Sequential steps during vasculogenesis and angiogenesis in the very early human placenta. Placenta 27, 535-539.

Djonov, V., Schmid, M., Tschanz, S. A., and Burri, P. H. (2000). Intussusceptive angiogenesis: its role in embryonic vascular network formation. Circ Res 86, 286-292.

Djonov, V. G., Kurz, H., and Burri, P. H. (2002). Optimality in the developing vascular system: branching remodeling by means of intussusception as an efficient adaptation mechanism. Dev Dyn 224, 391-402.

Dolle, P., and Duboule, D. (1989). Two gene members of the murine HOX-5 complex show regional and cell-type specific expression in developing limbs and gonads. Embo J 8, 1507-1515.

Downs, K. M. (2002). Early placental ontogeny in the mouse. Placenta 23, 116-131.

Downs, K. M., Gifford, S., Blahnik, M., and Gardner, R. L. (1998). Vascularization in the murine allantois occurs by vasculogenesis without accompanying erythropoiesis. Development 125, 4507-4520.

Dumont, D. J., Fong, G. H., Puri, M. C., Gradwohl, G., Alitalo, K., and Breitman, M. L. (1995). Vascularization of the mouse embryo: a study of flk-1, tek, tie, and vascular endothelial growth factor expression during development. Dev Dyn 203, 80-92.

Dumont, D. J., Gradwohl, G., Fong, G. H., Puri, M. C., Gertsenstein, M., Auerbach, A., and Breitman, M. L. (1994). Dominant-negative and targeted null mutations in the endothelial receptor tyrosine kinase, tek, reveal a critical role in vasculogenesis of the embryo. Genes Dev 8, 1897-1909.

Dye, J., Lawrence, L., Linge, C., Leach, L., Firth, J., and Clark, P. (2004). Distinct patterns of microvascular endothelial cell morphology are determined by extracellular matrix composition. Endothelium 11, 151-167.

Faber, J., and Thornburg K. Placental Physiology: Structure and Function of Fetomaternal Exchange. New York: Raven Press, 1983.

Ferrara, N., Carver-Moore, K., Chen, H., Dowd, M., Lu, L., O'Shea, K. S., Powell-Braxton, L., Hillan, K. J., and Moore, M. W. (1996). Heterozygous embryonic lethality induced by targeted inactivation of the VEGF gene. Nature 380, 439-442.

Ferrara, N., and Henzel, W. J. (1989). Pituitary follicular cells secrete a novel heparin-binding growth factor specific for vascular endothelial cells. Biochem Biophys Res Commun 161, 851-858.

Field, M. (1984). Placentophagy. Midwives Chron 97, 375-376.

Folkman, J. (2006). Angiogenesis. Annu Rev Med 57, 1-18.

Folkman, J., and D'Amore, P. A. (1996). Blood vessel formation: what is its molecular basis? Cell 87, 1153-1155.

Fong, G. H., Rossant, J., Gertsenstein, M., and Breitman, M. L. (1995). Role of the Flt-1 receptor tyrosine kinase in regulating the assembly of vascular endothelium. Nature 376, 66-70.

Frank, P. G., Marcel, Y. L., Connelly, M. A., Lublin, D. M., Franklin, V., Williams, D. L., and Lisanti, M. P. (2002). Stabilization of caveolin-1 by cellular cholesterol and scavenger receptor class B type I. Biochemistry 41, 11931-11940.

Fromental-Ramain, C., Warot, X., Messadecq, N., LeMeur, M., Dolle, P., and Chambon, P. (1996). Hoxa-13 and Hoxd-13 play a crucial role in the patterning of the limb autopod. Development 122, 2997-3011.

Gale, N. W., and Yancopoulos, G. D. (1999). Growth factors acting via endothelial cell-specific receptor tyrosine kinases: VEGFs, angiopoietins, and ephrins in vascular development. Genes Dev 13, 1055-1066.

Gao, J., Mazella, J., and Tseng, L. (2002). Hox proteins activate the IGFBP-1 promoter and suppress the function of hPR in human endometrial cells. DNA Cell Biol 21, 819-825.

Garcia-Cardena, G., Fan, R., Stern, D. F., Liu, J., and Sessa, W. C. (1996). Endothelial nitric oxide synthase is regulated by tyrosine phosphorylation and interacts with caveolin-1. J Biol Chem 271, 27237-27240.

Gekas, C., Dieterlen-Lievre, F., Orkin, S. H., and Mikkola, H. K. (2005). The placenta is a niche for hematopoietic stem cells. Dev Cell 8, 365-375.

Geva, E., Ginzinger, D. G., Moore, D. H., 2nd, Ursell, P. C., and Jaffe, R. B. (2005). In utero angiopoietin-2 gene delivery remodels placental blood vessel phenotype: a murine model for studying placental angiogenesis. Mol Hum Reprod 11, 253-260.

Geva, E., Ginzinger, D. G., Zaloudek, C. J., Moore, D. H., Byrne, A., and Jaffe, R. B. (2002). Human placental vascular development: vasculogenic and angiogenic (branching and nonbranching) transformation is regulated by vascular

endothelial growth factor-A, angiopoietin-1, and angiopoietin-2. J Clin Endocrinol Metab 87, 4213-4224.

Giraudo, E., Primo, L., Audero, E., Gerber, H. P., Koolwijk, P., Soker, S., Klagsbrun, M., Ferrara, N., and Bussolino, F. (1998). Tumor necrosis factor-alpha regulates expression of vascular endothelial growth factor receptor-2 and of its co-receptor neuropilin-1 in human vascular endothelial cells. J Biol Chem 273, 22128-22135.

Gnarra, J. R., Ward, J. M., Porter, F. D., Wagner, J. R., Devor, D. E., Grinberg, A., Emmert-Buck, M. R., Westphal, H., Klausner, R. D., and Linehan, W. M. (1997). Defective placental vasculogenesis causes embryonic lethality in VHL-deficient mice. Proc Natl Acad Sci U S A 94, 9102-9107.

Godwin, A. R., and Capecchi, M. R. (1998). Hoxc13 mutant mice lack external hair. Genes Dev 12, 11-20.

Goodman, F. R., and Scambler, P. J. (2001). Human HOX gene mutations. Clin Genet 59, 1-11.

Goshen, R., Ariel, I., Shuster, S., Hochberg, A., Vlodavsky, I., de Groot, N., Ben-Rafael, Z., and Stern, R. (1996). Hyaluronan, CD44 and its variant exons in

human trophoblast invasion and placental angiogenesis. Mol Hum Reprod 2, 685-691.

Gospodarowicz, D., Abraham, J. A., and Schilling, J. (1989). Isolation and characterization of a vascular endothelial cell mitogen produced by pituitary-derived folliculo stellate cells. Proc Natl Acad Sci U S A 86, 7311-7315.

Graba, Y., Aragnol, D., and Pradel, J. (1997). Drosophila Hox complex downstream targets and the function of homeotic genes. Bioessays 19, 379-388.

Gray, H. Anatomy of the Human Body. Philadelphia: Lea & Febiger,1918. Bartleby.com, 2000.

Gu, B., Alexander, J. S., Gu, Y., Zhang, Y., Lewis, D. F., and Wang, Y. (2006). Expression of lymphatic vascular endothelial hyaluronan receptor-1 (LYVE-1) in the human placenta. Lymphat Res Biol 4, 11-17.

Haack, H., and Gruss, P. (1993). The establishment of murine Hox-1 expression domains during patterning of the limb. Dev Biol 157, 410-422.

Hatano, N., Mori, Y., Oh-hora, M., Kosugi, A., Fujikawa, T., Nakai, N., Niwa, H., Miyazaki, J., Hamaoka, T., and Ogata, M. (2003). Essential role for ERK2

mitogen-activated protein kinase in placental development. Genes Cells 8, 847-856.

Hellgren, I., Sylven, C., and Magnusson, Y. (2000). Study of the beta1 adrenergic receptor expression in human tissues: immunological approach. Biol Pharm Bull 23, 700-703.

Hellqvist, M., Mahlapuu, M., Samuelsson, L., Enerback, S., and Carlsson, P. (1996). Differential activation of lung-specific genes by two forkhead proteins, FREAC-1 and FREAC-2. J Biol Chem 271, 4482-4490.

Hemberger, M., and Cross, J. C. (2001). Genes governing placental development. Trends Endocrinol Metab 12, 162-168.

Herzog, Y., Kalcheim, C., Kahane, N., Reshef, R., and Neufeld, G. (2001). Differential expression of neuropilin-1 and neuropilin-2 in arteries and veins. Mech Dev 109, 115-119.

Hombria, J. C., and Lovegrove, B. (2003). Beyond homeosis--HOX function in morphogenesis and organogenesis. Differentiation 71, 461-476.

Huang, S. S., Liu, I. H., Smith, T., Shah, M. R., Johnson, F. E., and Huang, J. S. (2006). CRSBP-1/LYVE-I-null mice exhibit identifiable morphological and functional alterations of lymphatic capillary vessels. FEBS Lett 580, 6259-6268.

Ingram, D. A., Caplice, N. M., and Yoder, M. C. (2005). Unresolved questions, changing definitions, and novel paradigms for defining endothelial progenitor cells. Blood 106, 1525-1531.

Innis, J. W., Mortlock, D., Chen, Z., Ludwig, M., Williams, M. E., Williams, T. M., Doyle, C. D., Shao, Z., Glynn, M., Mikulic, D., et al. (2004). Polyalanine expansion in HOXA13: three new affected families and the molecular consequences in a mouse model. Hum Mol Genet 13, 2841-2851.

Jackson, D. G., Prevo, R., Clasper, S., and Banerji, S. (2001). LYVE-1, the lymphatic system and tumor lymphangiogenesis. Trends Immunol 22, 317-321.

Kaufmann, P., Mayhew, T. M., and Charnock-Jones, D. S. (2004). Aspects of human fetoplacental vasculogenesis and angiogenesis. II. Changes during normal pregnancy. Placenta 25, 114-126.

Kawasaki, T., Kitsukawa, T., Bekku, Y., Matsuda, Y., Sanbo, M., Yagi, T., and Fujisawa, H. (1999). A requirement for neuropilin-1 in embryonic vessel formation. Development 126, 4895-4902.

Kayisli, U. A., Cayli, S., Seval, Y., Tertemiz, F., Huppertz, B., and Demir, R. (2005). Spatial and Temporal Distribution of Tie-1 and Tie-2 During Very Early Development of the Human Placenta. Placenta.

Kim, I., Kim, J. H., Moon, S. O., Kwak, H. J., Kim, N. G., and Koh, G. Y. (2000). Angiopoietin-2 at high concentration can enhance endothelial cell survival through the phosphatidylinositol 3'-kinase/Akt signal transduction pathway. Oncogene 19, 4549-4552.

Kim, I. M., Zhou, Y., Ramakrishna, S., Hughes, D. E., Solway, J., Costa, R. H., and Kalinichenko, V. V. (2005). Functional characterization of evolutionarily conserved DNA regions in forkhead box f1 gene locus. J Biol Chem 280, 37908-37916.

Kingdom, J., Huppertz, B., Seaward, G., and Kaufmann, P. (2000). Development of the placental villous tree and its consequences for fetal growth. Eur J Obstet Gynecol Reprod Biol 92, 35-43.

Knosp, W. M., Scott, V., Bachinger, H. P., and Stadler, H. S. (2004). HOXA13 regulates the expression of bone morphogenetic proteins 2 and 7 to control distal limb morphogenesis. Development 131, 4581-4592.

Knosp, W. M., Saneyoshi, C., Shou, S., Bachinger, H. P., and Stadler, H. S. (2006). Elucidation, quantitative refinement, and in vivo utilization of the HOXA13 DNA binding site. Journal of Biological Chemistry, in press.

Koblizek, T. I., Runting, A. S., Stacker, S. A., Wilks, A. F., Risau, W., and Deutsch, U. (1997). Tie2 receptor expression and phosphorylation in cultured cells and mouse tissues. Eur J Biochem 244, 774-779.

Krebs, C., Macara, L. M., Leiser, R., Bowman, A. W., Greer, I. A., and Kingdom, J. C. (1996). Intrauterine growth restriction with absent end-diastolic flow velocity in the umbilical artery is associated with maldevelopment of the placental terminal villous tree. Am J Obstet Gynecol 175, 1534-1542.

Krebs, L. T., Xue, Y., Norton, C. R., Shutter, J. R., Maguire, M., Sundberg, J. P., Gallahan, D., Closson, V., Kitajewski, J., Callahan, R., et al. (2000). Notch signaling is essential for vascular morphogenesis in mice. Genes Dev 14, 1343-1352.

Krumlauf, R. (1994). Hox genes in vertebrate development. Cell 78, 191-201.

Kumar, S., West, D. C., and Ager, A. (1987). Heterogeneity in endothelial cells from large vessels and microvessels. Differentiation 36, 57-70.

Lamont, R. E., and Childs, S. (2006). MAPping out arteries and veins. Sci STKE 2006, pe39.

Lee, S., Kozlov, S., Hernandez, L., Chamberlain, S. J., Brannan, C. I., Stewart, C. L., and Wevrick, R. (2000). Expression and imprinting of MAGEL2 suggest a role in Prader-willi syndrome and the homologous murine imprinting phenotype. Hum Mol Genet 9, 1813-1819.

Lewis, E. B. (1978). A gene complex controlling segmentation in Drosophila. Nature 276, 565-570.

Li, Y., and Behringer, R. R. (1998). Esx1 is an X-chromosome-imprinted regulator of placental development and fetal growth. Nat Genet 20, 309-311.

Long, E. C. (1963). The Placenta in Lore and Legend. Bull Med Libr Assoc 51, 233-241.

Louey, S., and Thornburg, K. L. (2005). The prenatal environment and later cardiovascular disease. Early Hum Dev 81, 745-751.

Lyden, T. W., Anderson, C. L., and Robinson, J. M. (2002). The endothelium but not the syncytiotrophoblast of human placenta expresses caveolae. Placenta 23, 640-652.

Macchiarelli, G., Jiang, J. Y., Nottola, S. A., and Sato, E. (2006). Morphological patterns of angiogenesis in ovarian follicle capillary networks. A scanning electron microscopy study of corrosion cast. Microsc Res Tech 69, 459-468.

Mahlapuu, M., Enerback, S., and Carlsson, P. (2001a). Haploinsufficiency of the forkhead gene Foxf1, a target for sonic hedgehog signaling, causes lung and foregut malformations. Development 128, 2397-2406.

Mahlapuu, M., Ormestad, M., Enerback, S., and Carlsson, P. (2001b). The forkhead transcription factor Foxf1 is required for differentiation of extra-embryonic and lateral plate mesoderm. Development 128, 155-166.

Maisonpierre, P. C., Suri, C., Jones, P. F., Bartunkova, S., Wiegand, S. J., Radziejewski, C., Compton, D., McClain, J., Aldrich, T. H., Papadopoulos, N., et al. (1997). Angiopoietin-2, a natural antagonist for Tie2 that disrupts in vivo angiogenesis. Science 277, 55-60.

Makanya, A. N., Stauffer, D., Ribatti, D., Burri, P. H., and Djonov, V. (2005). Microvascular growth, development, and remodeling in the embryonic avian kidney: the interplay between sprouting and intussusceptive angiogenic mechanisms. Microsc Res Tech 66, 275-288.

Malek, A. M., and Izumo, S. (1995). Control of endothelial cell gene expression by flow. J Biomech 28, 1515-1528.

Manley, J. L., and Levine, M. S. (1985). The homeo box and mammalian development. Cell 43, 1-2.

Manley, N. R., and Capecchi, M. R. (1995). The role of Hoxa-3 in mouse thymus and thyroid development. Development 121, 1989-2003.

Mann, R. S., and Affolter, M. (1998). Hox proteins meet more partners. Curr Opin Genet Dev 8, 423-429.

Martinez-Pomares, L., Hanitsch, L. G., Stillion, R., Keshav, S., and Gordon, S. (2005). Expression of mannose receptor and ligands for its cysteine-rich domain in venous sinuses of human spleen. Lab Invest 85, 1238-1249.

Matsumoto, K., Taniura, H., Uetsuki, T., and Yoshikawa, K. (2001). Necdin acts as a transcriptional repressor that interacts with multiple guanosine clusters. Gene 272, 173-179.

McCabe, C. D., and Innis, J. W. (2005). A genomic approach to the identification and characterization of HOXA13 functional binding elements. Nucleic Acids Res 33, 6782-6794.

McGinnis, W., Garber, R. L., Wirz, J., Kuroiwa, A., and Gehring, W. J. (1984a). A homologous protein-coding sequence in Drosophila homeotic genes and its conservation in other metazoans. Cell 37, 403-408.

McGinnis, W., Hart, C. P., Gehring, W. J., and Ruddle, F. H. (1984b). Molecular cloning and chromosome mapping of a mouse DNA sequence homologous to homeotic genes of Drosophila. Cell 38, 675-680.

Migdal, M., Huppertz, B., Tessler, S., Comforti, A., Shibuya, M., Reich, R., Baumann, H., and Neufeld, G. (1998). Neuropilin-1 is a placenta growth factor-2 receptor. J Biol Chem 273, 22272-22278.

Morgan, E. A., Nguyen, S. B., Scott, V., and Stadler, H. S. (2003). Loss of Bmp7 and Fgf8 signaling in Hoxa13-mutant mice causes hypospadia. Development 130, 3095-3109.

Morley, R. (2006). Fetal origins of adult disease. Semin Fetal Neonatal Med 11, 73-78.

Mortlock, D. P., and Innis, J. W. (1997). Mutation of HOXA13 in hand-foot-genital syndrome. Nat Genet 15, 179-180.

Mouta Carreira, C., Nasser, S. M., di Tomaso, E., Padera, T. P., Boucher, Y., Tomarev, S. I., and Jain, R. K. (2001). LYVE-1 is not restricted to the lymph vessels: expression in normal liver blood sinusoids and down-regulation in human liver cancer and cirrhosis. Cancer Res 61, 8079-8084.

Myers, C., Charboneau, A., and Boudreau, N. (2000). Homeobox B3 promotes capillary morphogenesis and angiogenesis. J Cell Biol 148, 343-351.

Myers, C., Charboneau, A., Cheung, I., Hanks, D., and Boudreau, N. (2002). Sustained expression of homeobox D10 inhibits angiogenesis. Am J Pathol 161, 2099-2109.

Nadano, D., Sugihara, K., Paria, B. C., Saburi, S., Copeland, N. G., Gilbert, D. J., Jenkins, N. A., Nakayama, J., and Fukuda, M. N. (2002). Significant differences between mouse and human trophinins are revealed by their expression patterns and targeted disruption of mouse trophinin gene. Biol Reprod 66, 313-321.

Nam, S. W., Clair, T., Kim, Y. S., McMarlin, A., Schiffmann, E., Liotta, L. A., and Stracke, M. L. (2001). Autotaxin (NPP-2), a metastasis-enhancing motogen, is an angiogenic factor. Cancer Res 61, 6938-6944.

Neufeld, G., Kessler, O., and Herzog, Y. (2002). The interaction of Neuropilin-1 and Neuropilin-2 with tyrosine-kinase receptors for VEGF. Adv Exp Med Biol 515, 81-90.

Ormestad, M., Astorga, J., and Carlsson, P. (2004). Differences in the embryonic expression patterns of mouse Foxf1 and -2 match their distinct mutant phenotypes. Dev Dyn 229, 328-333.

Papapetropoulos, A., Garcia-Cardena, G., Dengler, T. J., Maisonpierre, P. C., Yancopoulos, G. D., and Sessa, W. C. (1999). Direct actions of angiopoietin-1 on human endothelium: evidence for network stabilization, cell survival, and interaction with other angiogenic growth factors. Lab Invest 79, 213-223.

Patan, S. (1998). TIE1 and TIE2 receptor tyrosine kinases inversely regulate embryonic angiogenesis by the mechanism of intussusceptive microvascular growth. Microvasc Res 56, 1-21.

Peterson, R. S., Lim, L., Ye, H., Zhou, H., Overdier, D. G., and Costa, R. H. (1997). The winged helix transcriptional activator HFH-8 is expressed in the mesoderm of the primitive streak stage of mouse embryos and its cellular derivatives. Mech Dev 69, 53-69.

Pierrou, S., Hellqvist, M., Samuelsson, L., Enerback, S., and Carlsson, P. (1994). Cloning and characterization of seven human forkhead proteins: binding site specificity and DNA bending. Embo J 13, 5002-5012.

Ponting, J. M., and Kumar, S. (1995). Localisation and cellular origin of hyaluronectin. J Anat 187 (Pt 2), 331-346.

Poole, T. J., Finkelstein, E. B., and Cox, C. M. (2001). The role of FGF and VEGF in angioblast induction and migration during vascular development. Dev Dyn 220, 1-17.

Post, L. C., Margulies, E. H., Kuo, A., and Innis, J. W. (2000). Severe limb defects in Hypodactyly mice result from the expression of a novel, mutant HOXA13 protein. Dev Biol 217, 290-300.

Prevo, R., Banerji, S., Ferguson, D. J., Clasper, S., and Jackson, D. G. (2001). Mouse LYVE-1 is an endocytic receptor for hyaluronan in lymphatic endothelium. J Biol Chem 276, 19420-19430.

Puri, M. C., Rossant, J., Alitalo, K., Bernstein, A., and Partanen, J. (1995). The receptor tyrosine kinase TIE is required for integrity and survival of vascular endothelial cells. Embo J 14, 5884-5891.

Quinn, L. M., Johnson, B. V., Nicholl, J., Sutherland, G. R., and Kalionis, B. (1997). Isolation and identification of homeobox genes from the human placenta including a novel member of the Distal-less family, DLX4. Gene 187, 55-61.

Ratajska, A., Ciszek, B., and Sowinska, A. (2003). Embryonic development of coronary vasculature in rats: corrosion casting studies. Anat Rec A Discov Mol Cell Evol Biol 270, 109-116.

Razani, B., Engelman, J. A., Wang, X. B., Schubert, W., Zhang, X. L., Marks, C. B., Macaluso, F., Russell, R. G., Li, M., Pestell, R. G., et al. (2001). Caveolin-1 null mice are viable but show evidence of hyperproliferative and vascular abnormalities. J Biol Chem 276, 38121-38138.

Redline, R. W. (2006). Inflammatory responses in the placenta and umbilical cord. Semin Fetal Neonatal Med 11, 296-301.

Rhoads, K., Arderiu, G., Charboneau, A., Hansen, S. L., Hoffman, W., and Boudreau, N. (2005). A role for Hox A5 in regulating angiogenesis and vascular patterning. Lymphat Res Biol 3, 240-252.

Ribatti, D., Nico, B., Floris, C., Mangieri, D., Piras, F., Ennas, M. G., Vacca, A., and Sirigu, P. (2005). Microvascular density, vascular endothelial growth factor

immunoreactivity in tumor cells, vessel diameter and intussusceptive microvascular growth in primary melanoma. Oncol Rep 14, 81-84.

Rinkenberger, J., and Werb, Z. (2000). The labyrinthine placenta. Nat Genet 25, 248-250.

Risau, W. (1997). Mechanisms of angiogenesis. Nature 386, 671-674.

Rojas, A., De Val, S., Heidt, A. B., Xu, S. M., Bristow, J., and Black, B. L. (2005). Gata4 expression in lateral mesoderm is downstream of BMP4 and is activated directly by Forkhead and GATA transcription factors through a distal enhancer element. Development 132, 3405-3417.

Rossant, J., and Cross, J. C. (2001). Placental development: lessons from mouse mutants. Nat Rev Genet 2, 538-548.

Rossel, M., and Capecchi, M. R. (1999). Mice mutant for both Hoxa1 and Hoxb1 show extensive remodeling of the hindbrain and defects in craniofacial development. Development 126, 5027-5040.

Salsi, V., and Zappavigna, V. (2006). Hoxd13 and Hoxa13 Directly Control the Expression of the EphA7 Ephrin Tyrosine Kinase Receptor in Developing Limbs. J Biol Chem 281, 1992-1999.

Sapin, V., Dolle, P., Hindelang, C., Kastner, P., and Chambon, P. (1997a). Defects of the chorioallantoic placenta in mouse RXRalpha null fetuses. Dev Biol 191, 29-41.

Sapin, V., Ward, S. J., Bronner, S., Chambon, P., and Dolle, P. (1997b). Differential expression of transcripts encoding retinoid binding proteins and retinoic acid receptors during placentation of the mouse. Dev Dyn 208, 199-210.

Sarno, J. L., Schatz, F., Lockwood, C. J., Huang, S. T., and Taylor, H. S. (2006). Thrombin and interleukin-1beta regulate HOXA10 expression in human term decidual cells: implications for preterm labor. J Clin Endocrinol Metab 91, 2366-2372.

Sato, T. N., Qin, Y., Kozak, C. A., and Audus, K. L. (1993). Tie-1 and tie-2 define another class of putative receptor tyrosine kinase genes expressed in early embryonic vascular system. Proc Natl Acad Sci U S A 90, 9355-9358.

Sato, T. N., Tozawa, Y., Deutsch, U., Wolburg-Buchholz, K., Fujiwara, Y., Gendron-Maguire, M., Gridley, T., Wolburg, H., Risau, W., and Qin, Y. (1995). Distinct roles of the receptor tyrosine kinases Tie-1 and Tie-2 in blood vessel formation. Nature 376, 70-74.

Savani, R. C., Cao, G., Pooler, P. M., Zaman, A., Zhou, Z., and DeLisser, H. M. (2001). Differential involvement of the hyaluronan (HA) receptors CD44 and receptor for HA-mediated motility in endothelial cell function and angiogenesis. J Biol Chem 276, 36770-36778.

Sbaa, E., Frerart, F., and Feron, O. (2005). The double regulation of endothelial nitric oxide synthase by caveolae and caveolin: a paradox solved through the study of angiogenesis. Trends Cardiovasc Med 15, 157-162.

Schledzewski, K., Falkowski, M., Moldenhauer, G., Metharom, P., Kzhyshkowska, J., Ganss, R., Demory, A., Falkowska-Hansen, B., Kurzen, H., Ugurel, S., et al. (2006). Lymphatic endothelium-specific hyaluronan receptor LYVE-1 is expressed by stabilin-1+, F4/80+, CD11b+ macrophages in malignant tumours and wound healing tissue in vivo and in bone marrow cultures in vitro: implications for the assessment of lymphangiogenesis. J Pathol 209, 67-77.

Schweitzer, R., Chyung, J. H., Murtaugh, L. C., Brent, A. E., Rosen, V., Olson, E. N., Lassar, A., and Tabin, C. J. (2001). Analysis of the tendon cell fate using Scleraxis, a specific marker for tendons and ligaments. Development 128, 3855-3866.

Scott, V., Morgan, E. A., and Stadler, H. S. (2005). Genitourinary functions of Hoxa13 and Hoxd13. J Biochem (Tokyo) 137, 671-676.

Shalaby, F., Rossant, J., Yamaguchi, T. P., Gertsenstein, M., Wu, X. F., Breitman, M. L., and Schuh, A. C. (1995). Failure of blood-island formation and vasculogenesis in Flk-1-deficient mice. Nature 376, 62-66.

Silverman, M. D., Zamora, D. O., Pan, Y., Texeira, P. V., Planck, S. R., and Rosenbaum, J. T. (2001). Cell adhesion molecule expression in cultured human iris endothelial cells. Invest Ophthalmol Vis Sci 42, 2861-2866.

Simmons, D. G., and Cross, J. C. (2005). Determinants of trophoblast lineage and cell subtype specification in the mouse placenta. Dev Biol 284, 12-24.

Soker, S., Takashima, S., Miao, H. Q., Neufeld, G., and Klagsbrun, M. (1998). Neuropilin-1 is expressed by endothelial and tumor cells as an isoform-specific receptor for vascular endothelial growth factor. Cell 92, 735-745.

Stadler, H. S., Higgins, K. M., and Capecchi, M. R. (2001). Loss of Eph-receptor expression correlates with loss of cell adhesion and chondrogenic capacity in Hoxa13 mutant limbs. Development 128, 4177-4188.

Stupack, D. G., and Cheresh, D. A. (2002). ECM remodeling regulates angiogenesis: endothelial integrins look for new ligands. Sci STKE 2002, PE7.

Suri, C., Jones, P. F., Patan, S., Bartunkova, S., Maisonpierre, P. C., Davis, S., Sato, T. N., and Yancopoulos, G. D. (1996). Requisite role of angiopoietin-1, a ligand for the TIE2 receptor, during embryonic angiogenesis. Cell 87, 1171-1180.

Suzuki, N., Nakayama, J., Shih, I. M., Aoki, D., Nozawa, S., and Fukuda, M. N. (1999). Expression of trophinin, tastin, and bystin by trophoblast and endometrial cells in human placenta. Biol Reprod 60, 621-627.

Takashima, S., Kitakaze, M., Asakura, M., Asanuma, H., Sanada, S., Tashiro, F., Niwa, H., Miyazaki Ji, J., Hirota, S., Kitamura, Y., et al. (2002). Targeting of both mouse neuropilin-1 and neuropilin-2 genes severely impairs developmental yolk sac and embryonic angiogenesis. Proc Natl Acad Sci U S A 99, 3657-3662.

Teichert-Kuliszewska, K., Maisonpierre, P. C., Jones, N., Campbell, A. I., Master, Z., Bendeck, M. P., Alitalo, K., Dumont, D. J., Yancopoulos, G. D., and Stewart, D. J. (2001). Biological action of angiopoietin-2 in a fibrin matrix model of angiogenesis is associated with activation of Tie2. Cardiovasc Res 49, 659-670.

Tsoi, S. C., Wen, Y., Chung, J. Y., Chen, D., Magness, R. R., and Zheng, J. (2002). Co-expression of vascular endothelial growth factor and neuropilin-1 in ovine feto-placental artery endothelial cells. Mol Cell Endocrinol 196, 95-106.

Uetsuki, T., Takagi, K., Sugiura, H., and Yoshikawa, K. (1996). Structure and expression of the mouse necdin gene. Identification of a postmitotic neuron-restrictive core promoter. J Biol Chem 271, 918-924.

van Meeteren, L. A., Ruurs, P., Stortelers, C., Bouwman, P., van Rooijen, M. A., Pradere, J. P., Pettit, T. R., Wakelam, M. J., Saulnier-Blache, J. S., Mummery, C. L., et al. (2006). Autotaxin, a secreted lysophospholipase D, is essential for blood vessel formation during development. Mol Cell Biol 26, 5015-5022.

van Nes, J., de Graaff, W., Lebrin, F., Gerhard, M., Beck, F., and Deschamps, J. (2006). The Cdx4 mutation affects axial development and reveals an essential role of Cdx genes in the ontogenesis of the placental labyrinth in mice. Development 133, 419-428.

Vihanto, M. M., Vindis, C., Djonov, V., Cerretti, D. P., and Huynh-Do, U. (2006). Caveolin-1 is required for signaling and membrane targeting of EphB1 receptor tyrosine kinase. J Cell Sci 119, 2299-2309.

Vuorela, P., Hatva, E., Lymboussaki, A., Kaipainen, A., Joukov, V., Persico, M. G., Alitalo, K., and Halmesmaki, E. (1997). Expression of vascular endothelial growth factor and placenta growth factor in human placenta. Biol Reprod 56, 489-494.

Wang, Y., Zhang, Y., Lewis, D. F., Gu, Y., Li, H., Granger, D. N., and Alexander, J. S. (2003). Protease chymotrypsin mediates the endothelial expression of P- and E-selectin, but not ICAM and VCAM, induced by placental trophoblasts from pre-eclamptic pregnancies. Placenta 24, 851-861.

Ward, N. L., and Dumont, D. J. (2002). The angiopoietins and Tie2/Tek: adding to the complexity of cardiovascular development. Semin Cell Dev Biol 13, 19-27.

Warot, X., Fromental-Ramain, C., Fraulob, V., Chambon, P., and Dolle, P. (1997). Gene dosage-dependent effects of the Hoxa-13 and Hoxd-13 mutations on morphogenesis of the terminal parts of the digestive and urogenital tracts. Development 124, 4781-4791.

Wasserman, L., Ber, A., Goldman, J. A., and Allalouf, D. (1979). Composition of acidic glycosaminoglycans in human term placenta blood vessels. Artery 5, 45-60.

Whitaker, G. B., Limberg, B. J., and Rosenbaum, J. S. (2001). Vascular endothelial growth factor receptor-2 and neuropilin-1 form a receptor complex that is responsible for the differential signaling potency of VEGF(165) and VEGF(121). J Biol Chem 276, 25520-25531.

Williams, T. M., and Lisanti, M. P. (2004). The Caveolin genes: from cell biology to medicine. Ann Med 36, 584-595.

Williams, T. M., Williams, M. E., Kuick, R., Misek, D., McDonagh, K., Hanash, S., and Innis, J. W. (2005). Candidate downstream regulated genes of HOX group 13 transcription factors with and without monomeric DNA binding capability. Dev Biol 279, 462-480.

Yancopoulos, G. D., Davis, S., Gale, N. W., Rudge, J. S., Wiegand, S. J., and Holash, J. (2000). Vascular-specific growth factors and blood vessel formation. Nature 407, 242-248.

Zhang, E. G., Smith, S. K., Baker, P. N., and Charnock-Jones, D. S. (2001). The regulation and localization of angiopoietin-1, -2, and their receptor Tie2 in normal and pathologic human placentae. Mol Med 7, 624-635.

Zhang, Y. M., Xu, B., Rote, N., Peterson, L., and Amesse, L. S. (2002). Expression of homeobox gene transcripts in trophoblastic cells. Am J Obstet Gynecol 187, 24-32.

Zhou, Y., McMaster, M., Woo, K., Janatpour, M., Perry, J., Karpanen, T., Alitalo, K., Damsky, C., and Fisher, S. J. (2002). Vascular endothelial growth factor ligands and receptors that regulate human cytotrophoblast survival are

dysregulated in severe preeclampsia and hemolysis, elevated liver enzymes, and low platelets syndrome. Am J Pathol 160, 1405-1423.

Appendix 1

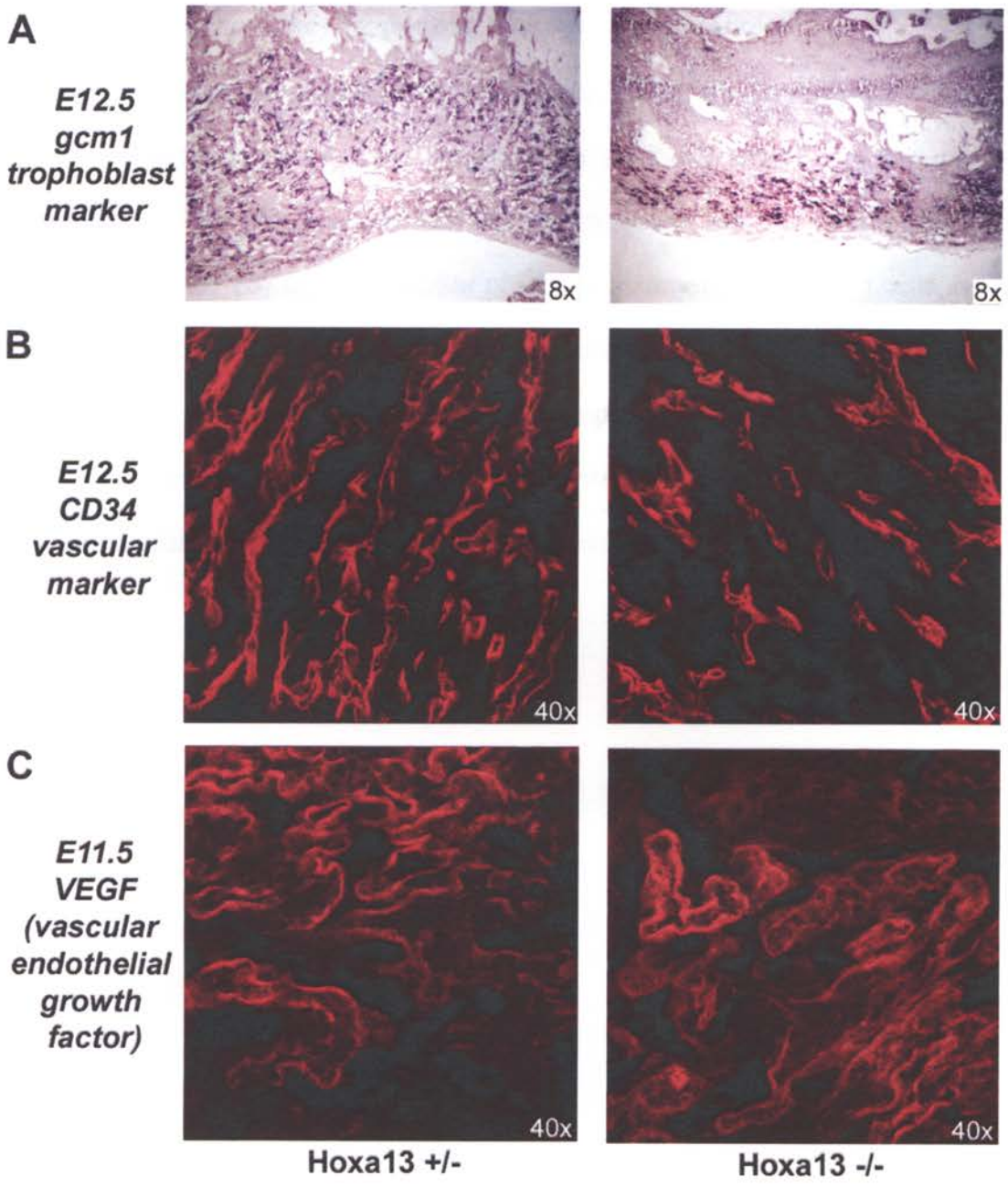
A
E12.5
gcm1
trophoblast
marker
8x
8x
B
E12.5
CD34
vascular
marker
40x
40x
C
E11.5
VEGF
(vascular
endothelial
growth
factor)
40x
40x
Hoxa13 +/-
Hoxa13 -/-

Appendix 1

Normal expression of key trophoblast and vascular markers

(A) *Gcm1*, a marker of labyrinth trophoblast cells, is strongly expressed in both the *Hoxa13* heterozygous and mutant placentas, as shown at E12.5 by ISH of wax sections. However, the reduction in the thickness of *Hoxa13* mutant labyrinths is clear. **(B)** CD34, a marker of ECs and hematopoietic stem cells, is present in the normal and mutant placental vasculature, as shown by IHC. CD34 was tested since the placenta is a site of hematopoiesis (Gekas et al., 2005). **(C)** As shown by IHC, VEGF is expressed by placental vasculature, and VEGF levels are indistinguishable between *Hoxa13* +/- and mutant labyrinths.

Appendix 2

Table C: Microarray gene information and statistical analysis

Color key
FDR p-value < 0.05 and FC > 2
FDR p-value < 0.05 and 0< FC <= 2
0.05 <= FDR p-value <0.1 and 0<FC<= 2
0.05 <= FDR p-value <0.1 and -2<=FC<0
FDR p-value <0.05 and -2<=FC<0
FDR p-value <0.05 and FC<-2

ProbeSetID	Gene Title	Gene Symbol	GO Molecular and/or Biological Function	FDR adjusted p-value	Fold Change (Mut/WT)
1434201_at	neuralin 1	Nrln1	development	0.0055	-4.4316
1417217_at	**melanoma antigen, family L, 2**	**Magel2**	---	0.0038	-2.8742
1439665_at	G protein-coupled receptor 23	Gpr23	receptor activity; 7tm_1	0.0038	-2.7686
1449533_at	RIKEN cDNA 1810057C19 gene	1810057C19Rik	---	0.0259	-2.5911
1448136_at	**ectonucleotide pyrophosphatase/phosphodiesterase 2**	**Enpp2**	nucleotide metabolism; nucleic acid binding; catalytic activity	0.0293	-2.3303
1460039_at	RIKEN cDNA 5930406N14 gene	5930406N14Rik	sugar binding	0.0123	-2.2925
1450883_a_at	**CD36 antigen**	**Cd36**	transport; cell adhesion; receptor activity	0.0103	-2.2849
1421201_a_at	**trophinin**	**Tro**	negative regulation of cell growth; cell adhesion	0.0419	-2.1552
1437360_at	hypothetical protein LOC279653	LOC279653	---	0.0164	-2.0695
1442865_at	hypothetical protein C130007D14	C130007D14	---	0.0002	-2.0609
1424233_at	mesenchyme homeobox 2	Meox2	development; somite specification; regulation of transcription	0.0477	-1.9817
1442368_at	potassium channel tetramerisation domain containing 12b	Kctd12b	voltage-gated potassium channel activity	0.0388	-1.9769
1423420_at	**adrenergic receptor, beta 1**	**Adrb1**	G-protein coupled receptor protein signaling pathway	0.0007	-1.9277
1416779_at	serum deprivation response	Sdpr	---	0.0953	-1.9266
1449145_a_at	**caveolin, caveolae protein**	**Cav**	endocytosis; protein binding	0.0703	-1.9237
1435382_at	**necdin**	**Ndn**	regulation of cell growth; regulation of transcription	0.0515	-1.8065
1452183_a_at	GTL2, imprinted maternally expressed untranslated mRNA	Gtl2	---	0.0515	-1.7955
1456326_at	Mus musculus similar to KIAA0970 protein (LOC333564), mRNA	---	---	0.0327	-1.7753
1418090_at	plasmalemma vesicle associated protein	Plvap	---	0.0264	-1.7753
1429310_at	fibronectin leucine rich transmembrane protein 3	Flrt3	---	0.0103	-1.6882

ProbeSetID	Gene Title	Gene Symbol	GO Molecular and/or Biological Function	FDR adjusted p-value	Fold Change (Mut/WT)
1434528_at	alanine and arginine rich domain containing protein	Aard	---	0.0830	-1.6841
1431094_at	retrotransposon-like 1	Rtl1	---	0.0751	-1.6799
1418788_at	**endothelial-specific receptor tyrosine kinase**	**Tek**	angiogenesis; kinase activity; cell-matrix and cell-cell adhesion; cell migration	0.0357	-1.5506
1447946_at	expressed sequence AW046396	AW046396	---	0.0281	-1.5239
1419468_at	RIKEN cDNA 1200003C23 gene	1200003C23Rik	heterophilic cell adhesion, sugar binding	0.0754	-1.5234
1432750_at	Mus musculus 10, 11 days embryo whole body cDNA, RIKEN full-length enriched library, clone:2810409C01	---	---	0.0561	-1.4863
1459913_at	Mus musculus adult male spinal cord cDNA, RIKEN full-length enriched library, clone:A330042I21	---	---	0.0882	-1.4839
1455096_at	mitogen-activated protein kinase kinase kinase kinase 5	Map4k5	pkinase;protein kinase activity	0.0477	-1.4713
1436367_at	Mus musculus transcribed sequences	---	---	0.0586	-1.3840
1450759_at	bone morphogenetic protein 6	Bmp6	cell growth and maintenance; cell differentiation; BMP signaling pathway	0.0327	-1.3467
1448501_at	transmembrane 4 superfamily member 6	Tm4sf6	---	0.0768	-1.3284
1416454_s_at	actin, alpha 2, smooth muscle, aorta	Acta2	cytoskeleton organization and biogenesis	0.0905	-1.3281
1416122_at	cyclin D2	Ccnd2	regulation of cell cycle; cytokinesis; cyclin-dependent protein kinase	0.0905	-1.3253

ProbeSetID	Gene Title	Gene Symbol	GO Molecular and/or Biological Function	FDR adjusted p-value	Fold Change (Mut/WT)
1427486_at	protein tyrosine phosphatase, receptor type, B	Ptprb	protein dephosphorylation; transmembrane receptor signaling	0.0629	-1.3099
1434939_at	**forkhead box F1a**	**Foxf1a**	vasculogenesis; organogenesis; transcription factor activity	0.0281	-1.3035
1418084_at	**neuropilin**	**Nrp**	angiogenesis; cell adhesion; neurogenesis; receptor activity	0.0953	-1.2908
1430415_at	RIKEN cDNA 4931428F02 gene	4931428F02Rik	---	0.0760	-1.2817
1448698_at	cyclin D1	Ccnd1	regulation of cell cycle; cytokinesis; kinase activity	0.0281	-1.2756
1447927_at	Mus musculus transcribed sequences	---	---	0.0650	-1.2498
1460674_at	RIKEN cDNA 2310021M12 gene	2310021M12Rik	receptor activity	0.0854	-1.2264
1436921_at	ATPase, Cu++ transporting, alpha polypeptide	Atp7a	metal and copper ion transport; metabolism	0.0650	-1.2183
1432387_at	RIKEN cDNA 1190003P12 gene	1190003P12Rik	carboxypeptidase activity	0.0518	-1.2172
1431296_at	coproporphyrinogen oxidase	Cpo	porphyrin and heme biosynthesis	0.0373	-1.2138
1427034_at	angiotensin converting enzyme	Ace	proteolysis and peptidolysis; zinc ion binding; hydrolase activity	0.0851	-1.2071
1433188_at	Mus musculus adult male corpora quadrigemina cDNA, RIKEN clone: B230112I24	---	---	0.0882	-1.2067
1457384_at	Mus musculus 0 day neonate head cDNA, RIKEN library, clone:4833438M18	---	---	0.0898	-1.2059
1454334_at	Mus musculus 10, 11 days embryo whole body cDNA, RIKEN library, clone:2810409C01	---	---	0.0694	-1.2006
1423292_a_at	periaxin	Prx	PDZ; intracellular signaling cascade	0.0703	-1.1945
1444893_at	Mus musculus transcribed sequences	---	---	0.0768	-1.1928
1433536_at	RIKEN cDNA 9830160H19 gene	9830160H19Rik	---	0.0629	-1.1887

ProbeSetID	Gene Title	Gene Symbol	GO Molecular and/or Biological Function	FDR adjusted p-value	Fold Change (Mut/WT)
1447508_at	Mus musculus 2 days pregnant adult female oviduct cDNA, RIKENlibrary, clone:E230011B21	---	---	0.0327	-1.1886
1421277_at	spectrin alpha 1	Spna1	G-protein coupled receptor protein signaling pathway; hemopoiesis; actin binding	0.0408	-1.1779
1457110_at	Mus musculus transcribed sequences	---	---	0.0987	-1.1697
1436582_at	Mus musculus transcribed sequence with strong similarity to protein sp:P00722 (E. coli) BGAL_ECOLI Beta-galactosidase (Lactase)	---	---	0.0649	-1.1649
1439514_at	CDC28 protein kinase 1	Cks1	cyclin-dependent protein kinase activity	0.0836	-1.1611
1430735_at	RIKEN cDNA 4930424G05 gene	4930424G05Rik	---	0.0586	-1.1610
1441735_at	Mus musculus transcribed sequences	---	---	0.0759	-1.1575
1441836_x_at	RIKEN cDNA 1700006H03 gene	1700006H03Rik	---	0.0357	-1.1549
1441941_x_at	serine (or cysteine) proteinase inhibitor, clade B, member 5	Serpinb5	serine-type endopeptidase inhibitor activity	0.0703	-1.1513
1441353_at	Mus musculus transcribed sequences	---	---	0.0515	-1.1486
1418286_a_at	ephrin B1	Efnb1	development; neurogenesis; axon guidance	0.0759	-1.1466
1453549_at	Mus musculus adult male testis cDNA, RIKEN full-length enriched library, clone:4930500G05	---	---	0.0479	-1.1448
1435487_at	Mus musculus 10 days neonate cerebellum cDNA, RIKEN library, clone:6530411F08	---	---	0.0948	-1.1378
1459214_at	Mus musculus transcribed sequences	---	---	0.0601	-1.1359
1444680_at	positive cofactor 2, multiprotein complex, glutamine/Q-rich-associated protein	Pcqap	regulation of transcription, DNA-dependent	0.0836	-1.1349
1459366_at	RIKEN cDNA 1110059F19 gene	1110059F19Rik	---	0.0282	-1.1319

ProbeSetID	Gene Title	Gene Symbol	GO Molecular and/or Biological Function	FDR adjusted p-value	Fold Change (Mut/WT)
1432339_at	Mus musculus adult male testis cDNA, RIKEN full-length enriched library, clone:4933432I03 product:unclassifiable, full insert sequence	---	---	0.0907	-1.1312
1431451_at	RIKEN cDNA 4933411C14 gene	4933411C14Rik	---	0.0479	-1.1264
1445915_at	Mus musculus transcribed sequences	---	---	0.0293	-1.1246
1435119_at	Mus musculus transcribed sequences	---	---	0.0882	-1.1240
1445481_at	Mus musculus transcribed sequence with weak similarity to protein ref:NP_286085.1 (E. coli) beta-D-galactosidase	---	---	0.0601	-1.1180
1453883_at	Mus musculus adult male testis cDNA, RIKEN full-length enriched library, clone:4933425B07	---	---	0.0970	-1.1176
1459959_at	Mus musculus transcribed sequences	---	---	0.0629	-1.1167
1447463_at	Mus musculus transcribed sequence with moderate similarity to protein pdb:1LBG (E. coli) B Chain B	---	---	0.0928	-1.1123
1433364_at	Mus musculus adult retina cDNA, RIKEN full-length enriched library, clone:A930036I15	---	---	0.0754	-1.1110
1457263_at	Mus musculus transcribed sequence with moderate similarity to protein ref:NP_038607.1 (M.musculus) L1 repeat, Tf subfamily	---	lipocalin; transporter activity	0.0649	-1.1109
1442063_at	RIKEN cDNA 5930437A14 gene	5930437A14Rik	---	0.0830	-1.1070
1458993_at	Mus musculus transcribed sequences	---	---	0.0907	-1.0969
1457435_x_at	myomesin 2	Myom2	muscle contraction and development	0.0907	-1.0931
1428424_at	RIKEN cDNA 2310035N15 gene	2310035N15Rik		0.0759	-1.0925
1439578_at	RIKEN cDNA 2210404M20 gene	2210404M20Rik	pre-mRNA splicing factor activity	0.0768	-1.0895
1446060_at	RIKEN cDNA 9230109A22 gene	9230109A22Rik	---	0.0446	-1.0778
1443460_at	Mus musculus transcribed sequences	---	---	0.0759	-1.0738

ProbeSetID	Gene Title	Gene Symbol	GO Molecular and/or Biological Function	FDR adjusted p-value	Fold Change (Mut/WT)
1442942_at	Williams-Beuren syndrome chromosome region 1 homolog (human)	Wbscr1	protein biosynthesis; nucleic acid binding	0.0694	-1.0702
1420495_a_at	vacuolar protein sorting 26 (yeast)	Vps26	intracellular protein transport	0.0759	1.0912
1460167_at	aldehyde dehydrogenase family 7, member A1	Aldh7a1	hearing; metabolism	0.0479	1.1481
1424438_a_at	leptin receptor gene-related protein	Obrgrp	receptor activity	0.0882	1.1666
1416075_at	salvador homolog 1 (Drosophila)	Sav1	---	0.0533	1.2029
1447849_s_at	avian musculoaponeurotic fibrosarcoma (v-maf) AS42 oncogene homolog	Maf	regulation of cell cycle, cell growth, and transcription	0.0736	1.2082
1417235_at	EH-domain containing 3	Ehd3	calcium ion binding; protein binding; ATP binding	0.0813	1.2575
1423062_at	insulin-like growth factor binding protein 3	Igfbp3	regulation of cell growth;growth factor binding	0.0016	1.8732
1429379_at	**extra cellular link domain-containing 1**	**Xlkd1**	cell adhesion receptor activity; hyaluronic acid binding	0.0023	3.5750

Appendix 3

HOXA13 directly regulates *EphA6* and *EphA7* expression in the genital tubercle vascular endothelia

Carley A. Shaut[1a], Chie Saneyoshi[1a], Emily A. Morgan[1], Wendy M. Knosp[3], Diane R. Sexton[2], and H. Scott Stadler[1,2,*]

[1] Department of Molecular and Medical Genetics, Oregon Health and Science University, Portland, OR 97239

[2] Shriners Hospital for Children Research Division, Portland, OR 97239

[3] Postdoctoral Scholar, UCSF-Mission Bay Campus

Rock Hall 381, 1550 4th Street, San Francisco, CA 94158-232

[a] (These individuals contributed equally to this work)

[*]Author of correspondence (email:hss@shcc.org)

Keywords: *Hoxa13*, Hypospadias, genital tubercle, vascular endothelia, *EphA6*, *EphA7*

As of December 20th, 2006, this manuscript was accepted for publication with revisions in Developmental Dynamics, and the revised copy was submitted to the publisher on December 18th, 2006.

Abstract

Hypospadias, a common defect affecting the growth and closure of the external genitalia, is often accompanied by gross enlargements of the genital tubercle (GT) vasculature. Because *Hoxa13* homozygous mutant mice also exhibit hypospadias and GT vessel expansion, we examined whether genes playing a role in angiogenesis exhibit reduced expression in the GT. From this analysis reductions in *EphA6* and *EphA7* were detected. Analysis of the *EphA6* and *EphA7* promoter regions revealed a series of highly conserved *cis*-regulatory elements bound by HOXA13 with high affinity. GT chromatin immunoprecipitation confirmed that HOXA13 binds these gene-regulatory elements *in vivo*. *In vitro*, HOXA13 activates gene expression through the *EphA6* and *EphA7* gene-regulatory elements. Together these findings reveal a novel site for HOXA13 activity in GT vascular endothelia where it directly regulates *EphA6* and *EphA7* expression, providing a transcriptional link between HOXA13, its target genes, and malformations affecting the growth and closure of the external genitalia.

Introduction

Hypospadias, a defect affecting the growth and closure of the external genitalia, is highly prevalent in the birth populations of industrialized nations, including the United States, United Kingdom, Sweden, and Japan (Giwercman et al., 1993; Paulozzi et al., 1997; Gallentine et al., 2001). While the frequency of hypospadias ranges as high as 1 in 125 live births, the molecular mechanisms underlying this defect are poorly understood (Svensson et al., 1997; Paulozzi et al., 1997; Stadler, 2003). One phenotype commonly associated with hypospadias is the enlargement of blood vessels supplying the glans or prepuce (Baskin et al., 1998; Baskin, 2000). At present, no molecular link between hypospadias and vessel enlargement in the genitalia has been identified; however, studies examining perturbations in Eph-ephrin signaling may provide important clues towards understanding the pathology of hypospadias and its associated vascular malformations (reviewed by Eichmann et al., 2005a; and Eichmann et al., 2005b; Hinck, 2004; Klagsbrun and Eichmann, 2005; Davy and Soriano, 2005). Indeed, Eph-ephrin signaling is essential for the patterning of multiple tissues and cell types including vascular endothelial cell assembly, cell migration, mesenchymal cell condensation, vascular bed formation, tumor neovascularization, and the closure of the external genitalia (Wang et al., 1998; Ogawa et al., 2000; Stadler et al., 2001; Chan et al., 2001; Dravis et al., 2004; Davy et al., 2004; Marquardt et al., 2005; Egea et al., 2005).

Recently, we and others have shown that HOXA13 function is necessary for *EphA7* expression in the developing limb (Stadler et al., 2001; Salsi and Zappavigna, 2006). Recognizing that Hoxa13-deficient mice also exhibit hypospadias and capillary

vessel enlargement (Morgan et al., 2003), we hypothesized that Eph-ephrin signaling may be affected in the genital tubercle (GT) vasculature, providing a transcriptional link between *Hoxa13* and the genes whose products are essential for normal GT vessel development. Testing this hypothesis, we report that *Hoxa13* directly regulates *EphA6* and *EphA7* expression in the GT vascular endothelia. Analysis of the *EphA6* and *EphA7* promoter regions revealed a conserved series of DNA sequences bound with high affinity by the HOXA13 DNA binding domain (A13). *In vivo*, direct interactions between HOXA13 and the *EphA6* and *EphA7* promoter elements were detected in the GT using *Hoxa13*-directed chromatin immunoprecipitation. *In vitro*, HOXA13 can utilize the bound gene-regulatory elements in the *EphA6* and *EphA7* promoters to direct gene expression. Together these findings indicate that *EphA6* and *EphA7* are direct transcriptional targets of HOXA13 in the genital tubercle vascular endothelia, providing new insight into the cell-signaling mechanisms functioning during the growth and development of the external genitalia.

Results

Vessel expansion is present throughout GT development in *Hoxa13*-GFP homozygous mutants

Analysis of the distal GT from embryonic days (E) 12.5 to 15.5 revealed average vessel diameters of 15 μm (± 0.5 μm; n=12 independent samples) in diameter in *Hoxa13-GFP* wild type and heterozygous mutants. In contrast, the GT vasculature of age-matched homozygous mutants exhibited greatly enlarged vessels with average diameters of 85 μm (± 15 μm; n=12 independent samples) (Figure 1). Interestingly, embryonic sex did not influence the presentation of the vascular phenotype as homozygous mutant male and female embryos exhibited similar increases in GT vessel diameter (Figure 1; compare E-H with I-L).

EphA6 and *EphA7* are reduced in the GT vascular endothelia of *Hoxa13* homozygous mutants

Recognizing that defects in vascular patterning are strongly associated with perturbations in Eph-ephrin signaling, we examined whether the affected GT vasculature exhibited changes in the expression of Eph receptors or their ephrin ligands. While no changes in EPHA2, EPHA4, EPHA5, EPHB2, EPHRIN A2, or EPHRIN A5 expression were detected in the *Hoxa13*-GFP homozygous mutants (data not shown), both EPHA6 and EPHA7 were consistently reduced in the GT vascular endothelia compared to heterozygous mutant controls (Figure 2 A-D), which do not exhibit a GT phenotype (Morgan et al., 2003). In the vasculature, HOXA13-GFP, EPHA6, and EPHA7 were strongly co-localized in the endothelial layer of heterozygous controls, whereas the reduced levels of EPHA6 and

EPHA7 in the homozygous mutants minimized our detection of co-localization in the expanded GT vasculature (Figure 2 E-L). PECAM-1 expression was also present in the affected GT vasculature, suggesting that endothelial cell identity was not affected by the loss of Hoxa13 function (Figure 2 M-P).

Semi-quantitative RT-PCR analysis confirmed the levels of *EphA6* and *EphA7* expression detected by immunohistochemistry. In particular, a uniform level of *EphA6* and *EphA7* expression was detected throughout the GT mesenchyme in *Hoxa13-GFP* heterozygous and homozygous mutant embryos (Figure 3A). Next, because cell-specific changes in gene expression are often not detectable in whole tissue RNA samples, we examined whether endothelial cells purified GT vasculature exhibited reductions in *EphA6* and *EphA7* expression, as observed by immunohistochemistry. RT-PCR analysis of GT endothelial cell isolates confirmed that *EphA6* and *EphA7* are expressed in the endothelial component of the GT vessels along with *Hoxa13* and PECAM-1 in *Hoxa13-GFP* heterozygous mutants (Figure 3B). In contrast, the expression of *EphA6* and *EphA7* was consistently reduced (n=3 independent assessments) in the purified GT vascular endothelia of *Hoxa13*-GFP homozygous mutants, although no difference in PECAM-1 expression was observed (Figure 3B).

HOXA13 binds discrete regions of the *EphA6* and *EphA7* promoters

DNA sequence analysis of the *EphA6* and *EphA7* promoter regions revealed several A-T rich regions matching sequences we previously identified as sites bound by HOXA13 (Knosp et al., 2004) (Figure 4A). Since key gene regulatory regions are often conserved between species, we examined whether

the *EphA6* and *EphA7* regions containing the clustered HOXA13 binding sites are conserved using the UCSC Genome Browser (Kent et al., 2002). For the *EphA6* element, a high degree of conservation was observed between mouse (*Mus musculus*), human (*Homo sapien*), rat (*Rattus norvegicus*), and opossum (*Monodelphis domestica*) with complete identity in several A-T rich regions where HOXA13 is thought to bind (Knosp et al., 2004; Salsi and Zappavigna, 2006; McCabe and Innis, 2005) (Figure 4B). For the *EphA7* fragment, strong sequence conservation was also detected between mouse, human, and rat, and opossum and several additional mammalian species including: dog (Canis familiarus), armadillo (*Asypus novemcinctus*), and elephant (*Loxodonta africana*) with strong identity within the putative HOXA13 binding site (Figure 4B).

EMSA analysis of the *EphA6* region (-2410 to -2067) revealed consistent binding by the HOXA13 DNA binding peptide, which could be competitively removed using identical non-labeled DNA fragments (Figure 4C). Similar binding was also observed for the 325 bp *EphA7* promoter region (-839 to -514) as well as an additional HOXA13-regulated region previously characterized by Salsi and Zappavigna (2006) (data not shown) (Figure 4C). Interestingly, both the *EphA6* and *EphA7* regions exhibited a staggered series of mobility-shifted bands when incubated with 0.2 μM A13 peptide, suggesting that multiple binding sites are present in the *EphA6* and *EphA7* conserved regions which require a higher protein concentration to be completely saturated (Figure 4C). Increasing the HOXA13 DNA binding peptide concentration to 2 μM produced a single higher

molecular weight product for the *EphA6* and *EphA7* promoter elements, indicating saturation of all Hoxa13 binding sites (Figure 4C).

Next, to establish whether the HOXA13 DNA binding domain peptide binds DNA as monomer or as higher order complex, we performed sedimentation equilibrium analysis. Analysis of the sedimentation the HOXA13 DNA binding peptide bound to a DNA identified a 1:1 stoichiometric ratio of peptide to DNA, suggesting that the staggered bands detected by EMSA most likely reflect the concentration-dependent saturation of multiple binding sites by the monomeric protein, rather than higher order complexes.

HOXA13 binds the *EphA6* and *EphA7* *cis*-regulatory elements *in vivo*

Next, to determine whether HOXA13 directly interacts with the *EphA6* and *EphA7* promoter sequences *in vivo*, we examined whether GT-specific chromatin containing the conserved *EphA6* and *EphA7* regions was immunoprecipitated with a HOXA13 antibody (αA13). Previous characterization of the HOXA13 antibody confirmed that it can bind both HOXA13 wildtype and mutant proteins and facilitate the immunoprecipitation of gene regulatory elements directly bound by wildtype HOXA13 (Knosp et al., 2004). PCR amplification of wildtype αA13-chromatin immunoprecipitates consistently detected the *EphA6* and *EphA7* promoter fragments (n= 5 independent assessments) (Figure 5). In homozygous mutants, the *EphA6* and *EphA7* promoter fragments could not be detected in the αA13-immunoprecipitated chromatin (n= 5 independent assessments) (Figure 5), suggesting that HOXA13's DNA binding function, which is absent in the mutant

HOXA13-GFP protein is necessary for the immunoprecipitation of these gene regulatory sequences.

In vitro utilization of the *EphA6* and *EphA7* promoter elements by full length HOXA13

The capacity of full length HOXA13 to regulate gene expression through the *EphA6* and *EphA7* promoter fragments was assessed in NG108-15 cells. In the absence of the *EphA6* or *EphA7* promoter fragments the empty pGL4.1 luciferase plasmid produced insignificant amounts of luciferase when co-transfected with a *Hoxa13* expression plasmid (pCMV*Hoxa13*) (Figure 6). Co-transfection of pCMV*Hoxa13* with pGL4.1 plasmid containing the forward orientation of the *EphA6* promoter fragment produced nearly a four-fold increase in luciferase expression (Figure 6). Interestingly, co-transfection of pCMV*Hoxa13* with the pGL4.1 plasmid containing the reverse orientation of *EphA6* promoter fragment produced no increase in luciferase expression, suggesting the *EphA6* gene-regulatory region functions in an orientation-specific manner. In contrast, activation of the *EphA7* promoter fragment by HOXA13 facilitated luciferase expression at levels 3-4 fold higher than controls independent of its orientation, suggesting the sequence bound by HOXA13 may function as an enhancer (Figure 6).

The loss of EphA7 is not sufficient to cause gross enlargement of the GT vasculature

The individual function of *EphA7* was assessed in the developing GT vasculature using a null *EphA7* allele (Holmberg et al., 2000). A comparison of

the GT vessel diameters between wildtype and *EphA7* homozygous mutant embryos revealed no significant expansions of the GT vessels (Figure 7), suggesting that the expression of *EphA6* in the GT vasculature may be sufficient to compensate for the loss of *EphA7* function, or that *EphA7* does not play a role in regulating vessel wall diameter. The effect of a combinatorial loss of *EphA6* and *EphA7* in the GT vasculature could not be assessed as *EphA6* null mutations are early embryonic lethal (Brown et al., 2000).

Discussion

In humans, the loss of HOXA13 function causes Hand-Foot-Genital Syndrome (HFGS), an autosomal dominant disorder that profoundly affects the development of the external genitalia (hypospadias), uterus, vagina, cervix, bladder, and ureter (Stern et al., 1970; Mortlock and Innis, 1997; Warot et al., 1997; Morgan et al., 2003; Stadler, 2003). An important step towards understanding the developmental basis for the genitourinary defects associated with HFGS is the identification of the genes directly regulated by HOXA13. In this report we identify *EphA6* and *EphA7* as direct transcriptional targets of HOXA13 in the GT. The *in vivo* association of HOXA13 with gene-regulatory elements present in *EphA6* and *EphA7*, as well as their *in vitro* utilization by HOXA13 to direct gene expression, provides strong evidence that HOXA13 can regulate the tissue-specific expression of these receptor tyrosine kinases.

Studies examining the functional consequences of perturbations in Eph receptor signaling indicate that changes in cell migration, morphology, and

adhesion are the major phenotypes in tissues lacking one or more Eph receptor or ephrin ligand (Shamah et al., 2001; Wahl et al., 2000; reviewed by Pasquale 2005; Cooke et al., 2005). In the developing vasculature, functional studies of *EphA2, ephrin A1, ephrin B2,* and *EphB4* firmly establish a role for Eph-ephrin signaling throughout the angiogenic process, including endothelial cell proliferation, assembly, and extracellular matrix remodeling (Adams et al., 2001; Gerety et al., 1999; McBride and Ruiz, 1998; Hunter et al., 2006).

A link between Hox proteins and the expression of ephrin ligands and Eph receptors has also been established. In the hindbrain, the loss of *Hoxa1* and *Hoxb1* directly affect the expression of *EphA2* in rhombomere 4, whereas in the developing microvasculature, antisense oligos directed towards *Hoxb3* also caused reductions in *ephrin A1* in the vascular endothelia (Chen et al., 1998; Myers et al., 2000). Finally the loss of HOXA13 function has also been linked to reductions in *EphA7* in the developing limb mesenchyme and *EphA7* and *EphA4* in the umbilical artery endothelia (Stadler et al., 2001).

While the characterization of the combinatorial functions of *EphA6* and *EphA7* in the GT vasculature await the production of a conditional *EphA6* allele, the present body of evidence linking perturbations in Eph receptor signaling to angiogenic defects suggests that the combined reduction of *EphA6* and *EphA7* in the GT vasculature may cause a change in cell adhesion, which under vascular load could affect the overall diameter of the GT vessels. Functionally, the loss of *EphA7* in the embryo causes defects in cell adhesion and anencephaly, although no defects in the developing vasculature were reported (Holmberg et al., 2000).

Furthermore, the loss of HOXA13 function also affects the morphology of the umbilical artery endothelia, which exhibit reduced levels of *EphA4* and *EphA7* expression (Stadler et al., 2001).

In the limb, HOXA13 and HOXD13 function in a redundant manner to regulate *EphA7* expression (Salsi and Zappavigna, 2006). This finding provides a possible explanation for the maintenance of *EphA7* expression in the GT mesenchyme of *Hoxa13* homozygous mutants as both *Hoxa13* and *Hoxd13* are co-expressed strongly in this region (Warot et al., 1997, Scott et al., 2005). More importantly, among the group 13 HOX proteins, only Hoxa13 has been reported to be expressed in vascular endothelia (this work, Warot et al., 1997, Stadler et al., 2001). Thus, in the GT vasculature, the loss of *Hoxa13* function should affect *EphA7* expression more severely, due to the absence of functionally redundant factors such as HOXD13.

Interestingly, our ChIP analysis in the GT did not detect HOXA13 binding to the site described by Salsi and Zappavigna (2006) in the limb, although we did verify that the A13 DNA binding domain peptide could bind this site *in vitro*. One possible explanation for this discrepancy is that the HOXA13 co-factor, MEIS-1B does not co-localize with HOXA13 in the limb, but strongly co-localizes in the genitourinary tissue, providing a mechanism to facilitate genitourinary-specific interactions between HOXA13 and its target DNA sequences (Williams et al., 2005). Alternatively, DNA accessibility may also vary in limb versus genitourinary chromatin which could also account for the differential binding of

HOXA13 to specific gene-regulatory sequences in the limb versus genitourinary tissues (Vashee et al., 1998; Kodadek, 1998).

Interestingly, a common theme emerging from studies of HOXA13-deficient genitourinary tissues is that epithelial lineages appear to be affected in a similar manner. Indeed, the urethral plate epithelium (which serves as a signaling center for the genital tubercle), the vascular endothelia of the umbilical arteries, and the epithelia lining the developing bladder and ureter (data not shown), all exhibit changes in cell morphology and stratification with the loss of functional HOXA13 (present study, Perriton et al., 2002; Morgan et al., 2003). While alterations in epithelial cell morphology and stratification could reflect a loss in cellular identity, this possibility is unlikely as *sonic hedgehog* expression is maintained in the mutant urethral plate epithelium, and PECAM-1 expression is also maintained in the mutant vascular endothelia (this study; Morgan et al., 2003). Thus, altered epithelial morphology and stratification in the mutant GT vasculature is more likely to reflect a change in key matrix or cytoskeletal components. These factors are necessary for a tissue-specific morphological state, and it has been recently demonstrated that they are regulated by Eph-ephrin signaling (Hunter et al., 2006; Harbott and Nobes, 2005; reviewed by Cheng et al., 2002; Marston and Goldstein, 2006).

Experimental procedures

Mouse strains

Hoxa13-GFP mutant embryos were derived from heterozygous intercrosses as described (Stadler et al., 2001; Morgan et al., 2003). The mutant HOXA13 allele encodes a fusion protein of HOXA13 and green fluorescent protein where the last 34 amino acids of HOXA13, encoding the DNA contacting third helix (ISATTNLSERQVTIWFQNRRVKEKKVINKLKTTS), is removed and replaced with the EGFP protein. The nuclear localization, turnover, and tissue-specific expression of the HOXA13-GFP protein appeared identical to the wild type protein (Stadler et al., 2001). Timed matings were used to establish embryonic gestational age in embryonic days (E) where E0.5 represents the first day of vaginal plug detection. *EphA7* homozygous mutant embryos were produced by intercrosses of *EphA7* heterozygous mutant mice, kindly provided by Jonas Frisén (Karolinska Institute, Stockholm, Sweden). *EphA7* embryo genotypes were determined by PCR of yolk sac derived DNA using the following primers: *EphA7* mutant allele: 5'-CTAAGGTCCTATTTTGCCTG-3', 5'-CATTACACTTCCAGACCTGGGAC-3'. *EphA7* wild type allele: 5'-CAGGAGTGGCCCGGGAA-3', 5'-CATTACACTTCCAGACCTGGGAC-3' and 40 cycles of 94°C (30 sec), 54°C (30 sec), 72°C (30 sec). All procedures using mice were done in accordance with an approved institutional animal protocol (A729 to HSS).

GT histology and immunohistochemistry

Paraffin (Paraplast Plus, Fisher) embedded *Hoxa13* wild type and homozygous mutant embryos (E 12.5-15.5) were sectioned at 7μm intervals and placed sequentially onto Superfrost plus slides (Fisher) and stained with hematoxylin and eosin as described by Stadler and Solursh (1994). Sections containing the GT and its associated vasculature were photographed using a Leica DMLB2 microscope and a Q Imaging Digital camera.

E13.5 *Hoxa13* heterozygous and homozygous mutant embryos were embedded in OCT (Tissue Tek) and sectioned as previously described (Morgan et al., 2003). Antibodies specific for *EphA6* (R&D Systems MAB6071), *EphA7* (R&D Systems MAB1495), and PECAM-1 (BD Pharmingen 553708) were used at dilutions of 1:200 and incubated on the sections at 4°C overnight. Secondary antibodies labeled with Cy5 were used as described by the manufacturer (Jackson Immunological). Imaging was performed on a Bio-Rad MRC1024 confocal microscope using Kalman filtering. Identical laser level, iris, and black level settings were used for all samples.

GT endothelial cell isolation and RT-PCR

The distal half of the E13.5 genital tubercles were isolated by micro-dissection in 1X phosphate buffered saline. E13.5 embryos were chosen because they strongly express *Hoxa13*, *EphA6*, and *EphA7* within the genital tubercle vasculature as shown by immunohistochemistry and *in situ* hybridization. Approximately 5-8 GTs of identical *Hoxa13* genotype were combined to gain

adequate amounts of endothelial cells and isolated RNA. The tissues were pooled in individual Netwells (Costar) and treated with 0.2% Collagenase Type IV (Gibco) at 37°C for 30 minutes with occasional shaking. After collagenase treatment the tissues were placed in digestion media (0.1% Trypsin/EDTA [Gibco], 0.2% Collagenase IV, in PBS) for 15 minutes at 37°C, using gentle pipetting every 5 minutes to dissociate the tissue. Cell flow-through was collected in 15mL tubes with 10mL quenching buffer (15% fetal bovine serum [#26140-087, Gibco] and 0.1% Bovine Serum Albumin in D-PBS [BP1605-100, Fisher]). Finally, to collect any residual cells, the Netwell baskets were rinsed with 0.1% BSA/PBS and added to the cell flow-through. Cells were stored on ice for 5 minutes and spun at 3000 rpm for 5 minutes, followed by an additional quenching wash and spin. Dynabeads were coated with PECAM-1 antibody (MEC 13.3, #553369 BD Pharmingen) as described by the manufacturer (Dynal). 2.5×10^6 cells were combined with the Dynabeads-antibody complex (3x more beads than cells), and mixture was incubated for 1 hour at 4°C on a rotating platform. The bead-antibody-cell complexes were isolated with a magnet, and the remaining PECAM negative cells were collected as a control. The cells were gently washed with 0.1% BSA/PBS and collected for RNA extraction using RNA Stat-60 (CS-110, Tel-Test). GT mesenchyme RNA was isolated in a similar manner using dissected genital tubercles from E13.5 embryos. RNA quality was analyzed by agarose gel electrophoresis and UV spectroscopy. One µg of RNA was used for cDNA synthesis using the Superscript First-Strand Synthesis system (Invitrogen).

Semi-quantitative RT-PCR:

cDNAs derived from distal GT RNA or endothelial cell RNA was used for semi-quantitative RT-PCR to detect the expression levels of *EphA6*, *EphA7*, *Gapdh*, *Pecam-1*, and *Hoxa13* in *Hoxa13* wild type and homozygous mutants. For RT-PCR, each cDNA template was diluted 1:1 with water. The following gene-specific primer sequences were used: *EphA6*-For: 5'-GAGAGACCGTACTGGGAAATG-3'; *EphA6*-Rev: 5'-GCCTGTGGTTTCTCTCCTTC-3' (NM007938, bp2901-3042); *EphA7*-For: 5'-CTCTTCGCTGCTGTTAGCAT-3'; *EphA7*-Rev: 5'-GTGATGACTCCATTGGGATG-3' (BC026153, bp1433-1566); *Pecam1*-For: 5'-CCAGTGCAGAGCGGATAAT-3'; and *Pecam1*-Rev: 5'-GCACCGAAGTACCATTTCAC-3' (NM008816, bp1487-1634); *Hoxa13*-For: 5'-CTGGAACGGCCAAATGTACT-3'; *Hoxa13*-Rev: 5'-TATAGGAGCTGGCGTCTGAA-3' (NM008264, bp952-1058).

Gapdh primers were previously described (Shou et al 2005). All RT PCR primer pairs were designed to flank an intronic sequence to distinguish any PCR products derived from genomic DNA contamination. Each RT-PCR analysis was tested from at least three independent RNA isolates.

EphA6 and EphA7 promoter analysis

Sequence analysis of the *EphA6* promoter (Ensembl: ENSMUST00000068860) identified a single region (-2410 to -2067) containing multiple T-A-A motifs we

previously identified as being bound by HOXA13 (Knosp et al., 2004). Analysis of the *EphA7* locus (Ensembl: ENSMUSG00000028289) identified the HOXA13 binding site characterized by Salsi and Zappavigna (2006) as well as a novel region (-839 to -514) containing several T-A-A motifs which we examined in this report for HOXA13 binding and gene regulation. PCR amplification of the *EphA6* and *EphA7* promoter regions was performed using the following primers: *EphA6*P1F 5'-GATAGGCAGAATGCCAGGTG-3'; *EphA6*P1R 5'-GGAGCAAGGAAAGCTCAGAA-3'; *EphA7*P1F 5'-TGCCTCTCGAGTTACAGAACAG-3'; *EphA7*P1R 5'-GGGAGCACTTGGCTTTTAGC-3'. HOXA13 binding to the PCR amplified *EphA6* and *EphA7* promoter fragments was determined using an electrophoretic mobility shift assay (EMSA) as previously described (Knosp et al., 2004). Briefly, the amplified PCR products were radio-labeled with T4 Polynucleotide kinase and assessed for HOXA13 binding by incubation with a HOXA13 DNA binding domain peptide (A13) followed by non-denaturing acrylamide gel electrophoresis. Competitor DNA consisting of the identical unlabeled PCR product was used to assess the binding affinity for the *EphA6* and *EphA7* promoter sequences as described (Knosp et al., 2004). Interspecies comparisons of the *EphA6* and *EphA7* regions containing the HOXA13 binding sites were performed using the UCSC Genome Browser (Kent et al., 2002).

Oligomerization analysis of the HOXA13 DNA binding peptide and DNA

Complexes of the A13 DNA binding domain peptide and DNA were assessed for their oligomerization state using sedimentation equilibrium ultracentrifugation on a Beckman Coulter XL-1A Protein Analysis System as previously described (Huffman et al., 2001). A self annealing fluorescein-labelled oligonucleotide, 5'-6-FAM-CCCATAAACCCCCCCGGTTTATGGG-3' (5μM) was combined with the A13 DNA binding peptide (6μM to 10 μM) in a buffer containing 80mM KCl, 10mM $MgCl_2$, 0.2mM EDTA, 1mM DTT, and 20mM Tris.HCl pH 7.8. The samples were centrifuged at 4°C at 26,000 or 32,000 rpm in a AN-60Ti rotor equipped with 12mm-path length Epon double sector cells. The absorbance was monitored at 480 nm as a function of radial distance. Molecular weights of the DNA and DNA + protein complexes were calculated from a non-linear least squares fit of the absorbance data using the software supplied with the Model XL-1A system. A density value for the solvent of 1.005g/ml was used for the calculations. The partial specific volumes of the peptide-DNA complexes were estimated by taking the mass-weighted average of the partial specific volumes for the free oligonucleotide (8100 daltons) and free peptide (8137 daltons). Using the additivity method of Cohn and Edsall (1943) the partial specific volume of the free peptide was estimated to be 0.745 ml/g. The partial specific volume of the free oligonucleotide was determined using a separate sedimentation equilibrium analysis in identical buffers without peptide. The partial specific volume of unbound oligonucleotide was determined to be 0.512 ml/g. Using the

mass weighted partial specific volume averages for the peptide and DNA, a partial specific volume of 0.629 g/ml was calculated for the samples containing peptide and DNA in a 1:1 ratio. Using this value, the molecular weight of the complex was determined to be 16,900 daltons, indicating that the peptide + DNA complex was present in a 1:1 stoichiometric ratio, confirming that the A13 DNA binding peptide binds monomerically to its DNA binding site.

Chromatin immunoprecipitation assays

Chromatin immunoprecipitation (ChIP) was performed using a *Hoxa13* antibody and whole genital tubercles dissected from E 12.5 embryos. Multiple attempts to isolate sufficient quantities of endothelial cells for ChIP were not successful as each genital tubercle yielded less than 1000 endothelial cells, whereas 10^6 cells are required to produce sufficient chromatin quantities for immunoprecipitation (Lavrrar and Farnham, 2004). Therefore all PCR amplification of the HOXA13 bound DNA regions were derived from whole genital tubercle chromatin isolates. 300 bp fragments encompassing bases -3000 to +1 of the EphA6 (Ensembl: ENSMUST00000068860) and EphA7 (Ensembl: ENSMUSG00000028289) promoters were examined for *in vivo* association with HOXA13. The genital tubercles were dissected in PBS containing 15 μL/mL protease inhibitor cocktail (PIC) (Sigma).

Tissues were fixed in 1% formaldehyde/ PBS and rocked at room temperature for 10 min. Protein-DNA cross linking was stopped by the addition of glycine to a final concentration of 0.125 M for 5 minutes. Next the samples

were centrifuged at low speed, and the pellet was washed once with cold PBS containing PIC and centrifuged at low speed. The pellet was re-suspended in 100 µL cell lysis buffer (5 mM PIPES, pH 8.0 / 85 mM KCl / 0.5% NP40) plus PIC and incubated on ice for 10 min. Next, the lysate suspension was micro-centrifuged at 5,000 rpm for 5 min at 4°C, followed by resuspension in 50 µL nuclear lysis buffer (50 m Tris-HCl, pH 8.1, 10 mM EDTA, 1% SDS) plus PIC and incubation for 10 min on ice. The lysed nuclei were sonicated for 20 periods of 30 sec ON and 1 min OFF at 4°C using a Bioruptor (Cosmo Bio) to produce sheared chromatin of an average length of 200-1000 bp. The sheared chromatin was micro-centrifuged at 13,000 rpm for 10 min at 4°C and the supernatant was transferred to a new tube.

ChIP was performed using a ChIP Assay Kit as described by the manufacturer (Upstate Biotechnologies/Millipore). Each chromatin supernatant was pre-cleared with 40 µL of Salmon Sperm DNA/ Protein A Agarose (Upstate Biotechnology). The chromatin samples were incubated with the *Hoxa13* antibody or IgG control antibody on a rotating platform at 4°C for 3 hours. Washes, DNA elution, and reverse cross-linking were performed as described in the Upstate ChIP Assay Kit. Samples were ethanol precipitated, resuspended in 100 µl of TE, and DNA purified using the Qiaquick PCR Purification kit (Qiagen).

The eluted DNA from the *Hoxa13* antibody, control IgG, or no antibody samples were assessed for the presence of the EphA6 and EphA7 promoter DNA using PCR. Primers used to amplify the ChIP positive regions were

identical to those used to amplify the candidate binding site regions described above.

Epha6 and Epha7 Luciferase Assays

NG108-15 cells (ATCC#HB-12317) were maintained and transfected as previously described (Knosp et al., 2004). Transfections were performed in 12 well plates (Costar) using 1.5 µg of a pGL4 plasmid containing either the forward (PGL4.1-*EphA6*F or PGL4.1-*EphA7*F) or reverse (PGL4.1*EphA6*R or PGL4.1-*EphA7*R) orientations of the *EphA6* or *EphA7* ChIP positive regions as well as 0.25 µg of the normalization vector, pRL-CMV Renilla, and 0.5 µg pCMV-*Hoxa13*-HA or an empty pCMV control plasmid per well. Cell lysates were processed to detect luciferase activity using the Dual-Glo Luciferase Assay System (Promega) in OptiPlate-96F black plates (Packard) as described (Knosp et al., 2004). Luciferase activity was detected using a Packard Fusion Microplate Analyzer (Perkin Elmer). Sample wells were read 3 times for 1 sec each and averaged. Three replicates of each transfection were performed and each transfection assay was repeated 3 times. Results were normalized for transfection efficiency using relative Renilla luciferase expression levels as described by the manufacturer (Promega) and plotted using SigmaPlot 9.0 (Systat).

Figures and Figure Legends

Figure 1. Hoxa13-deficient mice display enlarged blood vessels in the developing genital tubercle

Hematoxylin and eosin staining of sectioned genital tubercles from wild type (**A-D**), homozygous mutant male (**E-H**), and homozygous mutant female (**I-L**) embryos at embryonic days (E) 12.5-15.5. Arrows denote a typical example of normal vessel diameters in wild type embryos (**A-D**) or enlarged vessels in homozygous mutants (**E-L**). UPE= urethral plate epithelium. Bar is 100 μm.

Figure1:

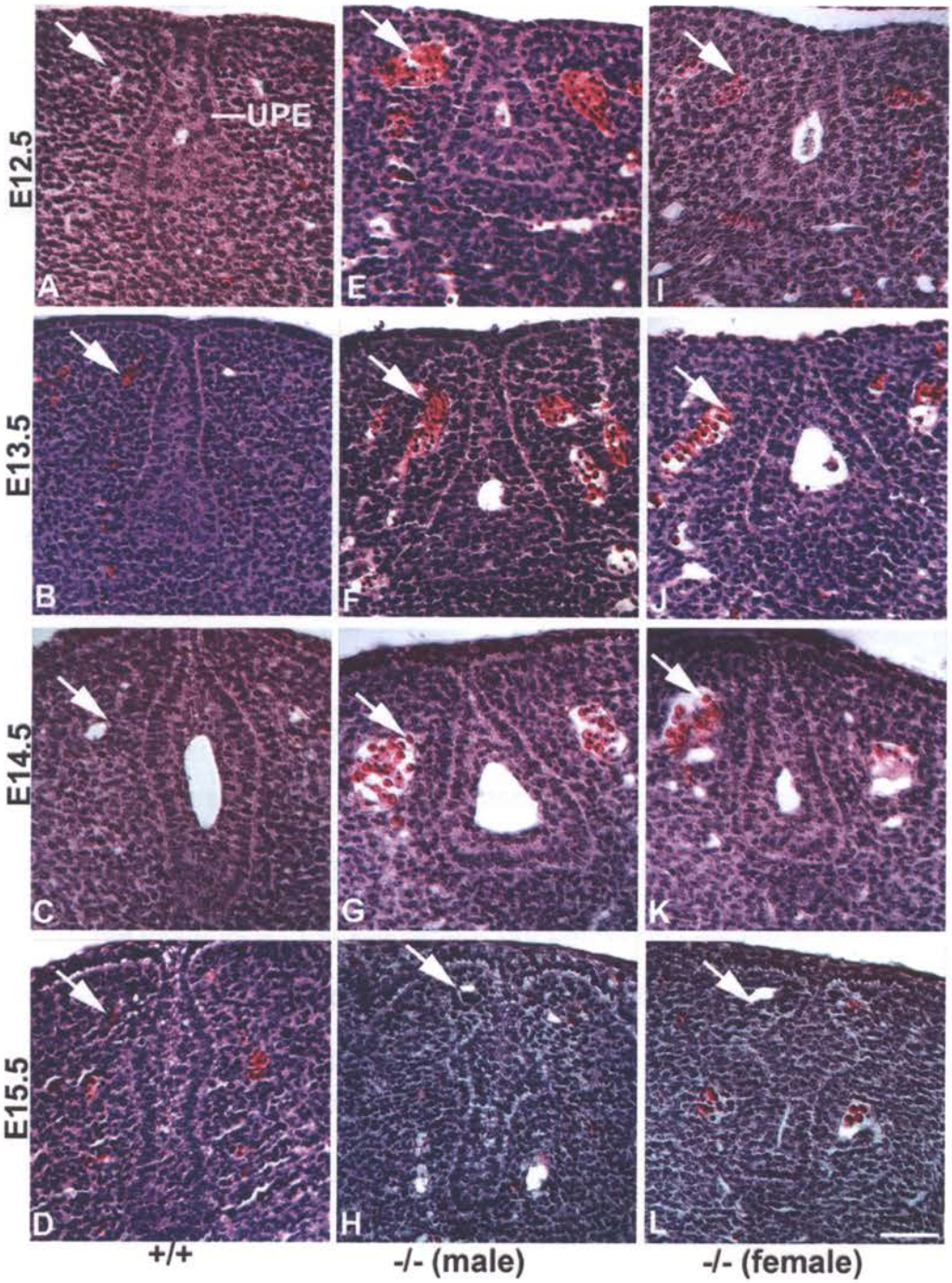

Figure 2. Immunohistochemical localization of EphA6 and EphA7 in the Genital Tubercle of E13.5 Hoxa13-GFP mice.

(A and C) *EphA6* and *EphA7* (red signal) are expressed in the GT mesenchyme (MES) as well as the endothelial cells lining the GT vasculature (arrows) of heterozygous *Hoxa13-GFP* embryos. (**B** and **D**) *EphA6* and *EphA7* expression is reduced in the enlarged GT vessels of age-matched *Hoxa13* homozygous mutants (arrows). (**E** and **G**) Co-localization (yellow signal) of *Hoxa13*-GFP with *EphA6* and *EphA7* in the GT vascular endothelia of heterozygous embryos. Arrows denote co-localization in the GT endothelia. (**F** and **H**) Reduced expression of *EphA6* and *EphA7* in the homozygous mutant vascular endothelia. Arrows denote the enlarged vasculature. (**I-L**) Higher magnification images of the heterozygous control and homozygous mutant vessels depicted in panels E-H. (**M-P**) PECAM-1 expression (red) is maintained in the GT vascular endothelia of *Hoxa13*-GFP (green) heterozygous mutant controls and age-matched homozygous mutants. UPE: urethral plate epithelium, MES: mesenchymal tissue, R: red blood cells. Bar represents 140 μm for A-H, 20 μm for I-L, and 70 μm for M-P. For clarity, only male GTs are shown, although similar vascular defects were observed in mutant female GTs.

Figure 2:

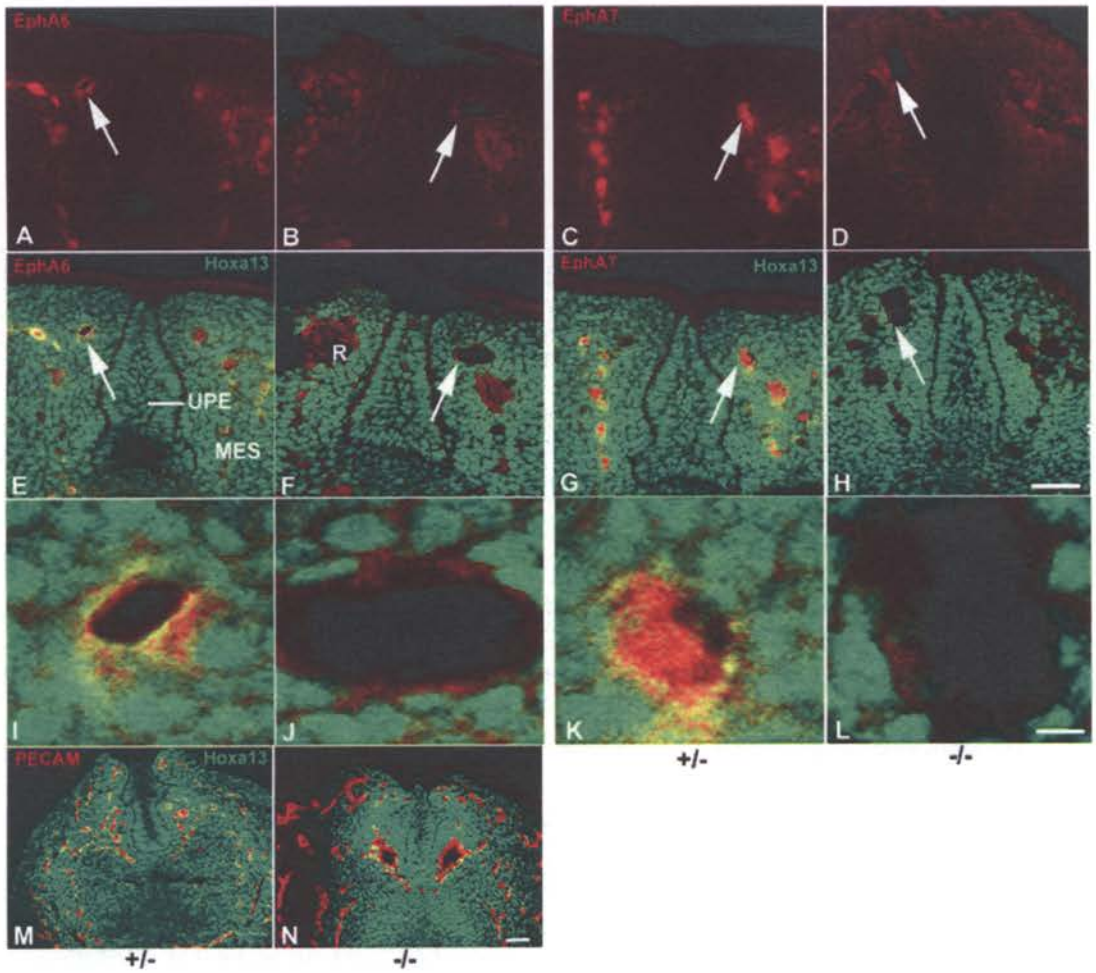
EphA6
A
B
EphA7
C
D
EphA6
Hoxa13
UPE
MES
E
R
F
EphA7
Hoxa13
G
H
I
J
K
L
+/-
-/-
PECAM
Hoxa13
M
N
+/-
-/-

Figure 3:

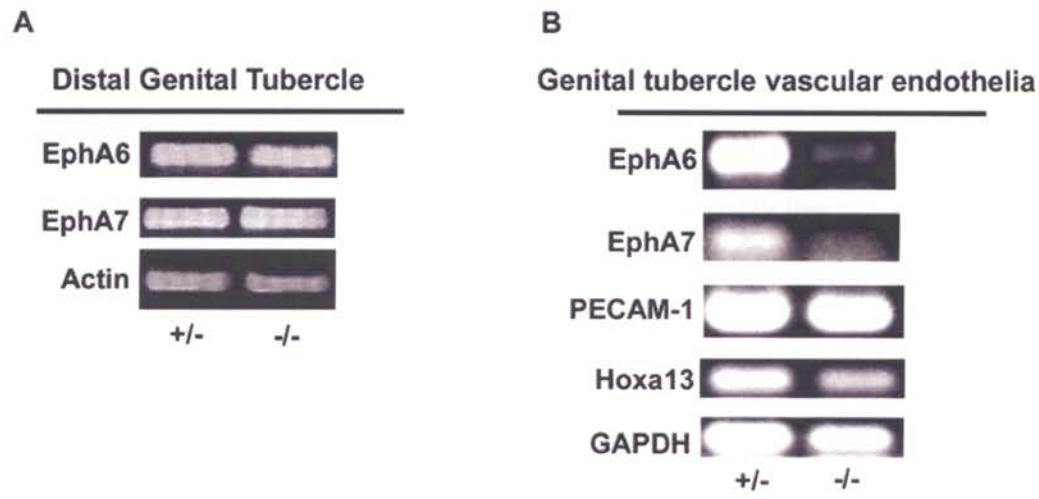

Figure 3. Quantitation of Hoxa13, EphA6, and EphA7 expression in the GT mesenchyme and vascular endothelia.

(A) Semi-quantitative RT-PCR of *EphA6* and *EphA7* transcripts revealed no differences in *EphA6* and *EphA7* expression in the whole distal GT. (**B**) *Hoxa13*, *EphA6*, and *EphA7* are co-expressed in the GT vascular endothelium by semi-quantitative RT-PCR on PECAM-positive endothelial-specific isolates. Furthermore, both *EphA6* and *EphA7* expression levels were reduced in vascular endothelial cells of *Hoxa13* homozygous mutant GT compared to *Hoxa13* heterozygous controls. The GAPDH housekeeping gene was used as a cDNA control.

Figure 4. HOXA13 binds discrete regions of the EphA6 and EphA7 promoters.

(A) Sequences of the murine *EphA6* and *EphA7* promoter regions. Underlined nucleotides denote regions exhibiting high conservation among multiple species. Lower case nucleotides denote primer sites used to amplify the promoter region for EMSA analysis and chromatin immunoprecipitation in Figure 5. **(B)** Species conservation of the *EphA6* and *EphA7* promoter regions bound by the HOXA13 DNA binding domain peptide (A13). Sequence conservation and alignment were determined using BLAST analysis software and the UCSC Genome Browser Database (Karolchik et al., 2003; Kent et al., 2002; Kent et al., 2005). **(C)** EMSA analysis of the *EphA6* and *EphA7* promoter regions. At 0.2 μM, the HOXA13 DNA binding domain peptide (A13) exhibits non-saturating levels of binding to several *Hoxa13* binding sites present in the *EphA6* and *EphA7* promoter fragments whereas at 2.0 μM of A13, all binding sites present in the *EphA6* and *EphA7* promoter fragments appear bound, producing a single reduced mobility DNA fragment. Note that the addition of 0.2 μM unlabeled *EphA6* or *EphA7* promoter fragments was sufficient to competitively displace the A13 peptide from the radiolabeled promoter fragments.

Figure 4:

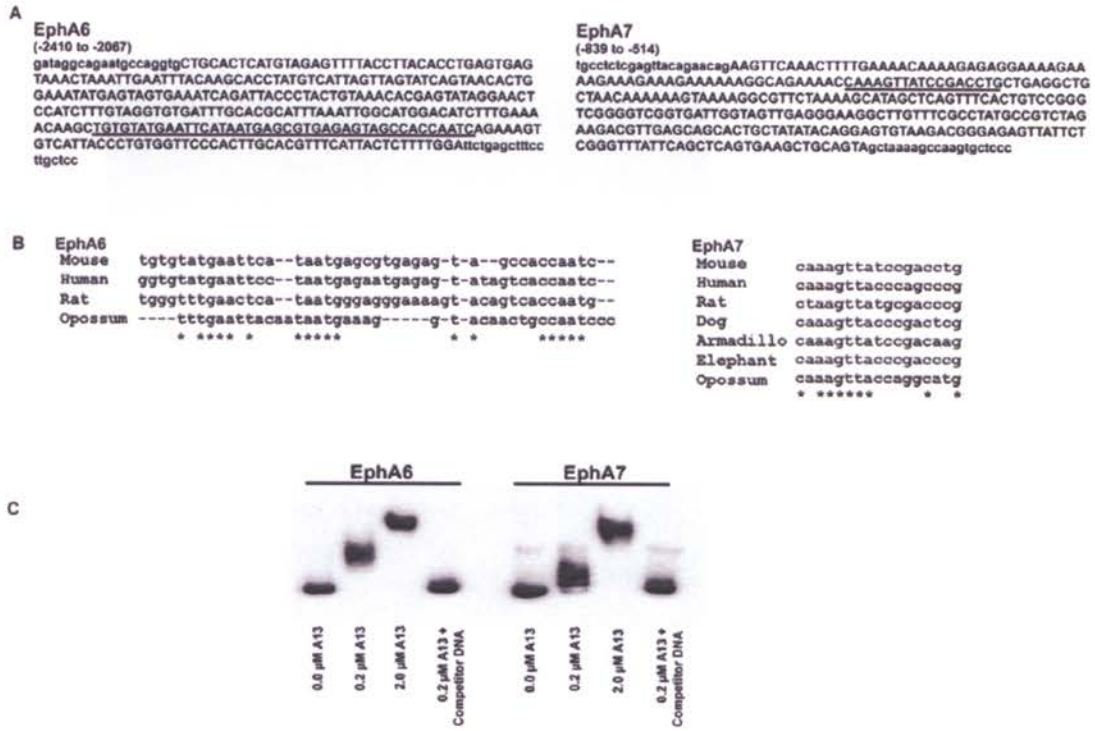
A
EphA6
(-2410 to -2067)
gataggcagaatgccaggtgCTGCACTCATGTAGAGTTTTACCTTACACCTGAGTGAG
TAAACTAAATTGAATTTACAAGCACCTATGTCATTAGTTAGTATCAGTAACACTG
GAAATATGAGTAGTGAAATCAGATTACCCTACTGTAAACACGAGTATAGGAACT
CCATCTTTGTAGGTGTGATTTGCACGCATTTAAATTGGCATGGACATCTTTGAAA
ACAAGCTGTGTATGAATTCATAATGAGCGTGAGAGTAGCCACCAATCAGAAAGT
GTCATTACCCTGTGGTTCCCACTTGCACGTTTCATTACTCTTTTGGAttctgagctttcc
ttgctcc
EphA7
(-839 to -514)
tgcctctcgagttacagaacagAAGTTCAAACTTTTGAAAACAAAAGAGAGGAAAAGAA
AAGAAAGAAAGAAAAAAGGCAGAAAACCAAAGTTATCCGACCTGCTGAGGCTG
CTAACAAAAAAGTAAAAGGCGTTCTAAAAGCATAGCTCAGTTTCACTGTCCGGG
TCGGGGTCGGTGATTGGTAGTTGAGGGAAGGCTTGTTTCGCCTATGCCGTCTAG
AAGACGTTGAGCAGCACTGCTATATACAGGAGTGTAAGACGGGAGAGTTATTCT
CGGGTTTATTCAGCTCAGTGAAGCTGCAGTAgctaaaagccaagtgctccc
B
EphA6
Mouse tgtgtatgaattca--taatgagcgtgagag-t-a--gccaccaatc--
Human ggtgtatgaattcc--taatgagaatgagag-t-atagtcaccaatc--
Rat tgggtttgaactca--taatgggagggaaaagt-acagtcaccaatg--
Opossum ----tttgaattacaataatgaaag-----g-t-acaactgccaatccc
EphA7
Mouse caaagttatccgacctg
Human caaagttacccagcccg
Rat ctaagttatgcgacccg
Dog caaagttacccgactcg
Armadillo caaagttatccgacaag
Elephant caaagttacccgacccg
Opossum caaagttaccaggcatg
C
EphA6
EphA7
0.0 μM A13
0.2 μM A13
2.0 μM A13
0.2 μM A13 + Competitor DNA
0.0 μM A13
0.2 μM A13
2.0 μM A13
0.2 μM A13 + Competitor DNA

Figure 5:

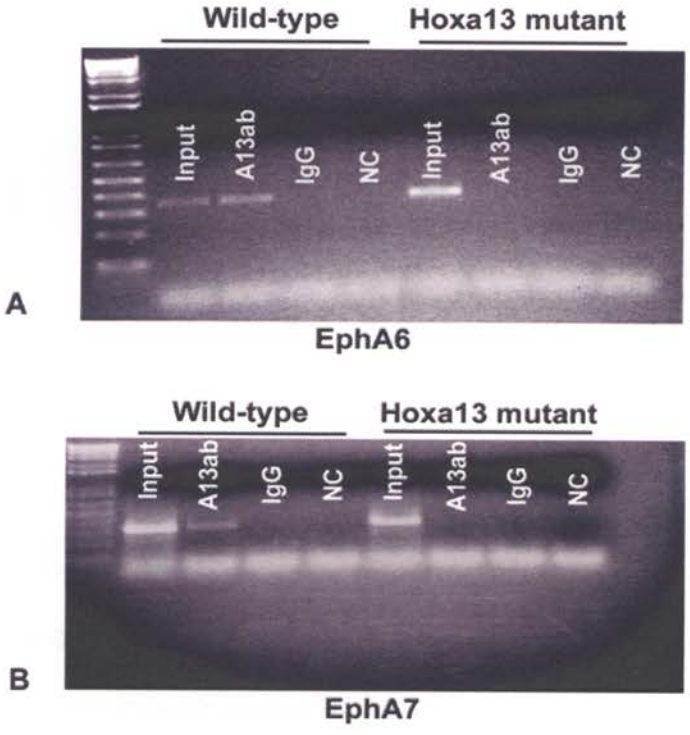

Figure 5. HOXA13 associates with the EphA6 and EphA7 promoter fragments in vivo in the developing GT.

(A-B) Positive PCR amplification of the *EphA6* and *EphA7* conserved regions after HOXA13 chromatin immunoprecipitation (ChIP) confirms that wild type HOXA13 binds the *EphA6* (**A**) and *EphA7* (**B**) promoter regions in the E 12.5 GT. Note that parallel ChIP assays of GT chromatin from homozygous mutants did not detect these same DNA, suggesting that HOXA13's DNA binding function is necessary for the *in vivo* binding of HOXA13 to the conserved *EphA6* and *EphA7* regions. NC=negative PCR control; IgG= immunoglobulin antibody control; Input= positive control confirming the presence of the *EphA6* and *EphA7* conserved regions in the chromatin samples prior to immunoprecipitation.

Figure 6:

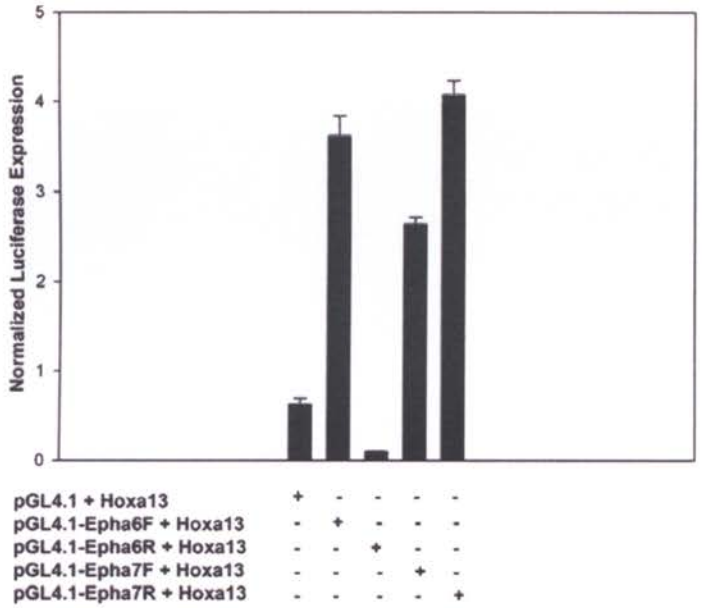

Figure 6. HOXA13 activates gene expression through the conserved EphA6 and EphA7 region in vitro

Co-transfection of NG108-15 cells with a pGL4.1 luciferase reporter plasmids containing forward or reverse orientations of the *EphA6* region bound by HOXA13 with a HOXA13 expression vector (pCMV-A13) resulted in increased luciferase expression (3.75 fold) only in the forward orientation compared to transfections with a control pCMV vector. Identical transfections using the conserved *EphA7* region bound by HOXA13 resulted in a 2.75-4 fold increase in relative luciferase expression, suggesting that this gene-regulatory region may be functioning as a HOXA13 directed enhancer of *EphA7* expression. Luciferase activity was normalized for transfection efficiency using a Renilla Luciferase control plasmid in all co-transfection assays. Bars represent the standard deviation of results derived from three independent assays.

Figure 7:

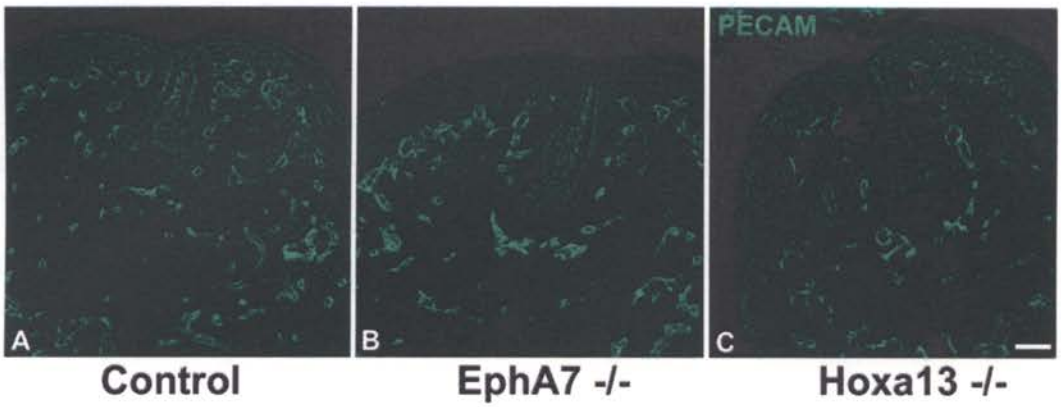

Figure 7. GT vessel diameter and endothelial cell identity are maintained in EphA7 homozygous mutants

(A) Typical GT vessel diameters and PECAM-1 expression in E13.5 wildtype control embryos. **(B)** The GT vasculature of *EphA7* homozygous mutants does not exhibit vessel enlargement or alteration in PECAM-1 expression when compared to the enlarged GT vasculature of *Hoxa13*-GFP homozygous mutants **(C).** Bar is 50 μm.

Acknowledgements

The authors thank Eric Steele and Hans Peter Bächinger for their assistance with the sedimentation equilibrium analysis. This work was supported by funding from the National Institutes of Health (HSS R01 DK66539) as well as Predoctoral Fellowships from the National Institutes of Health (WMK) and the American Heart Association (CS).

References

Adams RH, Diella F, Hennig S, Helmbacher F, Deutsch U, Klein R. 2001. The cytoplasmic domain of the ligand ephrinB2 is required for vascular morphogenesis but not cranial neural crest migration. Cell 104:57-69.

Baskin LS. 2000. Hypospadias and urethral development. J Urol 163:951-956.

Baskin LS, Erol A, Li YW, Cunha GR. 1998. Anatomical studies of hypospadias. J Urol 160:1108-1115; discussion 1137.

Brown A, Yates PA, Burrola P, Ortuno D, Vaidya A, Jessell TM, Pfaff SL, O'Leary DD, Lemke G. 2000. Topographic mapping from the retina to the midbrain is controlled by relative but not absolute levels of EphA receptor signaling. Cell 102:77-88.

Chan J, Mably JD, Serluca FC, Chen JN, Goldstein NB, Thomas MC, Cleary JA, Brennan C, Fishman MC, Roberts TM. 2001. Morphogenesis of prechordal plate and notochord requires intact Eph/ephrin B signaling. Dev Biol 234:470-482.

Chen J, Ruley HE. 1998. An enhancer element in the EphA2 (Eck) gene sufficient for rhombomere-specific expression is activated by HOXA1 and HOXB1 homeobox proteins. J Biol Chem 273:24670-24675.

Cheng N, Brantley DM, Chen J. 2002. The ephrins and Eph receptors in angiogenesis. Cytokine Growth Factor Rev 13:75-85.

Cooke JE, Kemp HA, Moens CB. 2005. EphA4 is required for cell adhesion and rhombomere-boundary formation in the zebrafish. Curr Biol 15:536-542.

Davy A, Aubin J, Soriano P. 2004. Ephrin-B1 forward and reverse signaling are required during mouse development. Genes Dev 18:572-583.

Davy A, Soriano P. 2005. Ephrin signaling *in vivo*: look both ways. Dev Dyn 232:1-10.

Dravis C, Yokoyama N, Chumley MJ, Cowan CA, Silvany RE, Shay J, Baker LA, Henkemeyer M. 2004. Bidirectional signaling mediated by ephrin-B2 and EphB2 controls urorectal development. Dev Biol 271:272-290.

Egea J, Nissen UV, Dufour A, Sahin M, Greer P, Kullander K, Mrsic-Flogel TD, Greenberg ME, Kiehn O, Vanderhaeghen P, Klein R. 2005. Regulation of EphA 4 kinase activity is required for a subset of axon guidance decisions suggesting a key role for receptor clustering in Eph function. Neuron 47:515-528.

Eichmann A, Le Noble F, Autiero M, Carmeliet P. 2005a. Guidance of vascular and neural network formation. Curr Opin Neurobiol 15:108-115.

Eichmann A, Yuan L, Moyon D, Lenoble F, Pardanaud L, Breant C. 2005b. Vascular development: from precursor cells to branched arterial and venous networks. Int J Dev Biol 49:259-267.

Gallentine ML, Morey AF, Thompson IM, Jr. 2001. Hypospadias: a contemporary epidemiologic assessment. Urology 57:788-790.

Gerety SS, Wang HU, Chen ZF, Anderson DJ. 1999. Symmetrical mutant phenotypes of the receptor EphB4 and its specific transmembrane ligand ephrin-B2 in cardiovascular development. Mol Cell 4:403-414.

Giwercman A, Carlsen E, Keiding N, Skakkebaek NE. 1993. Evidence for increasing incidence of abnormalities of the human testis: a review. Environ Health Perspect 101 Suppl 2:65-71.

Harbott LK, Nobes CD. 2005. A key role for Abl family kinases in EphA receptor-mediated growth cone collapse. Mol Cell Neurosci 30:1-11.

Hinck L. 2004. The versatile roles of "axon guidance" cues in tissue morphogenesis. Dev Cell 7:783-793.

Holmberg J, Clarke DL, Frisen J. 2000. Regulation of repulsion versus adhesion by different splice forms of an Eph receptor. Nature 408:203-206.

Hunter SG, Zhuang G, Brantley-Sieders D, Swat W, Cowan CW, Chen J. 2006. Essential role of Vav family guanine nucleotide exchange factors in EphA receptor-mediated angiogenesis. Mol Cell Biol 26:4830-4842.

Karolchik D, Baertsch R, Diekhans M, Furey TS, Hinrichs A, Lu YT, Roskin KM, Schwartz M, Sugnet CW, Thomas DJ, Weber RJ, Haussler D, Kent WJ. 2003. The UCSC Genome Browser Database. Nucleic Acids Res 31:51-54.

Kent WJ, Hsu F, Karolchik D, Kuhn RM, Clawson H, Trumbower H, Haussler D. 2005. Exploring relationships and mining data with the UCSC Gene Sorter. Genome Res 15:737-741.

Kent WJ, Sugnet CW, Furey TS, Roskin KM, Pringle TH, Zahler AM, Haussler D. 2002. The human genome browser at UCSC. Genome Res 12:996-1006.

Klagsbrun M, Eichmann A. 2005. A role for axon guidance receptors and ligands in blood vessel development and tumor angiogenesis. Cytokine Growth Factor Rev 16:535-548.

Knosp WM, Scott V, Bachinger HP, Stadler HS. 2004. HOXA13 regulates the expression of bone morphogenetic proteins 2 and 7 to control distal limb morphogenesis. Development 131:4581-4592.

Kodadek T. 1998. Mechanistic parallels between DNA replication, recombination and transcription. Trends Biochem Sci 23:79-83.

Marquardt T, Shirasaki R, Ghosh S, Andrews SE, Carter N, Hunter T, Pfaff SL. 2005. Coexpressed EphA receptors and ephrin-A ligands mediate opposing actions on growth cone navigation from distinct membrane domains. Cell 121:127-139.

Marston DJ, Goldstein B. 2006. Actin-based forces driving embryonic morphogenesis in Caenorhabditis elegans. Curr Opin Genet Dev 16:392-398.

McBride JL, Ruiz JC. 1998. Ephrin-A1 is expressed at sites of vascular development in the mouse. Mech Dev 77:201-204.

McCabe CD, Innis JW. 2005. A genomic approach to the identification and characterization of HOXA13 functional binding elements. Nucleic Acids Res 33:6782-6794.

Morgan EA, Nguyen SB, Scott V, Stadler HS. 2003. Loss of Bmp7 and Fgf8 signaling in *Hoxa13*-mutant mice causes hypospadia. Development 130:3095-3109.

Mortlock DP, Innis JW. 1997. Mutation of HOXA13 in hand-foot-genital syndrome. Nat Genet 15:179-180.

Myers C, Charboneau A, Boudreau N. 2000. Homeobox B3 promotes capillary morphogenesis and angiogenesis. J Cell Biol 148:343-351.

Ogawa K, Pasqualini R, Lindberg RA, Kain R, Freeman AL, Pasquale EB. 2000. The ephrin-A1 ligand and its receptor, EphA2, are expressed during tumor neovascularization. Oncogene 19:6043-6052.

Pasquale EB. 2005. Eph receptor signalling casts a wide net on cell behaviour. Nat Rev Mol Cell Biol 6:462-475.

Paulozzi LJ, Erickson JD, Jackson RJ. 1997. Hypospadias trends in two US surveillance systems. Pediatrics 100:831-834.

Perriton CL, Powles N, Chiang C, Maconochie MK, Cohn MJ. 2002. Sonic hedgehog signaling from the urethral epithelium controls external genital development. Dev Biol 247:26-46.

Salsi V, Zappavigna V. 2006. Hoxd13 and *Hoxa13* directly control the expression of the *EphA7* Ephrin tyrosine kinase receptor in developing limbs. J Biol Chem 281:1992-1999.

Shamah SM, Lin MZ, Goldberg JL, Estrach S, Sahin M, Hu L, Bazalakova M, Neve RL, Corfas G, Debant A, Greenberg ME. 2001. EphA receptors regulate growth cone dynamics through the novel guanine nucleotide exchange factor ephexin. Cell 105:233-244.

Shou S, Scott V, Reed C, Hitzemann R, Stadler HS. 2005. Transcriptome analysis of the murine forelimb and hindlimb autopod. Dev Dyn 234:74-89.

Stadler HS, Solursh M. 1994. Characterization of the homeobox-containing gene GH6 identifies novel regions of homeobox gene expression in the developing chick embryo. Dev Biol 161:251-262.

Stadler HS. 2003. Modelling genitourinary defects in mice: an emerging genetic and developmental system. Nat Rev Genet 4:478-482.

Stadler HS, Higgins KM, Capecchi MR. 2001. Loss of Eph-receptor expression correlates with loss of cell adhesion and chondrogenic capacity in *Hoxa13* mutant limbs. Development 128:4177-4188.

Stern AM, Gall JC, Jr., Perry BL, Stimson CW, Weitkamp LR, Poznanski AK. 1970. The hand-food-uterus syndrome: a new hereditary disorder characterized by hand and foot dysplasia, dermatoglyphic abnormalities, and partial duplication of the female genital tract. J Pediatr 77:109-116.

Svensson H, Reychman M, Troeng T, Aberg M. 1997. Staged reconstruction of hypospadias with chordee: outcome and costs. Scand J Plast Reconstr Surg Hand Surg 31:51-55.

Vashee S, Melcher K, Ding WV, Johnston SA, Kodadek T. 1998. Evidence for two modes of cooperative DNA binding *in vivo* that do not involve direct protein-protein interactions. Curr Biol 8:452-458.

Wahl S, Barth H, Ciossek T, Aktories K, Mueller BK. 2000. Ephrin-A5 induces collapse of growth cones by activating Rho and Rho kinase. J Cell Biol 149:263-270.

Wang HU, Chen ZF, Anderson DJ. 1998. Molecular distinction and angiogenic interaction between embryonic arteries and veins revealed by ephrin-B2 and its receptor Eph-B4. Cell 93:741-753.

Warot X, Fromental-Ramain C, Fraulob V, Chambon P, Dolle P. 1997. Gene dosage-dependent effects of the Hoxa-13 and Hoxd-13 mutations on morphogenesis of the terminal parts of the digestive and urogenital tracts. Development 124:4781-4791.